ANALYSIS AND SYNTHESIS ALGORITHMS for the ELECTRIC SCREEN JAUMAN ELECTROMAGNETIC WAVE ABSORBER

****

A Dissertation Presented in
Fulfillment of the Requirements for the
Degree of Doctor of Philosophy in Engineering
at the Faculty of Engineering,
University of Stellenbosch,
Stellenbosch, South Africa

by

Leendert Johannes du Toit
1993

****

Supervisor : Professor J.H. Cloete

stellenbosch University http://scholar.sun.ac.za

Abstract

An extensive literature study revealed numerous Jauman absorber examples with reasonable absorption properties. Unfortunately, tractable and detailed design techniques were found to be scarce, and often only applicable to absorbers with two or three layers. The research described in this report was therefore aimed at, and culminated in, general design methods for multilayered electric screen Jauman absorbers.

As a starting point, the synthesis problem is formulated by idealizing the spacers (assumed lossless and commensurate) and resistive sheets (assumed to have zero thickness), and by considering the absorption of a normally incident plane wave. An equivalent circuit model is derived, using the analogy between plane waves in stratified media, and guided waves in TEM transmission lines. The network is analyzed using Richard's frequency surrogate, $S = \tanh(s = \sigma + j\omega)$, and concise equations and algorithms are presented for symbolic and numerical analysis.

Maximum bandwidth synthesis of the classic one-layer absorber, or Salisbury screen, proved to be simple, clearly illustrates the analytic approach, and apparently has not been published before. The two-layer absorber was also found to be algebraically simple enough to be synthesized in closed form, is dealt with comprehensively, and the treatment consolidates and formalizes many of the design techniques available in the literature.

Networks comprising commensurate transmission lines and conductances have been investigated by Richards[1], but unfortunately the topology-driven realizability constraints on the input impedance of the Jauman network is only dealt with briefly. Fruitless investigations by the author showed this to be a formidable problem, and as a result the research concentrated on tractable and iterative synthesis algorithms for multilayered absorbers, instead of formal filter synthesis techniques.

These algorithms may be summarized as follows :

- A key concept in the multilayer zero-placement synthesis methods that will be presented, is the ability to physically realize a given set of reflection coefficient

[1] P.I. Richards, "Resistor-transmission-line circuits," *Proc. IRE*, vol. 36, pp. 217 – 220, Feb. 1948.

stellenbosch University http://scholar.sun.ac.za

zeros. This involves solving a set of highly non-linear equations, and a gradient-method iterative algorithm has been developed to achieve this.

- The first application of the aforementioned algorithm is to synthesize all reflection zeros at $S \rightarrow \infty$, thereby obtaining a maximally flat reflection coefficient magnitude response. Stable and rapid convergence was found for up to at least 20 layers, thereby extending the two- and three-layer algebraic solutions available in the literature. It was found that a stringent restriction exists on the maximum dielectric constant (ϵ_r) of the spacers, thereby limiting the practical implementation of these solutions.

- Through judicious manipulation of reflection zeros at distinct physical frequencies, an equiripple absorption response may be obtained. An elegant algorithm is presented to facilitate this, and it was found that these solutions represent substantial improvements over examples available in the literature. Restrictions still apply to the spacer ϵ_r, but these are more relaxed and practical equiripple absorbers are possible. In addition, the spread in sheet resistivities is much smaller than in comparable maximally flat solutions.

- Numerical searches indicated that the aforementioned equiripple responses are very close to, but not absolutely optimal, in the sense of maximum bandwidth. The small bandwidth and/or absorption improvements that were found were almost negligible from a practical viewpoint, but the optimal synthesis problem is academically very important. Through use of the general Chebyshev approximation method, an algorithm is developed which finds the local optimal response in the vicinity of such a parent equiripple solution. Although it might be tempting to classify the algorithm as a brute force method, it will be shown that this is not the case, and that its solutions provide the answer to the fundamental and unsolved optimal design problem.

These algorithms have been implemented, and tables of resistive sheet values are presented for N up to 8, a range of ϵ_r values corresponding to low loss foams, and for various absorption levels.

stellenbosch University http://scholar.sun.ac.za

Declaration

I, the undersigned, hereby declare that unless explicitly indicated otherwise, the contents of this document represents my own original work. It has not been presented for academic purposes elsewhere in its entirety or in part.

Leendert Johannes du Toit.

Signed : L du Toit.

Date : 28/11/93.

stellenbosch University http://scholar.sun.ac.za

Acknowledgements

I am indebted to the many people who contributed in various ways during the course of this dissertation. Specifically, I would like to use this opportunity to thank

- Professor John Cloete and the girls of La Rive, for many hours of advice, support, and encouragement, financial assistance, and a lot of fun;
- Professor Israel Navot, Technion, Haifa, Israel, who worked on the Jauman absorber problem during several visits to the University of Stellenbosch, and who made numerous contributions and suggestions;
- the staff at the Faculty, for my undergraduate education;
- my parents, for moral support and continuous encouragement;
- and lastly Scott and the boys from Huis Horings, without whom this would have been much quicker, less expensive, and also not remotely as enjoyable.

His coal stove is roaring, and he has arrived at that quiet hopelessness that cooks get on finally realizing that their work is never going to be finished, that there is no way of feeding a man once and for all.

– John Steinbeck[2]

[2] "Once there was a war," published by Corgi Books, London, 1964, pp. 66.

stellenbosch University http://scholar.sun.ac.za

Contents

stellenbosch University http://scholar.sun.ac.za

stellenbosch University http://scholar.sun.ac.za

stellenbosch University http://scholar.sun.ac.za

List of Tables

stellenbosch University http://scholar.sun.ac.za

List of Figures

stellenbosch University http://scholar.sun.ac.za

List of Definitions, Properties, Statements, Theorems and Conjectures

Definitions

Properties

Statements

Theorems

Conjectures

stellenbosch University http://scholar.sun.ac.za

Chapter 1

INTRODUCTION

1.1 History

The first concerted efforts to achieve practical microwave absorbers arose as radar became more and more important during World War II. Both Germany and the United States initiated projects which carried certain absorber ideas from research into at least limited operational use [1].

The German project was known by the code name "Schornsteinfeger" [2], [3], which translates to "chimney sweep" (the correlation between chimneys and microwave absorbers being carbon black!). One of the operational materials arising from this project was the Jauman absorber[1] (after J. Jauman), which was primarily used to camouflage submarine snorkels and periscopes. It was comprised of alternate layers of rigid plastic spacers and resistive sheets, $\pm$ 75mm thick in total, and provided about 20 dB absorption when utilized on flat or moderately curved conducting surfaces, at near normal incidence angles, over the range $2 - 15$ GHz.

The United States project in the $1941 - 1945$ period was led by Halpern at the M.I.T. Radiation Laboratory [4]. One of the materials developed was the Salisbury screen absorber (after W.W. Salisbury) [5], essentially a one-layer Jauman absorber. Interest in a practical version led the U.S. Rubber Company to manufacture a special resistive cloth, known as Uskon Cloth (or space cloth), with approximate surface resistance of 377 Ω/square. Construction of practical screens were simple, and the absorbers were useful over a $20 - 30$ % frequency range.

An interesting comment in [1] is the fact that the German effort was primarily directed towards radar camouflage, while the U.S. team concentrated on improving the performance of shipborne equipment by reducing unwanted reflections from the superstructure, and on providing indoor anechoic chambers for experimental purposes. Today radar cross section reduction of conducting objects is an active and extensive field[2], with the Jauman absorber one of many possibilities, e.g. [6].

---

[1] Although the spelling *Jaumann* often occurs in the literature, this dissertation will adhere to *Jauman*, as in [1].

[2] In the last few years microwave absorbing materials became increasingly known in the public domain. See for instance the rather amusing article on Stealth cars in [7].

stellenbosch University http://scholar.sun.ac.za

1.2 Engineering design problem

An idealized electric screen Jauman absorber is depicted in Figure 1.1. The perfect electric conductor (PEC), N identical and ideal (lossless) dielectric spacers, and N zero-thickness resistive surfaces (or sheets) are all assumed flat, and infinite in transverse dimensions. The stratified structure is illuminated by a normally incident uniform plane wave, and the resulting reflected wave magnitude is the quantity of interest.

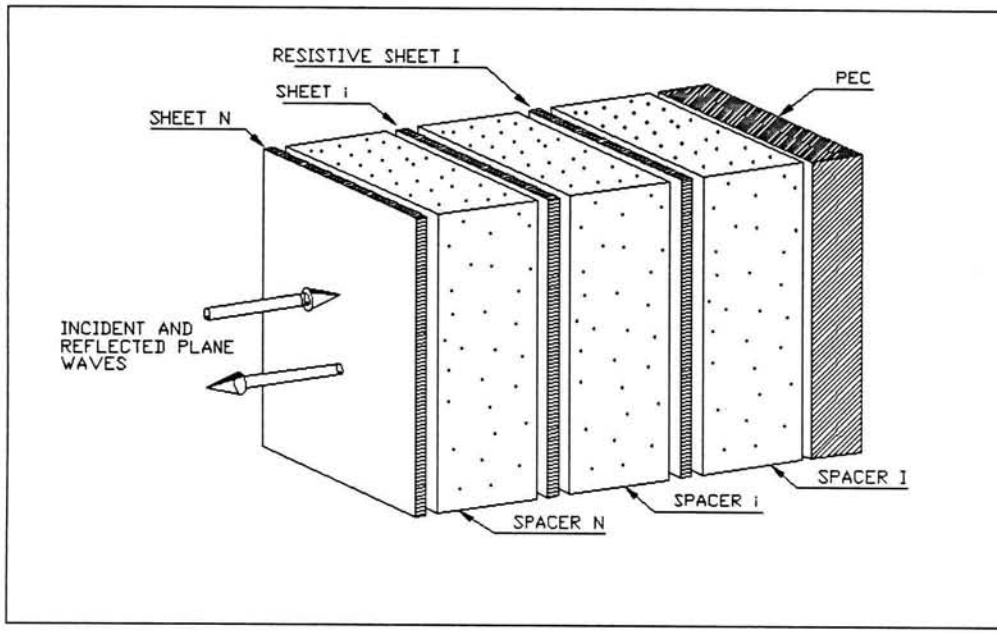

Figure 1.1: Physical topology of the Jauman absorber, with the infinite transverse dimensions truncated, and with the resistive sheets numbered from the PEC outwards.

Although the formal definitions of center frequency and bandwidth will only be introduced in the next Chapter, the engineering design problem which is solved in this dissertation, may now be stated as follows :

Statement 1 : *Assuming known spacers, what should the N sheet surface resistivities be, in order to*

- *minimize the reflected wave magnitude over a specified bandwidth, or alternatively*
- *maximize the bandwidth over which the reflected wave magnitude is less than a specified level?*

From what could be learned from the open literature, the solution to this design problem is still unsolved.

stellenbosch University http://scholar.sun.ac.za

1.3 Available synthesis techniques and classical solutions

An extensive literature study revealed numerous references to the Jauman absorber. Unfortunately, these were mostly example solutions, given without details of the particular design methods that were used. The few synthesis techniques that could be found, were either restricted to two and three- layer absorbers, or were vague. This section summarizes these methods and examples, grouped together according to the number of layers and/or the design method.

1.3.1 The one-layer absorber

Since being patented[3] by Salisbury [5], many sources have referred to the one-layer absorber, also known as the Salisbury screen, e.g. [8], [9], [10], [11], [12], [13, pp. 32-35 – 32-40], [14], [15, pp. 235, 239 – 244], [16, pp. 11.46 – 11.49] and [17, pp. 612 – 617]. Almost without exception these sources refer to the case where the resistive sheet has a surface resistivity of 377 Ω/square, i.e. the maximally flat solution. However, certain closed-form design and analysis equations, including the treatment of non-perpendicular incidence, were also found.

1.3.2 The two-layer absorber

- According to Severin [18] the first classical two-layer solution was developed[4] by Becker [19]. He discovered the existence of the two reflection zeros, and placed them judiciously in order to synthesize rippled absorption behaviors. Two numerical examples[5] are given, namely $R_1 = 270$, $R_2 = 1250$, and $R_1 = 230$, $R_2 = 2000$, all in Ω/square.

- Knott et al. [15, pp. 233 – 238] describe two-layer maximally flat and rippled synthesis using the approximate theory of small reflections, and in addition gives the exact maximally flat solution for $\epsilon_r = 1$, namely $R_1 = 266.579$ and $R_2 = 1287.159\Omega$/square.

- Ruck et al. [17, pp. 617] give[6] another reflection zero example, in particular

$$\epsilon_r = 1.76 \ , \ R_1 = 230 \ , \text{ and } R_2 = 552 \ \Omega/\text{square},$$

[3]The patent was applied for in 1943, but due to strategic reasons was only granted in 1952.

[4]Apparently and unfortunately not published.

[5]Inspection of (4.2) and (4.10) show that both these combinations will (almost) result in reflection zeros on the real or imaginary axes of the complex frequency plane, $s = \sigma + j\omega$. The specific zero positions (and ripple level for zeros at physical frequencies, i.e. on the imaginary s-axis), will depend on the spacer ϵ_r. In particular, the first example will exhibit a rippled response for all $\epsilon_r \geq 1$, and the second for all $\epsilon_r > 1.33$. Unfortunately it is not clear what ϵ_r was used to generate the graph in [18, Figure 4].

[6]They also propose multi-layered solutions with multiple reflection zeros, and suggest that it might be accomplished by solving $2N$ simultaneous equations. However, no information is given on how to determine these zero positions.

stellenbosch University http://scholar.sun.ac.za

which results in reflection coefficient ripples at approximately the −20 dB level. However, a radome forms an integral part of the design and (coincidentally) creates another reflection zero at the center frequency. This phenomena in effect transforms it into a three-layer example (see [23]).

- Naishadham and Kadaba [12, Figure 7] give a reflection zero example[7], in particular
$$\epsilon_r = 2.1 \ , \ R_1 = 282.8 \ , \text{ and } R_2 = 1130 \ \Omega/\text{square}.$$
- Fante and McCormack [9], [10], describe an algebraic procedure to synthesize two-layer[8] absorbers with maximally flat responses. Unfortunately, due to unmanageable algebraic complexity, their technique cannot be extended to general multilayered synthesis.

1.3.3 Multilayer exponential tapers

Various sources, e.g. [13, pp. 32-35 – 32-40], [18] and [21, pp. 396 – 399], refer to the same early exponential taper, with sheet resistivities increasing exponentially from the conductor outwards. In particular, the absorber had

$$\epsilon_r = 1.3 \ , \ R_1 = 300 \ \Omega/\text{square, and } R_{i+1} \approx 2.154 R_i \ , \ i = 1 \ldots 6 \ .$$

Presumably this specific solution was found by trial and error, and involved the evaluation of many different exponential generating laws. Exactly this approach was used by Nortier et al., [22]. They investigated many exponential tapers, and tabled those with good absorption properties. Note that their solutions assume an additional spacer at the incidence side, acting as a radome. The additional impedance transformation properties of such a radome prevent direct comparisons with radomeless absorbers, as the correspondence in [23] shows.

1.3.4 Multilayer quadratic tapers

Another old empiric law which is frequently encountered, is the quadratic taper. The following examples could be found :

- References to 2,3, and 4-layer absorbers in [15, pp. 247 – 248] and referred to by [16, pp. 11.46 – 11.49]. Only graphs of reflection coefficient magnitude versus frequency were given, however, without values for the sheet resistivities.

[7] There appear to be four inconsistencies in their example. First they incorrectly call it a maximally flat solution while the absorption has a rippled behavior; secondly usage of the particular two resistive sheets does in fact guarantee a reflection zero at a physical frequency, but with $\epsilon_r = 2.1$ the zero occurs at 5.864 GHz, and not at 7.5 GHz as they state; thirdly the reflection maximum is −10.1 dB and not $\approx$ −27 dB as in their Figure 7; and lastly their graph of reflection coefficient magnitude versus frequency shows total reflection at non-zero frequencies, which is impossible. It should be noted that their example is similar to the *approximate* (and coincidentally rippled) maximally flat solution for $\epsilon_r = 1$, obtained by Collin's theory of small reflections [20, pp. 224–237], which is described by Knott et al. [15, pp. 235, equation (8-51)].

[8] They also developed three-layer maximally flat design equations.

stellenbosch University http://scholar.sun.ac.za

- A reference in [15, p. 248] to a patent by Connolly and Luoma [24]. In particular, it was a six-layer absorber with $\epsilon_r = 1.03$, spacer thickness 3.56 mm, an "approximate" quadratic taper ($R_{1...6} = 236, 471, 943, 1508, 2513$ and 9425 Ω/square), and approximately 30 dB measured "average" absorption between 7 and 15 GHz.

- A five-layer taper given by Knott et al. [25] and referred to by [26]. In particular, it had $\epsilon_r = 1.035$, and $R_i = 75.4i^2$ Ω/square, $i = 1 \ldots 5$.

1.3.5 "Brute force" optimization

A summary of the empirical design methods described so far may be found in [27]. The least elegant, but sometimes sufficient solution to the design problem is to pose it as a numerical minimization problem, without exploiting any information of the physical problem under investigation. For example, a recent reference to such "brute force" methods, in particular the optimization of a Salisbury screen using microwave circuit analysis software, may be found in [28].

1.3.6 Specialized applications

Although this dissertation will not consider specialized applications, the following references are included for the sake of completeness :

- Magnetic spacers [10], [15, pp. 254 – 255].

- Chiral spacers [29].

- Polarization selective surfaces instead of resistive sheets and the PEC [30].

- The effect of curvature [25].

- Anisotropic spacers [26].

- The inclusion of periodic structures of magnetic elements [31].

- The use of lossy dichroic sheets [32].

1.3.7 The Wilkinson power divider connection

An interesting relationship exists between the classic multi-section two-way Wilkinson power divider hybrid [33], and the Jauman absorber. Cohn [34] developed a synthesis method where the circuit is bisected into odd and even excitation subcircuits. The odd mode circuit turns out to be similar to the Jauman problem, and thus the algorithms in this dissertation are applicable.

It should be noted that this dissertation considers identical spacers, while the quarterwave sections in the Wilkinson odd-mode circuit functions as an impedance transformer, and have dissimilar characteristic impedances. However, the algorithms

stellenbosch University http://scholar.sun.ac.za

are directly applicable, and the pertinent modifications are trivial. An IZP-response numerical example is presented in Section 7.5.4, and a substantial bandwidth improvement was found.

1.4 Overview of dissertation and original contributions

The preceding literature survey may be summarized as follows :

- Numerous references to the electric screen Jauman absorber occur in the open literature, and are mostly specific numerical examples, some of which exhibit reasonable absorption properties. The associated design techniques were almost without exception absent, empirical, vague or not applicable to multilayered absorbers. Lastly, without an optimal or close to optimal design method, the performance of the available numerical examples could not be rated.

In response to these stimuli, the research described in this dissertation was undertaken, and the more important issues will now be summarized Chapter-wise.

In **Chapter 2** the fundamental problem is posed unambiguously by idealizing the absorber parts (spacers and resistive sheets), investigating only the reflection of a normally incident[9] plane wave, assuming the absorber to be backed by a perfect electric conductor, and by assuming infinite transverse dimensions. The electromagnetic duality between plane waves in planar stratified layers, and guided waves in cascaded TEM transmission lines is exploited, and the physical absorber problem is transformed into an investigation of the input properties of a simple cascaded network.

Chapter 3 considers analysis of this network. In particular, the voltage cascade matrix approach was found to be suitable, using Richard's frequency surrogate, $S = \Sigma + j\Omega = \tanh s$. This analysis approach makes available a wealth of formal filter analysis and synthesis tools, is relatively simple, and it is surprising to note that it did not occur more often in the literature on the Jauman absorber.

To illustrate the simplicity of analysis, a rigorous treatment of the one-layer absorber, or Salisbury screen, is presented in **Appendix A**. It is interesting to note that none of the references in Section 1.3.1 described the optimal bandwidth solution, for which $R_{optimum} < 377\ \Omega$/square.

In **Appendix B** the symbolic analysis equations will be manipulated into recursive algorithms, suitable for numerical implementation. This should be seen as an extension of Chapter 3.

The algebraic complexity of the input port properties of the two-layer absorber

[9] In related work, oblique reflection from stratified structures was investigated [35], [36], and incorporated in a computer program.

stellenbosch University http://scholar.sun.ac.za

is manageable enough to be manipulated into closed-form synthesis equations. In **Chapter 4** a comprehensive treatment may be found, which consolidates and extends most of the two-layer design methods found in the literature. Four different synthesis methods are presented, namely

1. The maximally flat approach, with the two reflection zeros at $S \rightarrow \infty$.

2. A rippled response, with the two complementary reflection zeros at physical frequencies, i.e. on the imaginary S axis.

3. An optimal algebraic solution, where the frequency bandwidth is maximized by forcing a derivative to zero.

4. An iterative algorithm, where the points of maximum reflection are minimized simultaneously, over a fixed frequency bandwidth. This algorithm will be extended to multilayered absorbers in Chapter 8, and the two-layer implementation thus serves as a simple introduction.

It was found that the practical realization of two-layer maximally flat and rippled responses are limited by a restriction on the maximum spacer ϵ_r, and these limits are presented in closed form. Although some of the references described similar two-layer design methods, this fundamental restriction was never stated explicitly.

The same phenomenon was found in the multilayered case, and the two-layer ϵ_r limits and trends serve as verification for the multilayered conjectures[10] which will be developed later.

The developments of **Chapter 5** were vital to, and in fact suggested the multilayered zero placement synthesis algorithms. In particular, it will be shown that a given reflection coefficient numerator, i.e. known reflection zeros, contains enough information to synthesize[11] the corresponding absorber. This reconstruction of the sheet resistivities involves the solution of a set of N highly non-linear equations in N unknowns, and is accomplished with a Newton-Rhapson based algorithm. It is postulated (and verified for N=2 and 3) that $N!$ solutions exist for the unknown sheet resistivities, and that the conductances are complex in general.

The choice of starting values is crucial for convergence to a realizable set of resistivities, and will be dealt with carefully when the algorithm is used in later Chapters. It should also be stated that the algorithm behaved in a stable and tractable manner

[10]The multilayered synthesis algorithms work for $N \geq 2$, and should degenerate into the exact closed form solutions of Chapter 4. This has been verified.

[11]The fact that the reflection coefficient numerator alone completely specifies the absorber is worth expanding upon. Specifically, it prohibits the unconstrained use of formal 1-port synthesis techniques to obtain absorbers with wanted properties. Should such procedures be used, the process of manipulating wanted mathematical properties into rational input impedance or reflection coefficient functions should also consider the Jauman-topology-driven relationship between reflection coefficient numerator and denominator. This relationship might be in the form of an extension of the classical development by Brune [37], and was investigated by the author, but unfortunately could not be resolved.

stellenbosch University http://scholar.sun.ac.za

throughout the numerous syntheses that were done during the course of this dissertation.

Equipped with the ability to realize reflection zeros, an algorithm is developed in **Chapter 6** to synthesize multilayered maximally flat (MF-) responses, i.e. all reflection zeros at $S \to \infty$. These solutions were found for N up to at least 20, and significantly extends the two and three-layer solutions available in the literature.

As was stated before, these multilayered solutions are realizable only when the spacer ϵ_r is less than a certain maximum value, which is only marginally above 1. This places severe limitations on the practical implementation of multilayered absorbers with maximally flat responses. In addition, the sheet resistivity values exhibit a wide spread, and might not be practically feasible.

The Jauman absorber with $\epsilon_r = 1$ spacers, and the sheet resistivity law $R_i = 377i\ \Omega$/square, $i = 1 \ldots N$, surprisingly resulted in all reflection zeros distinct, and at physical frequencies. Even more surprising was the discovery that small frequency perturbations in these zero-positions did not affect realizability. In **Chapter 7** an algorithm will be developed to iteratively adjust the reflection zeros until the reflection coefficient magnitude exhibit an equiripple behavior. This solution will be named the IZP-solution, after **i**maginary-**z**ero-**p**lacement.

The algorithm proved to be stable for N up to at least 20 and for reasonable ripple levels, and numerical investigations indicated that these solutions are very close to optimal bandwidth[12]. In addition, these IZP-responses without exception exhibited wider bandwidths than comparable numerical examples in the literature. It was also found that the spacer restriction is more relaxed than in the MF-case, and the sheet resistivities exhibit a much smaller spread.

Although the IZP algorithm is iterative by nature, it leans heavily on intermediate properties of the Jauman structure, and should not be classified as a brute force numerical method[13]. The multilayered MF and IZP synthesis algorithms were presented at the IEEE AP-S/URSI International Symposium in 1990, [38].

The preceding IZP solutions were investigated for optimality by numerical searches[14], and small bandwidth and/or absorption level improvements were found in all cases. These improvements were extremely small, and would be negligible in practical absorbers, but are important academically.

Chapter 8 invokes the general formulation of Chebyshev approximation to develop another iterative algorithm, which minimizes the points of maximum reflection over the same bandwidth exhibited by a parent IZP-solution. The algorithm is felt to be an elegant implementation of the Chebyshev *no solution method* [51], and to the author's knowledge tractably solves the fundamental design problem of State-

[12]This may be heuristically motivated by the fact that the number of ripples is maximized for a given N.

[13]It is reminiscent of the Elliot-Orchard-Stern linear-array shaped-beam pattern synthesis [40], [41], which also involves iterative pattern zero position adjustments.

[14]And by using a circuit optimizer, similar to the procedure in [28].

stellenbosch University http://scholar.sun.ac.za

ment 1 for the first time. These solutions are tagged with the OPT mnemonic, and although the optimality is local, heuristic arguments very strongly support the conjecture that optimality is in fact global. Convergence was found to be stable, and the optimal sheet resistivities were found to be in the vicinity of the parent IZP values.

A description of the OPT synthesis algorithm is published in the 1992 IEEE AP-S/URSI International Symposium digest [39].

All the numerical algorithms have been implemented in MATLAB386[15], and a comprehensive set of lookup tables is presented in **Appendix E**. These results are useful for practical Jauman absorber design, and greatly extend and complement the solutions available in the literature.

[15]By MathWorks, Inc.

stellenbosch University http://scholar.sun.ac.za

Chapter 2

STRUCTURAL AND ELECTROMAGNETIC CONSIDERATIONS

2.1 Physical constraints

2.1.1 Topological

It will be assumed that the absorber is backed by a perfect electric conductor, that the spacers, resistive sheets and conductor have infinite transverse dimensions, and that the absorption of a normally incident[1] plane wave is to be investigated. These assumptions essentially reduce the analysis and synthesis problems to one dimension.

A spacer together with the resistive sheet adjacent to its incidence side, will be denoted a Jauman section, and the sections will be numbered from the conductor outwards to be consistent with the numbering scheme employed by early references to the Jauman absorber. During analysis, *and especially synthesis*, the number of sections[2] will be assumed known.

In some references the absorber is covered with an additional spacer with environmental protective properties. This geometry, which breaks down the sectioned symmetry and might cause ambiguity [23], will not be considered.

2.1.2 Spacers

The spacers will be assumed identical lossless homogeneous dielectrics, i.e. $\mu = \mu_o$ and with ϵ a real constant[3] $\geq \epsilon_o$, in particular $\epsilon = \epsilon_r \epsilon_0$ with $\epsilon_r \geq 1$. The spacer characteristic impedance,

$$Z_c = \frac{\eta_0}{\sqrt{\epsilon_r}} \approx \frac{376.7}{\sqrt{\epsilon_r}}\ \Omega\ , \tag{2.1}$$

[1] Oblique incidence will not be considered here. However, see [35], [36].

[2] Alternatively denoted layers.

[3] During analysis *and especially synthesis*, the spacer ϵ_r will be assumed known a priori.

stellenbosch University http://scholar.sun.ac.za

is therefore equal to or less than the intrinsic impedance of free space, η_0.

The spacers will be assumed commensurate, i.e. the same physical, and therefore electrical thickness. This restriction immediately defines the center frequency ω_0, where the physical spacer thickness equals a quarter-wavelength in the dielectric.

2.1.3 Resistive sheets

The resistive sheets interleaved with the spacers will be assumed of zero thickness. Such ideal sheets are completely characterized by a real, frequency-independent number, namely the sheet surface resistivity[4]. The assumptions involved are known [10], [43], and will not be expanded upon[5]. During analysis, all the sheets will be supposed present, i.e.

$$0 < R_{s,i} < \infty \text{ , with } R_{s,i} \text{ in } \Omega/\text{square, and } i = 1 \ldots N \text{ .} \tag{2.2}$$

2.2 Electromagnetic model and impedance normalizations

Exploiting the analogy between plane waves in stratified media, and TEM guided-waves in transmission lines [44, pp. 344 – 346], [45, pp. 501 – 502], it follows that the Jauman topology of Figure 1.1 may be modeled by interleaved and cascaded unit elements and shunt conductances, with the last unit element short-circuited. This network is shown in Figure 2.1. Without loss of generality, the characteristic

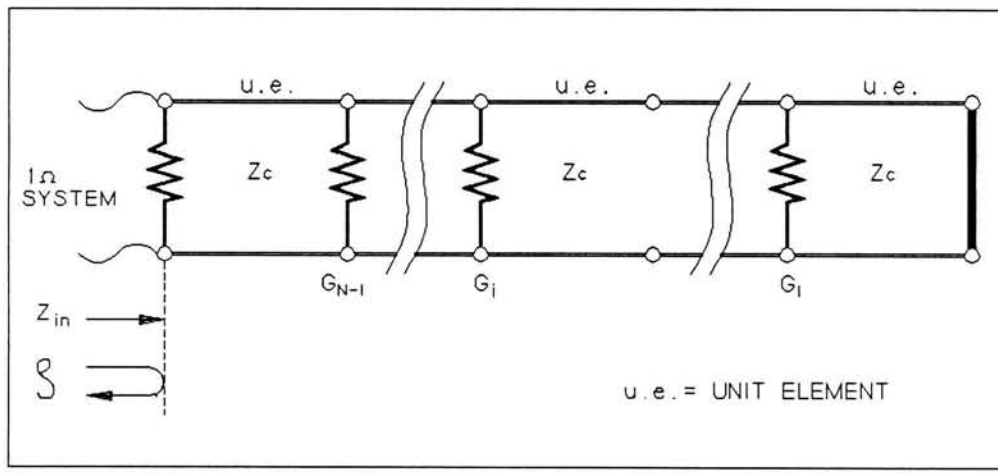

Figure 2.1: Equivalent network representation of the Jauman absorber.

impedance of the unit elements, Z_c, and the conductances, G_i, may be normalized

[4]The subscript s in (2.2) indicates that the quantity is expressed in Ω/square. The subscript was omitted in the examples of Section 1.3 for clarity.

[5]See [12] for a discussion on certain practical issues regarding the construction of resistive sheets.

stellenbosch University http://scholar.sun.ac.za

to the free space intrinsic impedance. In particular,

$$Z_c = \frac{1}{\sqrt{\epsilon_r}} \text{ , i.e. } 0 < Z_c \leq 1, \text{ and} \tag{2.3}$$

$$G_i = \frac{\eta_0}{R_{s,i}} \text{ , i.e. } 0 < G_i < \infty \text{ , } i = 1 \ldots N \text{ .} \tag{2.4}$$

From here onwards, any reference to a conductance refers to a G_i defined as in (2.4), and shown in Figure 2.1. It should be noted, however, that some of the later numerical results will be given as normalized resistivities, $R_i = 1/G_i$. This notation should not be confused with $R_{s,i}$, defined in (2.2).

The incidence medium, free space, is now represented by embedding the network in a system with characteristic impedance of 1Ω.

2.3 Frequency surrogates and normalizations

Although measurable electrical properties will be a function of the physical frequency ω, analytic continuation into the complex plane $s = \sigma + j\omega$ is obvious. Without loss of generality, the center frequency is normalized to $\omega_0 = \frac{\pi}{2}$, thereby implying that the delay times of the unit elements have been chosen to be 1 second.

Due to the nature of the unit elements [46], there will be a periodicity of π in ω, and a mirror image around $\omega = \pi/2$. It follows that the network will therefore exhibit the same electrical performance at the multiple frequencies $\omega + n\pi$ and $-\omega + n\pi$, for n any integer. The unique region in the complex s-plane will be defined as the band $\omega \in [-\frac{\pi}{2} , \frac{\pi}{2}]$.

Also due to the unit elements, the input impedance and voltage reflection coefficient will contain unwanted exponential components when expressed in terms of s. Richards [46], [47, p. 337] proposed the use of a frequency surrogate, $S = \Sigma + j\Omega = \tanh s$, which removes the exponentials, and which retains the real rational property of the input impedance of a so-called normal network, which fortunately includes the Jauman absorber network[6]. The imaginary axis of the $s-$plane now maps periodically, with $\Omega = \tan\omega$, onto the $j\Omega-$axis in the $S-$plane, with the segment $\omega \in [-\frac{\pi}{2} , \frac{\pi}{2}]$ mapping onto the whole imaginary S-axis.

Most of the research reported here was done in the S-plane. However, other frequency surrogates were used by Navot[7] and Cloete[8], and will briefly be described. The high-to-low pass transformation $p \stackrel{\text{def}}{=} S^{-1}$ retains the structural form of the equations involved, but simplify certain conditions at infinity. Mapping the closed right half of the S- and p-planes into the unit circle with $\xi \stackrel{\text{def}}{=} \mathrm{e}^{-2s}$, simplifies certain recursion relations when $Z_c = 1$. The interdependence between the different surrogates is summarized in Table 2.1.

[6]The equivalent network contains both lumped and distributed elements, but the conductances are assumed frequency independent, and thus the usual complexities arising from such mixed circuits do not occur.

[7]Prof. I. Navot, Technion, Haifa, Israel, worked on the Jauman problem during several visits to the University of Stellenbosch, and used p in most of his reports.

[8]Prof. J.H. Cloete, research supervisor, used ξ in most of his investigations.

stellenbosch University http://scholar.sun.ac.za

	$\mathcal{F}(s)$	$\mathcal{F}(S)$	$\mathcal{F}(p)$	$\mathcal{F}(\xi)$
$s =$	s	$\tanh^{-1} S$	$\coth^{-1} p$	$-0.5 \ln \xi$
$S =$	$\tanh s$	S	p^{-1}	$(1-\xi)/(1+\xi)$
$p =$	$\coth s$	S^{-1}	p	$(1+\xi)/(1-\xi)$
$\xi =$	$\exp(-2s)$	$(1-S)/(1+S)$	$(p-1)/(p+1)$	ξ

Table 2.1: Relationships between frequency surrogates.

Since the multilayered synthesis algorithms often refer to physical frequencies, it will be convenient to introduce

$$f = 200\omega/\pi \ . \tag{2.5}$$

It follows that one traversing of the imaginary axis of the S-plane is now transformed into the range $f \in [0, 200]$. Unless otherwise indicated, f will refer to (2.5) throughout this dissertation, and not to the conventional $f = \frac{\omega}{2\pi}$. It will also be used as abscissa in all graphs of $|\rho|$ versus frequency.

An important measurable property is the frequency bandwidth, defined as

$$\mathcal{B} \stackrel{\text{def}}{=} 100 \ \frac{\omega_2 - \omega_1}{\omega_0} = 2(100 - f_c) = 200 \left(1 - \frac{2 \arctan(\Omega_c)}{\pi}\right) \ \% \ , \tag{2.6}$$

where $\omega_1 + \omega_2 = 2\omega_0 = \pi$, $f_c = 200\omega_1/\pi$, $\Omega_c = \tan(\omega_1)$, and with the reflection coefficient magnitude less than a specified value for $\omega_1 \leq \omega \leq \omega_2$.

2.4 Fundamental problem restated

With reference to the equivalent network in Figure 2.1, the design problem of Statement 1 may be restated as follows :

> **Statement 2** : *With $N \geq 1$ and $0 < Z_c \leq 1$ known, what choice of real positive finite conductances $G_{1\ldots N}$, will either*
>
> - *minimize the maximum input reflection coefficient magnitude over a given bandwidth, or alternatively*
> - *maximize the bandwidth over which the maximum reflection coefficient magnitude is less than a certain allowable level?*

stellenbosch University http://scholar.sun.ac.za

Chapter 3

ANALYSIS

The input impedance and voltage reflection coefficient of the Jauman equivalent network in Figure 2.1 will now be derived, using S as frequency surrogate. The development is straightforward and almost trivial, but necessary, and the reader's patience is requested.

3.1 Voltage ABCD-matrix approach

An isolated section of the Jauman network is shown in Figure 3.1. Such a section

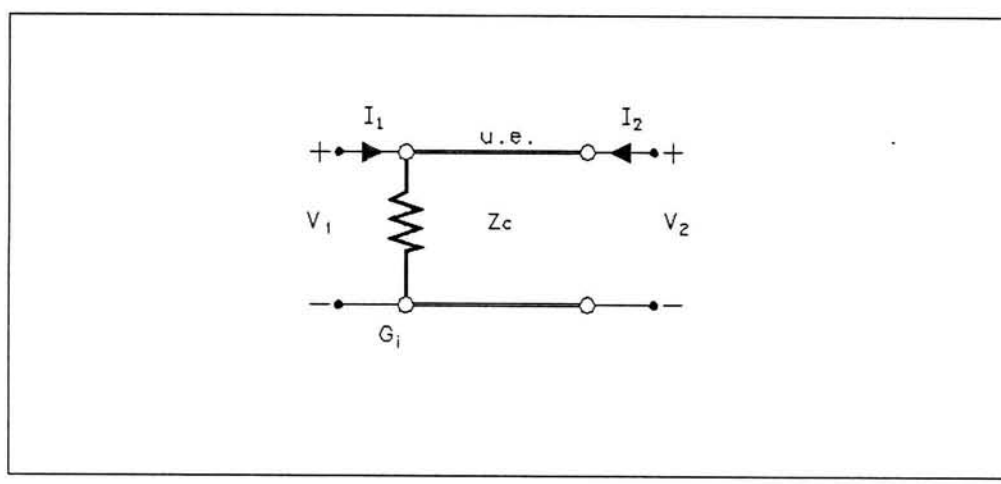

Figure 3.1: Section i isolated from the Jauman network of Figure 2.1.

may be characterized by cascade parameters in the form of the voltage $ABCD$-matrix $\mathbf{T}_i$ [47, pp. 132 – 136 and 337]. Using S as frequency variable, this matrix is given by

$$\begin{bmatrix} V_1 \\ I_1 \end{bmatrix} = \begin{bmatrix} 1 & Z_c S \\ \frac{S}{Z_c} + G_i & Z_c G_i S + 1 \end{bmatrix} \begin{bmatrix} V_2 \\ -I_2 \end{bmatrix} \frac{1}{\sqrt{1 - S^2}} \,. \tag{3.1}$$

stellenbosch University http://scholar.sun.ac.za

Cascading the Jauman sections is accomplished by multiplying the individual matrices of the different sections into a final 2x2 matrix, $\mathbf{F}_N$. In particular, and with the numbering scheme in mind,

$$\mathbf{F}_N = \begin{bmatrix} A_N & B_N \\ C_N & D_N \end{bmatrix} \frac{1}{\left(\sqrt{1-S^2}\right)^N} = \prod_{i=0}^{N-1} \mathbf{T}_{N-i} \,. \tag{3.2}$$

The input impedance of the shorted structure is given by

$$Z_{in}(S) = \left.\frac{V_1}{I_1}\right|_{V_2=0} = \frac{B_N}{D_N} \,, \tag{3.3}$$

with the common radical cancelling in both numerator and denominator. With the $e^{+j\omega t}$ time-dependence assumed and suppressed, the reflection coefficient is given by

$$\rho(S) = \frac{Z_{in}-1}{Z_{in}+1} = \frac{B_N - D_N}{B_N + D_N} \,. \tag{3.4}$$

To obtain the measurable reflection coefficient in terms of the normalized physical frequency ω, compute

$$|\rho|^2 = \rho(S)\rho(-S)|_{S=j\tan\omega} \,. \tag{3.5}$$

Both Z_{in} and ρ will be rational functions of two real polynomials in S of order N in general, and the coefficients of S will be sums of products[1] in the conductances, and the characteristic impedance Z_c. In Appendix A the optimal bandwidth solution of the one-layer absorber, or Salisbury screen, is found. The development uses the analysis method developed here, and serves as a simple example.

To accommodate the repetitive numerical computations of the multilayered algorithms, certain recursive extensions to the basic analysis method were developed. These may be found in Appendix B, and will be introduced in Section 5.2.1.

[1] Navot [49] investigated the coefficient buildup in detail, in particular the use of continuants [50, pp. 41 – 48] to derive closed form expressions.

stellenbosch University http://scholar.sun.ac.za

3.2 Standard forms of Z_{in} and ρ

To ensure consistency, the input impedance[2] and reflection coefficient from the previous Section will now be formalized regarding notation.

Property 1 : *The input impedance of the Jauman network depicted in Figure 2.1, with $1 \leq N < \infty$ sections, $0 < Z_c \leq 1$, all the conductances positive real finite, and with S as frequency variable, will always be expressible in the following standard form,*

$$Z_{in}(S) = \frac{\sum_{i=1}^{N} a_i S^i}{1 + \sum_{i=1}^{N} b_i S^i} \ , \tag{3.9}$$

with the a_i and b_i positive real finite coefficients.

Proof : *This follows from (3.1) to (3.3).*

Property 2 : *The reflection coefficient of the Jauman network, under the same conditions as in Property 1, will always be expressible in the following standard form,*

$$\rho(S) = \frac{-1 + \sum_{i=1}^{N} a_i S^i}{1 + \sum_{i=1}^{N} b_i S^i} \ , \tag{3.10}$$

with the a_i and b_i real finite coefficients, not to be confused with those from Property 1.

Proof : *This follows from Property 1 and (3.4).*

[2] Navot [48] investigated the case where all the conductances are absent, and found certain lower limits of the odd a_i and even b_i in (3.9). In particular, with $G_{1\ldots N} = 0$, (B.9) reduces to

$$P_i = \sum_{k=0}^{\left[\frac{i-1}{2}\right]} \binom{i}{2k+1} S^{2k} \ , \text{ with } i = 1 \ldots N+1 \ , \text{ and with} \tag{3.6}$$

$$[x] = \text{the largest integer} \leq x, \text{ and} \tag{3.7}$$

$$\binom{i}{j} = \text{the binomial coefficient, } \frac{i!}{(i-j)!j!} \ . \tag{3.8}$$

From (3.6) to (3.8), (B.10) and the fact that the conductances are positive real finite, these limits may readily be computed.

stellenbosch University http://scholar.sun.ac.za

Chapter 4

CLOSED FORM SYNTHESIS OF THE TWO-LAYER ABSORBER

This Chapter investigates the two-layer absorber, in particular closed form analysis and synthesis. Two classical solutions will be found, and two optimization techniques will be developed to find optimal solutions. The development is straightforward, but important due to the following :

- It will consolidate and formalize most of the two-layer synthesis techniques found in the literature (see Section 1.3).
- Surprising limitations on the practical realizability of these solutions were discovered, and will be examined in detail.
- This Chapter should be seen as a simple introduction to some of the fundamental concepts of the multilayer iterative algorithms.

From (3.1) and (3.2) it follows that

$$B_1 = Z_c S \ , \ D_1 = Z_c G_1 S + 1 \ , \ B_2 = G_1 Z_c^2 S^2 + 2 Z_c S \ , \text{ and}$$

$$D_2 = (G_1 G_2 Z_c^2 + 1) S^2 + (\{G_1 + 2G_2\} Z_c) S + 1 \ , \tag{4.1}$$

and implementing (3.4) yields $\rho(S)$ in standard form,

$$\rho(S) = \frac{aS^2 + bS - 1}{cS^2 + dS + 1} \ , \text{ with}$$

$$\begin{aligned} a &= Z_c^2 G_1 (1 - G_2) - 1 \\ b &= Z_c (2 - G_1 - 2G_2) \\ c &= Z_c^2 G_1 (1 + G_2) + 1 \\ d &= Z_c (2 + G_1 + 2G_2) \ . \end{aligned} \tag{4.2}$$

The rest of this Chapter is devoted to the manipulation of (4.2).

stellenbosch University http://scholar.sun.ac.za

4.1 Maximally flat (MF) response

4.1.1 MF definition

This solution is the result of enforcing $|\rho(\omega)|$ to behave maximally flat [47, pages 515-525] around $\omega = \frac{\pi}{2}$, and is also known as the Butterworth response. It translates into two restrictions on the magnitude of the reflection coefficient, namely

$$|\rho|^2_{\omega\to\frac{\pi}{2}} = 0 \text{ , and } \left.\frac{\partial\,|\rho|^2}{\partial(\omega^2)}\right|_{\omega\to\frac{\pi}{2}} = 0 \text{ .} \tag{4.3}$$

From (4.2) we have

$$|\rho|^2 = \rho(S)\rho(-S)/_{S=j\tan\omega} = \frac{a^2\tan^4\omega + [b^2+2a]\tan^2\omega + 1}{c^2\tan^4\omega + [d^2-2c]\tan^2\omega + 1} \text{ .} \tag{4.4}$$

Applying the first restriction of (4.3) enforces $a = 0$, since we have c finite when G_1 and G_2 are finite. Evaluating next the derivative of (4.3) at $\omega \to \frac{\pi}{2}$, we have

$$\left.\frac{\partial\,|\rho|^2}{\partial(\omega^2)}\right|_{\omega\to\frac{\pi}{2}} = \left.\frac{-2b^2}{c^2\cos\omega}\right|_{\omega\to\frac{\pi}{2}} \tag{4.5}$$

resulting in a simple pole for $b \neq 0$ (assuming both G_1 and G_2 non-negative real and finite), and equating to zero when $b = 0$. It follows that the maximally flat solution is equivalent to finding conductances that will yield $a = b = 0$, i.e. the whole synthesis process operates only on the numerator of ρ, and the only design parameter is Z_c.

4.1.2 Solving for the conductances

It follows from (4.2) that two solutions for G_1 and G_2 exist :

$$\text{Solution A : } \begin{cases} G_1 = \frac{-b+\sqrt{\Delta}}{2Z_c} \\ G_2 = 1 + \frac{-b-\sqrt{\Delta}}{4Z_c} \end{cases} \qquad \text{with } \Delta = b^2 + 8(1+a). \tag{4.6}$$

$$\text{Solution B : } \begin{cases} G_1 = \frac{-b-\sqrt{\Delta}}{2Z_c} \\ G_2 = 1 + \frac{-b+\sqrt{\Delta}}{4Z_c} \end{cases}$$

With $a = b = 0$ solution B always yields a negative G_1, and therefore only solution A needs to be considered, simplifying to

$$G_1 = \frac{\sqrt{2}}{Z_c} \text{ , and } G_2 = 1 - \frac{1}{\sqrt{2}Z_c} \text{ .} \tag{4.7}$$

A lower bound on Z_c immediately becomes apparent, namely

$$Z_c \geq \frac{1}{\sqrt{2}} \text{ .} \tag{4.8}$$

stellenbosch University http://scholar.sun.ac.za

This abrupt failure of the solution is well worth noting, and this restriction on the unit element will be extended later in the form of Conjecture 2 to include multilayered absorbers.

4.1.3 Frequency bandwidth

The reflection coefficient magnitude decreases monotonically from 1 at $\Omega = 0$ to 0 at $\Omega \to \infty$, and from (4.2) and (4.7), and using the definition $|\rho|^2_{\Omega=\Omega_c} = \mathcal{R}^2$, it follows that the bandwidth $\mathcal{B}$ is given by (2.6) and

$$\Omega_c = \frac{1}{2\sqrt{Z_c}}\sqrt{\sqrt{2} - 4Z_c + \sqrt{2}\sqrt{\frac{1}{\mathcal{R}^2} - 4\sqrt{2}\,Z_c + 8Z_c^2}}\,. \tag{4.9}$$

4.1.4 Numerical examples

Example 1: Synthesize a two-layer absorber with a MF-response. Assume $\epsilon_r = 1.8$, and compute the -20 dB bandwidth.

⊗ We have $Z_c = 1/\sqrt{1.8} = 0.7454$, satisfying (4.8). From (4.7) we obtain the conductance solution $G_1 = 1.897$ and $G_2 = 0.05132$. To obtain the bandwidth we compute $\mathcal{R}^2 = 10^{-20/10} = 0.01$, use (4.9) to obtain $\Omega_c = 2.055$, and finally (2.6) to yield $\mathcal{B} = 57.66$ %. In Figure 4.1 the reflection coefficient magnitude versus frequency is shown.

Example 2: Synthesize a two-layer absorber with a MF-response, assuming $\epsilon_r = 2.5$.

⊗ We have $Z_c = 0.6325$, which violates the restriction of (4.8). No solution exists.

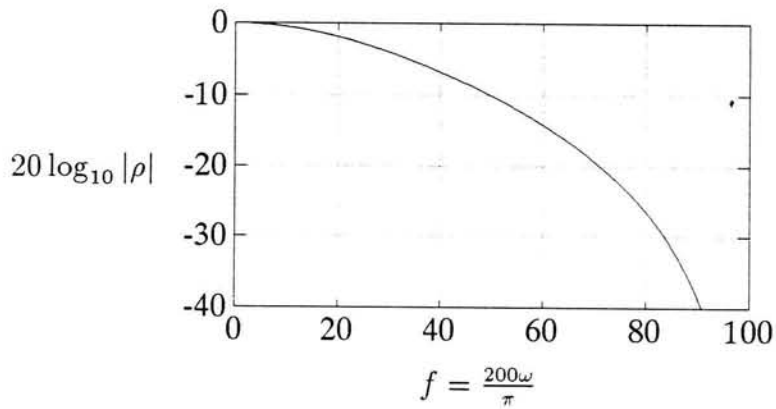

Figure 4.1: Reflection coefficient magnitude versus frequency, for MF numerical example 1.

stellenbosch University http://scholar.sun.ac.za

4.2 The rippled (IZP) response

4.2.1 Position of reflection zeros

In the MF-case two reflection coefficient zeros exist at infinity. The imaginary zero-placement (IZP) method operates by moving those zeros down the imaginary S-axis, to $\pm\Omega_z$, with $0 < \Omega_z \leq \infty$. The generic form of the reflection coefficient magnitude may be observed in Figure 4.2. From (4.2) it follows that in order to obtain the required reflection zero positions, we must have

$$b = 0 \text{ , and } a = -\frac{1}{\Omega_z^2} < 0 \text{ .} \tag{4.10}$$

Analogous to the MF case, the reflection zero placing operates only on the numerator of ρ, and again only solution A yields a potentially positive real G_1, reducing to

$$G_1 = \frac{\sqrt{2(a+1)}}{Z_c} \text{ , and } G_2 = 1 - \frac{G_1}{2} \text{ .} \tag{4.11}$$

It is important to note that the design process is finished once the reflection zero position is known. The rest of this Section will therefore be devoted to linking Ω_z to the ripple level ($\mathcal{R}$) and the frequency bandwidth ($\mathcal{B}$).

Studying (4.11) immediately brings forth another restriction. To ensure realness of G_1 a lower bound exists on a, thereby restricting the zero position. We have

$$a \geq -1 \text{ , or equivalently } \Omega_z \geq 1 \text{ .} \tag{4.12}$$

A third and last restriction merits special attention. To ensure positiveness of G_2 another (potential) restriction on a, and thus Ω_z, emerges. When $Z_c \leq \frac{1}{\sqrt{2}}$ we need

$$a \leq 2Z_c^2 - 1 \text{ , or equivalently } \Omega_z \leq \frac{1}{\sqrt{1-2Z_c^2}} \text{ .} \tag{4.13}$$

Keeping the generic form of the reflection coefficient magnitude in mind, this implies that the restriction on Z_c in the MF-case has relaxed, but not without reducing the solution space. In other words, with $Z_c < \frac{1}{\sqrt{2}}$ the MF-solution doesn't exist, whereas the IZP-solution does, but with a restriction on the zero position, and thus, as will be seen shortly, also on the minimum realizable ripple level. Once again this abrupt solution failure will be generalized in Conjecture 3.

As a check on consistency, it may be verified that the IZP-solution degenerates into the MF-solution when the zero positions are moved all the way to infinity. This is to be expected, since the MF solution is simply a specific case of the IZP solution.

4.2.2 Ripple level

With Ω_z within bounds, the solution may now be analyzed to obtain the ripple level in terms of the zero position. The maximum reflection coefficient magnitude for

stellenbosch University http://scholar.sun.ac.za

$\Omega > \Omega_z$ occurs at $\Omega \to \infty$, and $\mathcal{R} = \rho(\Omega \to \infty)$ is defined as the solution's ripple level, and is real-valued. To compute $\mathcal{R}$ it is now also necessary to compute the denominator of ρ. From (4.11) we have $G_2 \leq 1$, and thus from (4.2), (4.10) and (4.11), and by taking the limit, the following is obtained :

$$\mathcal{R} = \frac{-1}{1 + 2\sqrt{2}\, Z_c \Omega_z \sqrt{\Omega_z^2 - 1}} ,$$

$$\text{with } -1 < \mathcal{R} < 0 . \tag{4.14}$$

The restriction (of (4.13)) on Ω_z may be used in (4.14) to obtain the previously mentioned dependence of the minimum realizable ripple level on Z_c, in particular

$$|\mathcal{R}|_{min} = \frac{1 - 2Z_c^2}{1 + 2Z_c^2} , \text{ when } Z_c < \frac{1}{\sqrt{2}} . \tag{4.15}$$

Inverting (4.14) yields the **first design equation :**

$$\Omega_z = \frac{1}{\sqrt{2}} \sqrt{1 + \sqrt{1 + \frac{(\mathcal{R}+1)^2}{2Z_c^2 \mathcal{R}^2}}} . \tag{4.16}$$

If $Z_c < \frac{1}{\sqrt{2}}$, (4.13) or (4.15) should be used to verify that the solution exists, and then the conductances follow from (4.11) and the relationship $a = -1/\Omega_z^2$.

4.2.3 Frequency bandwidth

With Ω_z known, i.e. assuming a successful design, the resulting frequency bandwidth $\mathcal{B}$ may be computed with (2.6) and the frequency point $0 < \Omega_c < \Omega_z$ where $|\rho| = -\mathcal{R}$. After simple but quite tedious manipulations of (4.2), (4.10), (4.11) and (4.14), the following expression[1] is obtained :

$$\Omega_c = \Omega_z \sqrt{1 - \frac{2Z_c\, \Omega_z\, (\Omega_z^2 + 1)}{4Z_c\, \Omega_z^3 + \sqrt{2}\, \sqrt{\Omega_z^2 - 1}}} . \tag{4.17}$$

The **second design method** is to synthesize towards a specified bandwidth. Unfortunately Ω_z cannot be isolated from (4.17) into a closed form expression, and a numerical method should be used to solve for the zero-position in terms of Ω_c and Z_c. Again, for $Z_c < \frac{1}{\sqrt{2}}$ the validity of Ω_z should be verified with (4.13), and if realizable the conductance values and ripple level follow as before.

[1] It is seen that the zero position restriction (when $Z_c < \frac{1}{\sqrt{2}}$) translates into a minimum realizable bandwidth $\mathcal{B}_{min}$.

stellenbosch University http://scholar.sun.ac.za

4.2.4 Numerical examples

Example 1: Synthesize a -20 dB two-layer IZP-response, assuming $\epsilon_r = 1.3$.
$\otimes$ We have $Z_c = 0.8771$, $\mathcal{R} = -0.1$, and (4.16) yields $\Omega_z = 2.040$. The conductances follow from (4.11) as $G_1 = 1.406$ and $G_2 = 0.2973$, with the frequency bandwidth given by (2.6) and (4.17) as 81.86 %. The reflection coefficient magnitude $|\rho|$ versus frequency is shown in Figure 4.2.

Example 2: Synthesize a two-layer IZP-response with a 120 % bandwidth, assuming $Z_c = 0.6$.
$\otimes$ We have $\Omega_c = 0.7265$, and a numerical solution of (4.17) yields $\Omega_z = 1.2571$. Since $Z_c < 1/\sqrt{2}$ the realizability restriction of (4.13) should be investigated, and it follows that the solution is valid. From (4.11) we have $G_1 = 1.428$ and $G_2 = 0.2859$, and the ripple level follows from (4.14) as $\mathcal{R} = -0.3810$ (or -8.382 dB). Again $|\rho|$ versus frequency is shown in Figure 4.2.

Example 3: Synthesize a -40 dB two-layer IZP-response with $\epsilon_r = 10$ spacers.
$\otimes$ From (4.16) we have $\Omega_z = 10.54$, which violates the restriction of (4.13). Alternatively, (4.15) yields $|\mathcal{R}|_{min} = 0.6667 \equiv -3.5218$ dB, which violates the -40 dB specification. No solution exists.

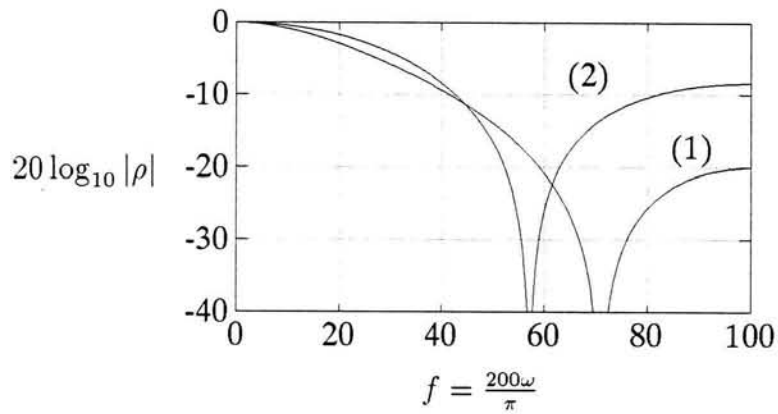

Figure 4.2: Reflection coefficient magnitude versus frequency, for IZP numerical examples 1 and 2.

stellenbosch University http://scholar.sun.ac.za

4.3 Optimal (OPT) response

Two methods will be developed. Both assume that a successful IZP-solution was possible, and then find the local optimal solution in its vicinity. It should be noted that the preceding IZP development strongly suggests that optimality is in fact global.

In particular, the following two improvement strategies will be used :

1. The bandwidth of a parent IZP solution will be maximized, keeping the ripple level constant. With great difficulty, this method might be applicable to three-layer synthesis, but it will become evident that the method will fail for $N > 3$.

2. The ripple level of a parent IZP solution will be minimized, keeping the bandwidth constant. This method will be generalized later in the multilayered OPT-response synthesis algorithm.

In both cases the improvements turned out to be marginal, with the optimal solution very close (in terms of the conductances) to the parent IZP solution.

4.3.1 Method 1: Maximizing the bandwidth

The main purpose of the parent IZP-solution will be to assist in conceptualizing the optimization technique, and the only parameter that will be shared by the two methods, is the ripple level $\mathcal{R}$.

Keeping in mind that for the IZP-solution we had $\rho(\Omega \rightarrow \infty) = \mathcal{R}$, with $-1 < \mathcal{R} < 0$, it follows from (4.2) that the relationship

$$G_1 = \frac{-(\mathcal{R}+1)}{Z_c^2(G_2\mathcal{R} + G_2 + \mathcal{R} - 1)} \tag{4.18}$$

will maintain $\rho(\Omega \rightarrow \infty) = \mathcal{R}$. Note that in order to keep G_1 positive a restriction on G_2 arises, namely

$$G_2 \leq \frac{1-\mathcal{R}}{1+\mathcal{R}} \, . \tag{4.19}$$

The problem is now reduced to finding the optimal[2] G_2 in the sense that Ω_c, the lowest frequency where $|\rho| = -\mathcal{R}$, will be minimized.

After manipulation[3] of (4.2) and (4.18), the following functional dependence of Ω_c on G_2 is found,

$$\Omega_c = \sqrt{\frac{(1-\mathcal{R}^2)(G_2\mathcal{R} + G_2 + \mathcal{R} - 1)^2 Z_c^2}{n}} \text{ , with}$$

$$n = c_4 G_2^4 + c_3 G_2^3 + c_2 G_2^2 + c_1 G_2 + c_0 \text{ , and}$$

[2] In the vicinity of the IZP parent solution.

[3] The symbolic manipulations that led to (4.20) and (4.21) are simple but extensive. It might therefore be possible to express them more simply.

stellenbosch University http://scholar.sun.ac.za

$$\begin{aligned}
c_4 &= 4(\mathcal{R}+1)^3(\mathcal{R}-1)Z_c^4 \\
c_3 &= 16(\mathcal{R}+1)^2(\mathcal{R}^2-\mathcal{R}+1)Z_c^4 \\
c_2 &= 4(\mathcal{R}+1)(\mathcal{R}-1)(6\mathcal{R}^2Z_c^2+6Z_c^2-\mathcal{R}^2-2\mathcal{R}-1)Z_c^2 \\
c_1 &= 4\left\{4Z_c^2(\mathcal{R}-1)(\mathcal{R}^3-1)-2\mathcal{R}^4-\mathcal{R}^3+2\mathcal{R}^2-\mathcal{R}-2\right\}Z_c^2 \\
c_0 &= (\mathcal{R}+1)(\mathcal{R}-1)\left\{4Z_c^4(\mathcal{R}^2-2\mathcal{R}+1)- \right. \\
&\quad \left. 4Z_c^2(\mathcal{R}^2-\mathcal{R}+1)+\mathcal{R}^2+2\mathcal{R}+1\right\} .
\end{aligned} \tag{4.20}$$

To illustrate the potential bandwidth improvement, a $\mathcal{R} = -0.1$, $Z_c = 0.8$ IZP-solution was used as parent, and Ω_c versus G_2 is shown in Figure 4.3.

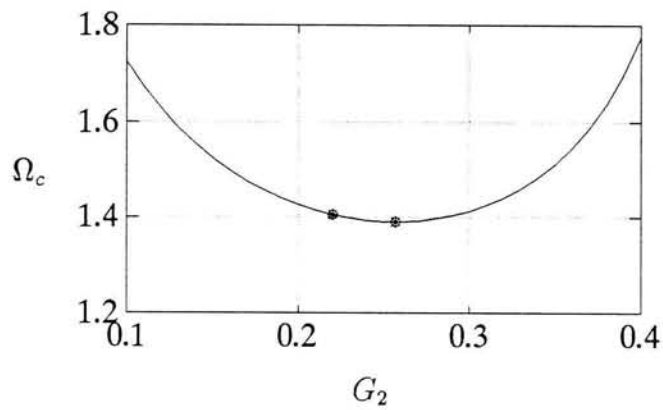

Figure 4.3: Relationship (i.e. (4.20)) between Ω_c and G_2, in the vicinity of the parent IZP-solution with $\mathcal{R} = -0.1$ and $Z_c = 0.8$. The two points indicated on the graph are the parent IZP solution for G_2 on the left, and the optimal point.

To find the G_2 that will yield $\Omega_{c,min}$, differentiate (4.20) with respect to G_2, and equate to zero. This results in

$$k_4G_2^4 + k_3G_2^3 + k_2G_2^2 + k_1G_2 + k_0 = 0 \text{ , with}$$

$$\begin{aligned}
k_4 &= 4(\mathcal{R}-1)(\mathcal{R}+1)^4Z_c^4 \\
k_3 &= 8(\mathcal{R}+1)^3(2\mathcal{R}^2-3\mathcal{R}+2)Z_c^4 \\
k_2 &= 24(\mathcal{R}-1)(\mathcal{R}+1)^2(\mathcal{R}^2-\mathcal{R}+1)Z_c^4 \\
k_1 &= 2(\mathcal{R}+1)\left\{4Z_c^2(2\mathcal{R}^4-5\mathcal{R}^3+6\mathcal{R}^2-5\mathcal{R}+2)+ \right. \\
&\quad \left. \mathcal{R}^3+2\mathcal{R}^2+R\right\}Z_c^2 \\
k_0 &= (\mathcal{R}-1)\left\{4Z_c^4(\mathcal{R}^4-2\mathcal{R}^3+2\mathcal{R}^2-2\mathcal{R}+1)+ \right. \\
&\quad \left. 2Z_c^2(\mathcal{R}^3+2\mathcal{R}^2+\mathcal{R})-\mathcal{R}^4-4\mathcal{R}^3-6\mathcal{R}^2-4\mathcal{R}-1\right\} .
\end{aligned} \tag{4.21}$$

The appropriate G_2 from (4.21), in particular the solution that is real, positive, satisfies (4.19) and which is in the vicinity of the parent value for G_2, together with G_1 obtained from (4.18), completes the solution. The bandwidth may be computed in the usual way via (4.20).

stellenbosch University http://scholar.sun.ac.za

4.3.2 Method 2: Minimizing the ripple level

In this section the Chebyshev "no-solution" methodology [51], [52] of finding a local optimal solution will be introduced. The starting point will be a realizable IZP-solution, i.e. Z_c and Ω_c^{IZP} were specified, and the IZP synthesis method resulted in G_1^{IZP}, G_2^{IZP}, Ω_z^{IZP}, and $\mathcal{R}^{IZP}$. The only parameter subsequently shared by both methods is Ω_c^{IZP}, defining the bandwidth over which the ripple level will be minimized. The various equations that will be developed are quite complex when expressed in closed form. For this reason, and keeping in mind that this section serves as introduction to the general multilayered iterative method, the solution development will be done in symbolic form. This particular approach may be summarized as follows :

- **Properties to be optimized :** $y_1 = |\rho|^2_{\Omega=\Omega_c^{IZP}}$, and $y_2 = |\rho|^2_{\Omega\to\infty}$, with initial value $y_1 = y_2 = (\mathcal{R}^{IZP})^2$.
- **Objectives :** Minimize y_1, y_2 and $|y_1 - y_2|$ simultaneously.
- **Variables :** G_1 and G_2, with initial values $G_1 = G_1^{IZP}$, and $G_2 = G_2^{IZP}$.

Optimality will have been reached when there exist no arbitrarily small perturbations in G_1 and G_2 that will decrease both y_1 and y_2 simultaneously. In [51] optimality in this sense is linked to the unsolvability of the following matrix equation,

$$\begin{bmatrix} \frac{\partial y_1}{\partial G_1} & \frac{\partial y_1}{\partial G_2} \\ \frac{\partial y_2}{\partial G_1} & \frac{\partial y_2}{\partial G_2} \end{bmatrix} \begin{bmatrix} x_1 \\ x_2 \end{bmatrix} = \begin{bmatrix} K_1 \\ K_2 \end{bmatrix} , \tag{4.22}$$

with K_1 and K_2 any two non-zero real numbers with the same sign. The determinant being square, this so-called *no-solution criterion* simply requires the determinant to vanish, yielding the first relationship between the optimal values of G_1 and G_2. The second (equiripple) objective, $y_1 = y_2$, supplies the second relationship between the two unknown conductances, and the solution to these two equations will yield the optimal conductances. The solution method is to define two error functions,

$$\mathcal{E}_1 = y_1 - y_2 \text{ , and } \mathcal{E}_2 = \frac{\partial y_1}{\partial G_1}\frac{\partial y_2}{\partial G_2} - \frac{\partial y_2}{\partial G_1}\frac{\partial y_1}{\partial G_2} , \tag{4.23}$$

in which the partial derivatives will be approximated[4] by finite differences. These errors may be approximated by linearizing them around some intermediate solution, $G_1^{\{i\}}$ and $G_2^{\{i\}}$, and a recursive improvement equation may then be extracted,

$$\begin{bmatrix} G_1^{\{i+1\}} \\ G_2^{\{i+1\}} \end{bmatrix} = \begin{bmatrix} G_1^{\{i\}} \\ G_2^{\{i\}} \end{bmatrix} - \begin{bmatrix} \frac{\partial \mathcal{E}_1}{\partial G_1} & \frac{\partial \mathcal{E}_1}{\partial G_2} \\ \frac{\partial \mathcal{E}_2}{\partial G_1} & \frac{\partial \mathcal{E}_2}{\partial G_2} \end{bmatrix}^{-1} \begin{bmatrix} \mathcal{E}_1 \\ \mathcal{E}_2 \end{bmatrix} , \tag{4.24}$$

[4]Care should be taken with the perturbations used to compute the nested partial derivatives. In the computation of $\mathcal{E}_2$ conductance perturbations of $10^{-6}\mho$ were used, while the partial derivatives of $\mathcal{E}_2$ with respect to G_1 and G_2 were computed with $10^{-5}\mho$ increments.

stellenbosch University http://scholar.sun.ac.za

with the partial derivatives evaluated at $G_1^{\{i\}}$ and $G_2^{\{i\}}$.

With the IZP values for G_1 and G_2 as starting point, (4.24) quickly converges, i.e. $\mathcal{E}_1, \mathcal{E}_2 \to 0$, and when done, the optimized ripple level is given by y_1 or y_2. Note that after each evaluation of (4.24), the process should repeat from (4.23).

4.3.3 Numerical examples

Example 1: Find the optimal two-layer -20 dB solution, assuming $\epsilon_r = 1.3$.

$\otimes$ Method 1 is applicable. The parent IZP-solution is $G_1^{IZP} = 1.406$, $G_2^{IZP} = 0.2973$, with $\Omega_c^{IZP} = 1.335$, or equivalently $\mathcal{B}^{IZP} = 81.86\%$. The improved conductance values follow from (4.21), $G_2 = 0.3340$, and from (4.18), $G_1 = 1.464$. The improved frequency bandwidth follows from (4.20) as $\Omega_c = 1.320$, or $\mathcal{B} = 82.56\%$. The absorption properties are shown in Figure 4.4.

Example 2: Find the optimal two-layer $\mathcal{B} = 70\%$ solution, assuming $Z_c = 0.9$.

$\otimes$ Method 2 is applicable. We have $\Omega_c^{IZP} = 1.6319$, and the parent IZP-solution is found to be $G_1^{IZP} = 1.433$, $G_2^{IZP} = 0.2836$, and $\mathcal{R}^{IZP} = -23.386$ dB.

Iteration 1:

Using the IZP-conductances as initial values, we have $y_1 = 0.0046$, $y_2 = 0.0046$, $\frac{\partial y_1}{\partial G_1} = 0.0224$, $\frac{\partial y_1}{\partial G_2} = -0.0562$, $\frac{\partial y_2}{\partial G_1} = -0.0354$, and $\frac{\partial y_2}{\partial G_2} = 0.0589$. Turning next to the two error functions, we have $\mathcal{E}_1 = 5.1969 \times 10^{-9}$ and $\mathcal{E}_2 = -6.7437 \times 10^{-4}$. The partial derivatives are $\frac{\partial \mathcal{E}_1}{\partial G_1} = 0.0578$, $\frac{\partial \mathcal{E}_1}{\partial G_2} = -0.1151$, $\frac{\partial \mathcal{E}_2}{\partial G_1} = 0.0098$, and $\frac{\partial \mathcal{E}_2}{\partial G_2} = 0.0177$. Evaluation of (4.24) results in the first set of improved conductances, $G_1^{\{1\}} = 1.46881$ and $G_2^{\{1\}} = 0.301699$.

Subsequent iterations:

$G_1^{\{2\}} = 1.47179$, $G_2^{\{2\}} = 0.304459$,

$G_1^{\{3\}} = 1.47178$, $G_2^{\{3\}} = 0.304475$,

with convergence to 6 digits reached after only 3 iterations. The improved ripple level turns out to be $\mathcal{R} = -23.497$ dB, with the absorption behavior shown in Figure 4.4.

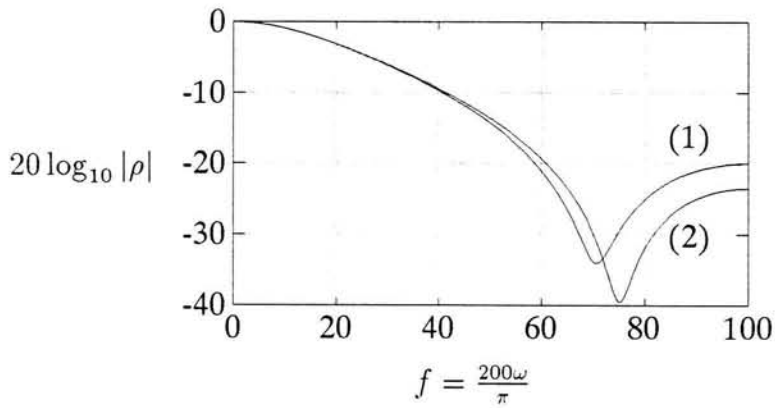

Figure 4.4: Reflection coefficient magnitude versus frequency, for the OPT numerical examples. *Note:* It has been verified that the two optimization methods degenerate into each other, when given the appropriate design parameters.

stellenbosch University http://scholar.sun.ac.za

Chapter 5

CONDUCTANCE RECONSTRUCTION

5.1 Introduction

It follows from Chapter 3 (in particular Property 2), that the reflection coefficient numerator will be a polynomial in S of degree N, in general, thus exhibiting N zeros in the complex $S-$plane. Should it be of a lesser degree, the rational character of $\rho(S)$ will enforce additional reflection zeros at $S \rightarrow \infty$. In the next two Chapters algorithms will be developed which repetitively and judiciously propose such a set of N zeros on the imaginary S-axis, and then subsequently solve for the N conductances. It is the purpose of this Chapter to :

- Show that the reflection coefficient numerator contains enough information to reconstruct the N conductances, and that the problem is in fact underdetermined (in the sense that multiple solutions exist);
- To introduce a classification which will aid in the evaluation of reconstructed solutions, by addressing the questions of solution uniqueness and existence;
- And to develop a general iterative algorithm for such reconstructions.

5.2 The reconstruction problem

5.2.1 The reflection coefficient numerator, $\mathcal{N}_\rho(S)$

The conductance reconstruction and multilayer synthesis algorithms will all refer extensively to the reflection coefficient numerator, expressed as in Property 2. It will therefore be advantageous to introduce the following :

stellenbosch University http://scholar.sun.ac.za

Definition 1 : *A proposed reflection coefficient numerator, to be realized with N layers and with $G_{1\ldots N}$ real, non-negative and finite, with or without the a priori knowledge that the realization is possible, will always be expressible as*

$$\mathcal{N}_\rho(S) = -1 + \sum_{i=1}^{N} a_i S^i \ , \tag{5.1}$$

with $a_{1\ldots N}$ real and finite. Such a proposed numerator will be denoted by $\mathcal{N}_\rho(S)$, and will implicitly be accompanied by a known $0 < Z_c \leq 1$.

Although the matrix method of Chapter 3 is sufficient to compute the numerator of $\rho(S)$ either symbolically or numerically, a more efficient method has been developed in Appendix B.1. In particular,

$$\mathcal{N}_\rho(S) = -1 + \sum_{i=1}^{N} a_i S^i = (Z_c S + 1)P_N - P_{N+1} \ , \text{ with}$$

$$P_{i+1} = (Z_c G_i S + 2)P_i + (S^2 - 1)P_{i-1} \text{ for } i = 1 \ldots N \ , \text{ and } P_0 = 0 \ , \ P_1 = 1 \ . \tag{5.2}$$

The numerator of ρ is now expressed in terms of the last two polynomials of a set, $P_{0\ldots N+1}(S)$, which is constructed[1] through a two-term recursive relation. Inspection of (5.2) shows that with increasing N, the number and complexity of the terms rapidly grow into unmanageable symbolic complexity. To illustrate this, the $\mathcal{N}_\rho$ coefficients for $N = 1$, 2 and 3 are shown in Table 5.1.

	$N = 1$	$N = 2$	$N = 3$
a_1	$Z_c(1 - G_1)$	$Z_c(2 - G_1 - 2G_2)$	$Z_c(3 - G_1 - 2G_2 - 3G_3)$
a_2	–	$Z_c^2 G_1(1 - G_2) - 1$	$(2Z_c^2[G_1 + G_2][1 - G_3] - Z_c^2 G_1 G_2 - 3)$
a_3	–	–	$Z_c([Z_c^2 G_1 G_2 + 1][1 - G_3] - G_1)$

Table 5.1: Symbolic expansions of $\mathcal{N}_\rho(S)$ for $N = 1$, 2 and 3.

To circumvent this symbolic complexity, a computational algorithm is presented in Appendix B.3 to facilitate the repetitive numerical computation of the coefficients a_i.

Returning to the conductance reconstruction problem, it follows that it entails finding a set of positive real conductances, $G_{1\ldots N}$, that will realize the wanted coefficients $a_{1\ldots N}$, thereby realizing the given reflection zeros. This process involves solving the N highly non-linear equations implicit in (5.2), and no tractable non-iterative method could be devised.

[1] An algorithm is presented in Appendix B.2 to compute the coefficients of $P_i(S)$ numerically.

stellenbosch University http://scholar.sun.ac.za

5.2.2 Examples of small N, multivalued reconstructions

Although the phenomenon was not explicitly pointed out during the development of Chapter 4, even the two-layer conductance reconstruction problem is potentially multivalued. Assume for example that the synthesis of $\mathcal{N}_\rho = -1.5S^2 - 3S - 1$ (with $N = 2$ and $Z_c = 1$) was required during some hypothetical design process. Clearly (4.6) will result in two physically realizable solutions for G_1 and G_2, namely $G_1 = \frac{3+\sqrt{5}}{2}$, $G_2 = 1 + \frac{3-\sqrt{5}}{4}$, and $G_1 = \frac{3-\sqrt{5}}{2}$, $G_2 = 1 + \frac{3+\sqrt{5}}{4}$, and it follows that additional information would be required to make the choice.

To illustrate ambiguity for $N = 3$, pose the rather premature[2] reconstruction problem of realizing $\mathcal{N}_\rho(S) = -1$, together with $Z_c = 1$. The three non-linear equations in the three conductances follow from Table 5.1, and a symbolic equation manipulator was used to find the following exhaustive set of 6 solutions,

G_1	G_2	G_3
1.64404	0.514261	0.109146
−1.64404	−0.514261	1.89085
$1.32394 + j0.595189$	$-1.83518 - j0.0116596$	$1.78214 - j0.190623$
$1.32394 - j0.595189$	$-1.83518 + j0.0116596$	$1.78214 + j0.190623$
$-1.32394 + j0.595189$	$1.83518 - j0.0116596$	$0.217856 - j0.190623$
$-1.32394 - j0.595189$	$1.83518 + j0.0116596$	$0.217856 + j0.190623$

and it is seen that only one set is physically realizable.

The last example involves the reconstruction algorithm, which will be developed in Section 5.3. Posing the same problem as above, namely $\mathcal{N}_\rho(S) = -1$, but with $N = 4$ and $Z_c = 1$, and using different starting points in the iterative algorithm (5.8), it was possible to converge on the following three real solutions :

R_1	R_2	R_3	R_4
0.56104	1.4936	4.2782	22.5545
−0.56104	−1.4936	−4.2782	0.51134
6.4650	0.59237	−0.52106	0.642411

This should sensitize the reader to the pitfalls associated with such iterative algorithms, and why they should be (and were) implemented with great care.

5.2.3 Conjecture on the number of solutions

An investigation into the buildup of the sums of products forming the coefficients of $\mathcal{N}_\rho$, led to the following heuristic conjecture :

> **Conjecture 1** : *Any given $\mathcal{N}_\rho$ has $N!$ different solution sets for the unknown $G_{1\ldots N}$, with the conductances complex in general.*

The reader should note that all these solutions will realize the given $\mathcal{N}_\rho(S)$, but will result in different reflection coefficient denominators.

[2] This is in fact the definition of the maximally flat solution, which will be formalized in the next Chapter.

stellenbosch University http://scholar.sun.ac.za

5.2.4 Realizability classification of $\mathcal{N}_\rho(S)$

The following classification of $\mathcal{N}_\rho$ is proposed to formalize future discussions on solution existence and uniqueness.

> **Definition 2** : *Amongst all the* real *conductance solution sets which realize a given* $\mathcal{N}_\rho$,
>
> *(a) not one set will comprise non-negative, finite conductances,*
> *(b) only one set will comprise non-negative, finite conductances, or*
> *(c) more than one set will comprise non-negative, finite conductances.*
>
> *The* $\mathcal{N}_\rho$ *under investigation will be assigned a Class-number,* **Class 0,1 or 2**, *depending on its realizability as in (a), (b) or (c) respectively.*

To briefly illustrate the Class nomenclature, the examples of Section 5.2.2 may be classified as follows : The two-layer $\mathcal{N}_\rho$ is Class 2, the three-layer $\mathcal{N}_\rho$ is Class 1, and the four-layer $\mathcal{N}_\rho$ is still unresolved[3].

5.2.5 Classification of the two-layer MF- and IZP-solutions

Armed with Definition 2, it will be instructive to classify the two-layer zero placement solutions of Sections 4.1 and 4.2. From (4.6) to (4.8) it follows that the MF-specification ($\mathcal{N}_\rho = -1$) will be of

$$\begin{aligned} &\text{Class 1 when} \quad \tfrac{1}{\sqrt{2}} \leq Z_c \leq 1 \text{ , and of} \\ &\text{Class 0 when} \quad 0 < Z_c < \tfrac{1}{\sqrt{2}} \text{ .} \end{aligned} \tag{5.3}$$

Since the IZP-solution might be seen as a generalization of the MF-method, it seems appropriate that the occurrence of its Class change relaxes[4]. With reference to (4.15) it follows that the $\mathcal{N}_\rho$ under investigation will be of

$$\begin{aligned} &\text{Class 1 when} \quad \tfrac{1}{\sqrt{2}} \leq Z_c \leq 1 \text{ ,} \\ &\text{Class 1 when} \quad 0 < Z_c < \tfrac{1}{\sqrt{2}} \text{ , } |\mathcal{R}| \geq |\mathcal{R}|_{min} \text{ , and} \\ &\text{Class 0 when} \quad 0 < Z_c < \tfrac{1}{\sqrt{2}} \text{ , } |\mathcal{R}| < |\mathcal{R}|_{min} \text{ .} \end{aligned} \tag{5.4}$$

[3] It will be proposed in Conjecture 2 that it is of Class 1.

[4] Put simply, with increasing ϵ_r, the minimum realizable ripple level ($|\mathcal{R}|$) increases. This was also found in the multilayered case, and will be generalized in Conjecture 3.

stellenbosch University http://scholar.sun.ac.za

5.3 Algorithm to realize $\mathcal{N}_\rho(S)$

In this section an algorithm will be developed that will attempt to realize a given $\mathcal{N}_\rho(S)$. It is an application of the well-known gradient-based Newton-Rhapson root finding method [54, pp. 5, 222–227], where some functional dependence is linearized, and from which an iterative improvement scheme may subsequently be extracted. Implicit in such procedures is the assumption that at least one solution exists, and convergence is guaranteed if the starting point is chosen to be in the immediate vicinity of such a solution. Note that the algorithm will be designed to operate with real conductances only.

At the heart of the algorithm is the repetitive computation of $\mathcal{N}_\rho(S)$. To simplify the development, the following matrix notation is introduced :

$$\mathbf{a} = [a_1 \dots a_N]^T \ , \ \mathbf{G} = [G_1 \dots G_N]^T \ . \tag{5.5}$$

The functional dependence of $\mathbf{a}$ on $\mathbf{G}$ is approximated by assuming the linear relationship

$$\mathbf{a}(\mathbf{G}) \approx \bar{\mathbf{a}} + \bar{\mathbf{D}}(\mathbf{G} - \bar{\mathbf{G}}) \ . \tag{5.6}$$

Notationwise, we have $\bar{\mathbf{a}}$ due to $\bar{\mathbf{G}}$, $\mathbf{G}$ assumed to be in the vicinity of $\bar{\mathbf{G}}$, and $\bar{\mathbf{D}}$ the square[5] Jacobian matrix[6]

$$\bar{\mathbf{D}} = [d_{ij}] \ , \text{ with } d_{ij} = \left.\frac{\partial a_i}{\partial G_j}\right|_{\bar{\mathbf{G}}} \ , \ i = 1, \dots, N \text{ and } j = 1, \dots, N \ . \tag{5.7}$$

To obtain the recursive improvement scheme, redefine $\mathcal{N}_\rho(S) = -1 + \sum_{i=1}^{N} \hat{a}_i S^i$, enforce $\mathbf{a} = \hat{\mathbf{a}} = [\hat{a}_1, \dots, \hat{a}_N]^T$ in (5.6), and denote intermediate solutions with superscripts. This results in

$$\mathbf{G}^{(i+1)} = \mathbf{G}^{(i)} + (\bar{\mathbf{D}}^{(i)})^{-1}(\hat{\mathbf{a}} - \mathbf{a}^{(i)}) \ . \tag{5.8}$$

Still missing in (5.8) is the starting point, $\mathbf{G}^{(1)}$. The choice is quite critical, since it defines the final solution that will be converged[7] upon.

Finally, (5.8) terminates when the convergence criterion,

$$\max\{|\hat{a}_1 - a_1|, \dots, |\hat{a}_N - a_N|\} \leq 10^{-9} \ , \tag{5.9}$$

is satisfied.

---

[5] The squareness is fortunate, and follows from the Jauman topology.

[6] Refer to Appendix B.4 for an efficient algorithm to iteratively construct the partial derivatives. They were approximated by finite differences in an early experimental routine, but speed and accuracy were not sufficient.

[7] It was found that intermediate conductance solutions (i.e. during convergence) sometimes included negative conductances. This is simply part of the convergence route in the G–domain, and should be ignored. The implication of negative conductances in the final solution is much more relevant, and will be treated implicitly in Conjectures 2 and 3.

stellenbosch University http://scholar.sun.ac.za

Chapter 6

MULTILAYERED MAXIMALLY FLAT (MF) SOLUTION

6.1 Solution definition

The definition of the multilayered maximally flat reflection coefficient magnitude response is a straightforward extension of the development in Section 4.1.1, namely

$$|\rho|^2_{\omega=\frac{\pi}{2}} = 0 \text{ , and } \left.\frac{\partial^i |\rho|^2}{\partial \omega^{2i}}\right|_{\omega=\frac{\pi}{2}} = 0 \text{ , with } i = 1 \ldots N-1 \text{ , and } N \geq 2 \text{ .} \qquad (6.1)$$

It was found that these requirements simplify considerably[1] when translated into the Richards' frequency domain, as the following illustrates :

> **Theorem 1** : *With N and Z_c specified, the maximally flat requirements of (6.1) will be satisfied when, and only when*
>
> $$\mathcal{N}_\rho(S) \equiv -1 \text{ ,}$$
>
> *for all S, i.e. when the N coefficients of S have vanished.*
>
> **Proof** : *See Appendix C.*

Statement 1 simply means that all reflection zeros are at $S \rightarrow \infty$.

[1] Navot [49] states a more general requirement,

$$\left.\frac{\partial^i \mathcal{N}_\rho(S)}{\partial S^i}\right|_{\text{any } s} = 0 \text{ , for } i = 1 \ldots N \text{ ,} \qquad (6.2)$$

using p (defined in Section 2.3) as frequency surrogate. This leads to a set of N constraints for each choice of S, with any N of these constraints linearly independent, and results in more freedom when doing symbolic manipulations. In particular, when $S = 0$ Theorem 1 follows from (6.2) by inspection.

stellenbosch University http://scholar.sun.ac.za

6.2 Realizing $\mathcal{N}_\rho(S) = -1$

The conductance reconstruction algorithm[2] of Section 5.3 will now be utilized. From Theorem 1 we have the requirement $\hat{\mathbf{a}} = \mathbf{0}$. To find a stable starting point for the iteration of (5.8), small N solutions were obtained with a symbolic manipulator and with early experimental iterative procedures. The results indicated that the conductances follow the general trend $G_{i+1} < G_i$, and that G_1 is in the vicinity of 1. It was therefore decided to start the algorithm with $G_i^{(1)} = i^{-1}$, irrespective of Z_c. This choice proved stable for N up to at least 20, and for any $0 < Z_c \leq 1$. The existence and uniqueness of these conductance solutions are dealt with in Section 6.4.

6.3 Symbolically worked example

To illustrate the above, it will be informative to implement the conductance reconstruction algorithm symbolically on the simple $N = 3$, $Z_c = 1$ example. We have from (5.2) that

$$\mathbf{a}^{(i)} = \begin{bmatrix} 3 - G_1 - 2G_2 - 3G_3 \\ -3 + 2G_1 + 2G_2 - G_1G_2 - 2G_1G_3 - 2G_2G_3 \\ 1 - G_1 - G_3 + G_1G_2 - G_1G_2G_3 \end{bmatrix},$$

and thus

$$\bar{\mathbf{D}}^{(i)} = \begin{bmatrix} -1 & -2 & -3 \\ 2 - G_2 - 2G_3 & 2 - G_1 - 2G_3 & -2G_1 - 2G_2 \\ -1 + G_2 - G_2G_3 & G_1 - G_1G_3 & -1 - G_1G_2 \end{bmatrix}. \tag{6.3}$$

Starting with $\mathbf{G}^{(1)} = [1, 0.5, 0.\dot{3}]^T$, and utilizing (5.8) and (6.3), the successive iterations of Table 6.1 were obtained.

Iteration i	$\mathbf{G}^{(i)}$	$\mathbf{a}^{(i)}$
1	$[1.000000, 0.500000, 0.333333]^T$	$[0.0000, -1.5000, 0.0000]^T$
2	$[1.725806, 0.572581, 0.043011]^T$	$[-0.0000, 0.4109, 0.1768]^T$
3	$[1.643460, 0.519005, 0.106177]^T$	$[-0.0000, 0.0128, 0.0128]^T$
4	$[1.644044, 0.514268, 0.109140]^T$	$[-0.0000, 0.0000, 0.0000]^T$
5	$[1.644042, 0.514261, 0.109146]^T$	$[-0.0000, 0.0000, 0.0000]^T$
≥ 6	As above (with same accuracy).	

Table 6.1: Intermediate results of the symbolically worked example of Section 6.3.

[2]The algorithm is briefly described in [38].

stellenbosch University http://scholar.sun.ac.za

6.4 Existence and uniqueness

As was stated in Section 6.2, the reconstruction algorithm always converged (for reasonable Z_c, i.e. not too close to 0). However, with $Z_c < 1$ and N big enough, it was found that some of the conductances turned out to be negative. The phenomenon was investigated numerically[3], and Conjecture 2, using the definition of Class, summarizes the results.

Conjecture 2 : *The maximally flat requirement, $\mathcal{N}_p(S) = -1$, is*

(a) of Class 1 when $Z_c \geq Z_{c,min}(N)$, or
(b) of Class 0 when $Z_c < Z_{c,min}(N)$.

Approximate values for the first few $Z_{c,min}$ are given in Table 6.2.

Motivation and notes :

- *$Z_{c,min}(1) = 0$ follows trivially from (A.2), Appendix A.*
- *$Z_{c,min}(2) = 1/\sqrt{2}$ has been derived in (4.8), Section 4.1.1.*
- *$Z_{c,min}(3 \ldots 8)$ have been found numerically by repetitively synthesizing solutions with decreasing Z_c, and noting when the solution changes Class. It was found without exception that G_N is the first to turn negative when Z_c is marginally smaller than $Z_{c,min}$, and that $G_N = 0$ when $Z_c = Z_{c,min}$. With Z_c decreasing substantially below $Z_{c,min}$, the conductance reconstruction algorithm starts behaving erratically, and with Z_c approaching 0, fails.*
- *For $Z_c = 1$, it is conjectured that $\mathcal{N}_p(S) = -1$ will be of Class 1 for $N \to \infty$, and that in the limit $G_1 = 2 - \delta$, with $\delta \to 0$ and $\delta > 0$, and that G_N will remain positive but will approach 0.*

N	1	2	3	4	5	6	7	8
$Z_{c,min}$	0_+	0.707	0.891	0.956	0.981	0.992	0.996	0.998
$\epsilon_{r,max}$	∞_-	2	1.260	1.095	1.039	1.017	1.007	1.003

Table 6.2: Minimum values for Z_c, and the corresponding maximum values for ϵ_r, which guarantee the MF-solution to be realizable.

[3]It should be noted that although a more formal proof would have been reassuring, the severe non-linearity of the pertinent equations, $\hat{\mathbf{a}} = \mathbf{0}$, discouraged such an approach.

stellenbosch University http://scholar.sun.ac.za

6.5 Representative numerical results

The ϵ_r restriction severely limits the practical realization of multilayered maximally flat responses. However, low dielectric constant foams are sometimes used, and in Appendix E many such solutions are tabled.

As was mentioned before, the MF solutions exhibit wide spreads in conductance values. To illustrate this, the $N = 20$, $\epsilon_r = 1$ solution is tabulated in Table 6.3, with the absorption behavior shown in Figure 6.1. The -20 dB absorption frequency bandwidth was found[4] to be 167.97 %.

R_1	R_6	R_{11}	R_{16}	0.50000458	3.0988071	12.962977	935.48405
R_2	R_7	R_{12}	R_{17}	1.0000955	3.7885643	21.940171	4257.4434
R_3	R_8	R_{13}	R_{18}	1.5009526	4.7275441	42.549731	27075.914
R_4	R_9	R_{14}	R_{19}	2.0060614	6.1570915	97.180655	270487.06
R_5	R_{10}	R_{15}	R_{20}	2.5277857	8.5541762	269.21309	5652534.8

Table 6.3: Normalized resistance values for a $N = 20$ MF-response solution, with $\epsilon_r = 1$.

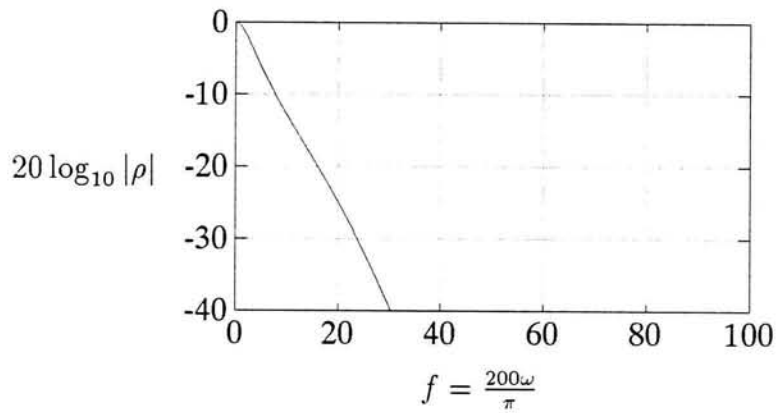

Figure 6.1: Reflection coefficient magnitude versus frequency, for the $N = 20$, $\epsilon_r = 1$ (see Table 6.3) multilayered MF-response numerical example.

[4]With **G** known, and with $|\rho|$ being a monotonically decreasing function with f, a simple gradient procedure was used to find the frequency point which defines the bandwidth.

stellenbosch University http://scholar.sun.ac.za

Chapter 7

MULTILAYERED IMAGINARY-ZERO-PLACEMENT (IZP) ALGORITHM

7.1 Introduction

Armed with the ability to realize reflection zeros[1], the synthesis of rippled absorption responses was investigated and successfully implemented. In particular, a feasibility investigation revealed the following :

- Extrapolating from the two-layer case, it was conjectured that multiple and distinct reflection zeros on the $j\Omega$ axis would cause a rippled absorption behavior. In addition, if the number of ripples could be maximized for a given number of layers, such responses would have wide bandwidths.

- Surprisingly, it was discovered by the author that the $G_i = i^{-1}$ starting point that was used in the conductance reconstruction algorithm during multilayered MF-synthesis, together with $Z_c = 1$, results in precisely this behavior. In particular, it exhibits $2\left[\frac{N}{2}\right]$ distinct and conjugate-paired zeros on the $j\Omega$ axis, and a single zero at $\Omega \to \infty$ when N is odd.

  This particular choice of conductances was subsequently investigated by Navot [55], with the following results : Proof that the reflection zeros will be distinct and will reside on the $j\Omega$ axis for all $N \geq 1$; proof that the zeros of an N layered and an $N+1$ layered structure will interlace on the $j\Omega$ axis; a recursive expression[2] to construct $\mathcal{N}_\rho$; and a closed form expression for the coefficients of S in $\mathcal{N}_\rho(S)$.

[1] Throughout this Chapter the term *zeros* will refer to reflection zeros, i.e. the zeros of $\rho(S)$, complex in general.

[2] The author derived the expression independently, but did not investigate this special case any further.

stellenbosch University http://scholar.sun.ac.za

- To investigate the feasibility of the proposed approach, small random on-axis perturbations were made in the zero positions resulting from $G_i = i^{-1}$, and subsequently realized with the algorithm of Chapter 5. The findings were encouraging, and may be summarized as follows :

  $\Rightarrow$ With $Z_c = 1$ it was found that almost any distinct[3] choice of N complementary pairs of Ω axis zeros were realizable, provided the zero closest to the origin was not too close[4]. Fortunately, the algorithm could be designed such that the zero position changes are driven[5] by the respective reflection maxima, and this situation never occurred during practical synthesis runs.

  $\Rightarrow$ With $Z_c < 1$, however, many of the attempted realizations resulted in one or more negative conductances, irrespective of the initial values fed to the reconstruction algorithm. This phenomenon will be treated more formally in Conjecture 3.

- A key concept that will be exploited is the fact that a local reflection maximum in $|\rho|$ is approximately proportional to the separation between its boundary zeros in the f domain. This is not surprising, as all the pertinent functions are well-behaved.

The zero placement scheme[6] should by now be obvious. The synthesis algorithm is cyclic, with each cycle implying the realization of a set of reflection zeros, an evaluation of the resulting rippled behavior, and an improvement in the zero positions. The reader should note that the only inputs to the synthesis will be N, Z_c, the initial conductance values, $G_i = i^{-1}$, $i = 1 \ldots N$, and the desired reflection ripple[7] level in dB, $\mathcal{R}_{dB}$. Once the final set of zero positions (with the specified equiripple response) have been realized, the synthesis is done. Additional properties, e.g. the frequency bandwidth, may subsequently be computed, but are not involved in the actual synthesis.

---

[3] Still with $Z_c = 1$, the realization of multiple zeros and zeros at $S \rightarrow \infty$ were investigated, and no additional realizability restrictions were found.

[4] In particular, the specific case where $G_{1 \ldots N-1} = 0$ and $G_N = 1$, i.e. a frequency-scaled one-layer maximally flat solution, provides a heuristic fundamental lower limit. Its zeros in the range $0 < f < 100$ are at $q_i = \frac{100}{N}(2i - 1)$, for $i = 1 \ldots [\frac{N}{2}]$ and $N > 1$, and the ripple magnitudes are at the 0 dB level. In practice, however, it was found that the conductance reconstruction algorithm starts behaving erratically when the lowermost zero is still realizable, but approaches the limit set by q_1. This was pointed out by I. Navot.

[5] Explaining the IZP nomenclature.

[6] The algorithm is briefly described in [38].

[7] To be consistent with Chapter 4, $\mathcal{R}_{dB}$ is defined as $\mathcal{R}_{dB} = 20 \log_{10}(-\mathcal{R})$.

stellenbosch University http://scholar.sun.ac.za

7.2 The IZP-algorithm

7.2.1 Reflection zero position nomenclature

The aim of the IZP-algorithm is to place the reflection zeros such that an equirippled absorption response is obtained over the range[8] $f \in (0, 200)$, with the number of ripples maximized for a given N. From the typical $N = 4$ and $N = 5$ responses

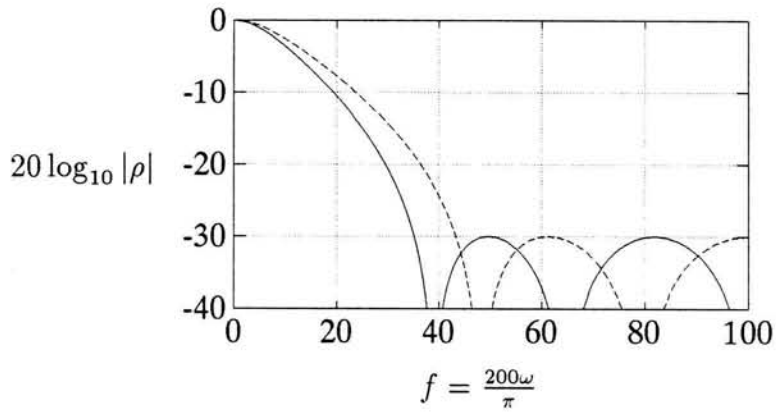

Figure 7.1: Reflection coefficient magnitude versus frequency, for typical $\mathcal{R}_{dB} = -30$ dB four-layer (dotted) and five-layer (solid) IZP-response numerical examples.

---

shown in Figure 7.1, and keeping the symmetry around $f = 100$ in mind, it may be observed that for N even a reflection maximum should occur at $f = 100$, while for N odd a zero should reside at $f = 100$, implying an $\mathcal{N}_\rho$ of order $N - 1$ in S. It should next be obvious that $M \stackrel{\text{def}}{=} \left[\frac{N}{2}\right]$ unique zero positions exist in the range $f \in (0, 100)$, i.e. not counting the zero at $f = 100$ when N is odd. They are numbered sequentially with decreasing f, and their f domain positions will be denoted $z_{1\ldots M}$.

The reflection coefficient magnitude will exhibit maxima in between these zeros, denoted $m_{1\ldots M}$, and each maximum will be linked notationwise to its two neighboring zeros. In particular, the spacings in between zeros will be denoted lobe-widths, $w_{1\ldots M}$, and will relate to the zero positions as follows :

$$N \text{ even} : z_i = \begin{cases} 100 - \frac{w_1}{2} & i = 1 \\ z_{i-1} - w_i & i = 2 \ldots M \end{cases} , \tag{7.1}$$

$$N \text{ odd} : z_i = \begin{cases} 100 - w_1 & i = 1 \\ z_{i-1} - w_i & i = 2 \ldots M \end{cases} . \tag{7.2}$$

Finally, in order to simplify the forthcoming development, the vectors[9] $\mathbf{w} = [w_1, \ldots, w_M]^T$, $\mathbf{z} = [z_1, \ldots, z_M]^T$, and $\mathbf{m} = [m_1, \ldots, m_M]^T$ are introduced. Also note that the maxima will be expressed in dB, i.e. $m_i = 20\log_{10}(|\rho|)$.

---

[8] The frequency surrogate f is defined in (2.5).

[9] The superscript T denotes the matrix transpose operation.

stellenbosch University http://scholar.sun.ac.za

7.2.2 Constructing and realizing $\mathcal{N}_\rho$

To initialize[10] the algorithm, assume the following lobe-widths :

$$\begin{cases} w_{1\ldots M-1} = \frac{200}{N+0.5} \text{ , and } w_M = \frac{150}{N+0.5} & \text{for } M > 1, \\ w_1 = \frac{150}{N+0.5} & \text{for } M = 1. \end{cases} \tag{7.3}$$

Next compute the zero positions using (7.1) or (7.2), and then the reflection coefficient numerator

$$\mathcal{N}_\rho(S) = -\prod_{i=1}^{M}\left(\frac{S^2}{\tan^2(\frac{z_i\pi}{200})} + 1\right) . \tag{7.4}$$

Note that $\mathcal{N}_\rho(S)$ will be an even polynomial in S, and of order M for any N. Using the reconstruction algorithm of Section 5.3, the next step is to find a set of conductances that will realize $\mathcal{N}_\rho$. Initially, i.e. to realize the lobe widths of (7.3), it was found that $G_i^{(1)} = 1/i$ always converged. During subsequent cycles, and for the computation of the Jacobian elements, the $\mathcal{N}_\rho$ to be realized will differ only marginally from that of the previous cycle, and therefore $\mathbf{G}$ from the previous cycle should be used to initialize (5.8).

7.2.3 Evaluating the maxima

After realizing $\mathcal{N}_\rho$, the reflection coefficient maxima in each of the lobes must be computed. It is important to point out that only the magnitudes are relevant, and not the corresponding frequency points where they occur. However, it is necessary to compute these maxima quite accurately[11], and with that in mind, an algorithm was developed to find the turning points f_i where the maxima occur, by finding the zeros of the derivative with a gradient-based method. With these f_i known, $m_i = 20\log_{10}|\rho(f = f_i)|$ can be evaluated with sufficient accuracy. Details on this procedure may be found in Appendix B.5.

With the maxima known, a termination check should be performed. In particular, the lobe maxima should all approach the specified[12] level ($\mathcal{R}_{dB}$ in dB),

$$\max\{|m_1 - \mathcal{R}_{dB}|, \ldots, |m_M - \mathcal{R}_{dB}|\} \leq 10^{-4} . \tag{7.5}$$

Assuming convergence, the synthesis is done, and the frequency bandwidth may be computed[13].

---

[10] Once the algorithm is under way, a set of intermediate lobe-widths will be known at this stage.

[11] The accuracy is needed when the partial derivatives in (7.7) are approximated by finite differences. An early experimental algorithm used a slow numerical search method, which exhibited convergence problems.

[12] The IZP algorithm becomes unstable when very high ($\mathcal{R}_{dB} \to 0$ dB, see footnote 4), or very low ($\mathcal{R}_{dB} \to -\infty$ dB, i.e. the MF-solution) levels are enforced. However, no anomalies were encountered during numerous synthesis runs for N up to 20, and for realistic $\mathcal{R}_{dB}$, i.e. $-40 \leq \mathcal{R}_{dB} \leq -10$.

[13] The bandwidth is defined by the frequency point f_c, slightly less than z_M, where $20\log_{10}|\rho| = \mathcal{R}_{dB}$. As in the MF-case, f_c is found numerically, and the bandwidth follows from (2.6).

stellenbosch University http://scholar.sun.ac.za

7.2.4 Judicious manipulation of the reflection zero positions

An unsatisfactory ripple behavior may be improved by judiciously perturbing the lobe-widths. This operation leans heavily on the fact that a reflection maximum in between two zeros is more or less proportional to its corresponding[14] lobe-width. With this in mind, the maxima are approximated by a linear function in *all* the widths, i.e.

$$\mathbf{m} \approx \bar{\mathbf{m}} + \bar{\mathbf{E}}(\mathbf{w} - \bar{\mathbf{w}}) \ . \tag{7.6}$$

Notationwise, we have $\bar{\mathbf{m}}$ due to $\bar{\mathbf{w}}$, $\mathbf{w}$ assumed to be in the vicinity of $\bar{\mathbf{w}}$, and $\bar{\mathbf{E}}$ the square[15] Jacobian matrix

$$\bar{\mathbf{E}} = [e_{ij}] \ , \text{ with } e_{ij} = \left.\frac{\partial m_i}{\partial w_j}\right|_{\bar{\mathbf{w}}} \ , i = 1, \ldots, M \text{ and } j = 1, \ldots, M \ . \tag{7.7}$$

The partial derivatives in $\bar{\mathbf{E}}$ are approximated by finite differences, in particular by perturbing[16] the lobe widths one by one, each time retracing the complete cycle (from (7.1)) up to the re-computation of $\mathbf{m}$, and finally observing the resulting changes in $\mathbf{m}$. These intermediate quantities are used only in computing $\bar{\mathbf{E}}$, and should be discarded afterwards.

Solving (7.6) for $\mathbf{w}$ by enforcing $m_{1\ldots M} = \mathcal{R}_{dB}$ results in the following width-improvement[17] matrix[18] equation :

$$\mathbf{w} = \bar{\mathbf{w}} + \beta(\Delta\mathbf{w}) \ , \text{ with } \Delta\mathbf{w} = (\bar{\mathbf{E}})^{-1}(\mathcal{R}_{dB} - \bar{\mathbf{m}}) \ , \tag{7.8}$$

and with β a damping constant $0 < \beta \leq 1$. It was sometimes found during the first few cycles of specific synthesis runs, that the algorithm behaved erratically. This behavior was corrected by restricting[19] the maximum lobe-width change to be $\frac{25}{N+2}$ f-domain units. This damping is implemented[20] by choosing β to be

$$\beta = \min\left(1, \frac{25}{(N+2)\max\{|\Delta w_1|, \ldots, |\Delta w_M|\}}\right) \ . \tag{7.9}$$

With (7.8) and (7.9) an improved set of lobe widths may be computed. These new widths should then be used in the next cycle, i.e. working from (7.1)).

---

[14]This simple assumption, namely $m_i = \bar{m}_i + \left.\frac{\partial m_i}{\partial w_i}\right|_{\bar{w}_i} (w_i - \bar{w}_i)$, was used in a preliminary algorithm, but was found to be less stable than the method in the text, and had convergence problems.

[15]Again the squareness is fortunate (see footnote 5 in Chapter 5).

[16]Width perturbations of 0.001 f-domain units was found to be sufficiently small for all reasonable $\mathcal{R}_{dB}$, and N up to at least 20. Note from (7.1) and (7.2), that a width-perturbation δw_j causes a shift in all the remaining zero positions, namely z_i, $i = j \ldots M$, with small corresponding shifts in the f-domain positions of the maxima.

[17]Note that (7.8) is not a recursive operation.

[18] Note that $\mathcal{R}_{dB} - \bar{\mathbf{m}}$ implies that each element of the vector $\bar{\mathbf{m}}$ should be subtracted from the scalar $\mathcal{R}_{dB}$, thereby again resulting in a vector.

[19]The errors in the linear approximation of (7.6) are sometimes too big, and induce unstable changes in $\mathbf{w}$. These big lobe-width changes result in big changes in the coefficients of $\mathcal{N}_\rho(S)$, which in turn cause the conductance reconstruction algorithm to become erratic.

[20]Note that final convergence is not affected, as by then we have $\beta = 1$.

stellenbosch University http://scholar.sun.ac.za

7.3 Symbolically worked example

The first few iterations in the $N = 3$, $\epsilon_r = 1$ and $\mathcal{R}_{dB} = -15$ dB IZP synthesis is shown in Table 7.1, and clearly illustrate the algorithm. Note in particular that $M = 1$, and that (5.8) may be implemented in closed form through the use of (6.3). The absorption behavior is shown in Figure 8.1.

Cycle	Equation	Results
0	(7.3)	$w_1 = 42\frac{6}{7}$
1	(7.2)	$z_1 = 57\frac{1}{7}$
	(7.4)	$\mathcal{N}_\rho(S) = -0.6360S^2 - 1$, i.e. $\hat{\mathbf{a}} = [0, -0.6360, 0]^T$
	(5.8), $i = 1$	$G_1 = 1.0000$, $G_2 = 0.50000$, $G_3 = 0.33333$
	(5.8), $i = 2$	$G_1 = 1.4181$, $G_2 = 0.54181$, $G_3 = 0.16610$
	(5.8), $i = 3$	$G_1 = 1.3896$, $G_2 = 0.51837$, $G_3 = 0.19121$
	(5.8), $i = 4$	$G_1 = 1.3897$, $G_2 = 0.51759$, $G_3 = 0.19170$
	(5.9)	Convergence reached.
	Appendix B.5	$m_1 = -26.623$ dB
	(7.7)	$e_{1,1} = 0.792$
	(7.8)	$\Delta w_1 = 14.68$
	(7.9)	$\beta = 0.341$
	(7.8)	We have $\bar{w}_1 = 42\frac{6}{7}$, therefore $w_1 = 47\frac{6}{7}$.
2	(7.2)	$z_1 = 52\frac{1}{7}$
	(7.4)	$\mathcal{N}_\rho(S) = -0.8739S^2 - 1$, i.e. $\hat{\mathbf{a}} = [0, -0.8739, 0]^T$
	(5.8), $i = 1$	$G_1 = 1.3897$, $G_2 = 0.51759$, $G_3 = 0.19170$
	(5.8), $i = 2$	$G_1 = 1.2898$, $G_2 = 0.51733$, $G_3 = 0.22528$
	(5.8), $i = 3$	$G_1 = 1.2878$, $G_2 = 0.51626$, $G_3 = 0.22650$
	(5.9)	Convergence reached.
	Appendix B.5	$m_1 = -22.719$ dB
	(7.7)	$e_{1,1} = 0.775$
	(7.8)	$\Delta w_1 = 9.963$
	(7.9)	$\beta = 0.502$
	(7.8)	We have $\bar{w}_1 = 47\frac{6}{7}$, therefore $w_1 = 52\frac{6}{7}$.
3	(7.2)	$z_1 = 47\frac{1}{7}$
	(7.4)	$\mathcal{N}_\rho(S) = -1.1969S^2 - 1$, i.e. $\hat{\mathbf{a}} = [0, -1.1969, 0]^T$
	(5.8), $i = 1$	$G_1 = 1.2878$, $G_2 = 0.51626$, $G_3 = 0.22650$
	(5.8), $i = 2$	$G_1 = 1.1468$, $G_2 = 0.51335$, $G_3 = 0.27556$
	(5.8), $i = 3$	$G_1 = 1.1430$, $G_2 = 0.51099$, $G_3 = 0.27840$
	(5.9)	Convergence reached.
	Appendix B.5	$m_1 = -18.819$ dB
	(7.7)	$e_{1,1} = 0.792$
	(7.8)	$\Delta w_1 = 4.820$
	(7.9)	$\beta = 1$
	(7.8)	We have $\bar{w}_1 = 52\frac{6}{7}$, therefore $w_1 = 57.677$.
Cycle 4 : $m_1 = -14.851$ dB.		
Cycle 5 : $m_1 = -14.999$ dB.		
Cycle 6 $\Rightarrow$ Final solution : $G_1 = 0.94645$, $G_2 = 0.49410$, $G_3 = 0.35512$.		

Table 7.1: Intermediate results of the symbolically worked IZP-response example of Section 7.3.

stellenbosch University http://scholar.sun.ac.za

7.4 Solution existence and uniqueness

Numerous applications of the IZP-algorithm, for N up to 20, $0 < Z_c \leq 1$ and $-40 \leq \mathcal{R}_{dB} \leq -10$, converged smoothly. Upon equiripple convergence according to (7.5), the $\mathcal{N}_\rho$ for the specific synthesis is known, and may be classified as follows :

Conjecture 3 : *The resultant $\mathcal{N}_\rho$, assuming equiripple convergence according to (7.5), will either*

(a) be of Class 1 when $Z_c \geq Z_{c,min}(N, \mathcal{R}_{dB})$, or
(b) be of Class 0 when $Z_c < Z_{c,min}(N, \mathcal{R}_{dB})$.

Approximate values for the first few $Z_{c,min}$ are given in Table 7.2.

Motivation and notes :

1. $Z_{c,min}(2, \mathcal{R}_{dB}) = \sqrt{\frac{1-10^{\mathcal{R}_{dB}/20}}{2\left(1+10^{\mathcal{R}_{dB}/20}\right)}}$ *follows from (4.15), Section 4.2.2.*

2. $Z_{c,min}(3 \ldots 8, \mathcal{R}_{dB})$ *have been found numerically by repetitively synthesizing solutions with decreasing Z_c, and noting when the solution changes Class. It was found without exception that G_N is the first to turn negative when Z_c is marginally smaller than $Z_{c,min}$, and that $G_N = 0$ when $Z_c = Z_{c,min}$. With Z_c decreasing substantially below $Z_{c,min}$, the conductance reconstruction algorithm starts behaving erratically, and with Z_c approaching 0, fails.*

3. *With reference to Conjecture 2, it is seen that the restriction on $Z_{c,min}$ is less stringent than in the MF-case.*

4. *With $Z_c = 1$ it is conjectured that IZP solutions will exist for any $\mathcal{R}_{dB}$, and for $N \to \infty$.*

N	$\mathcal{R}_{dB} = -20$ dB		$\mathcal{R}_{dB} = -30$ dB		$\mathcal{R}_{dB} = -40$ dB	
	$Z_{c,min}$	$\epsilon_{r,max}$	$Z_{c,min}$	$\epsilon_{r,max}$	$Z_{c,min}$	$\epsilon_{r,max}$
2	0.6396	2.444	0.6851	2.131	0.7001	2.040
3	0.7669	1.700	0.8368	1.428	0.8667	1.331
4	0.8137	1.510	0.8890	1.265	0.9225	1.175
5	0.8372	1.427	0.9132	1.199	0.9465	1.116
6	0.8512	1.380	0.9266	1.165	0.9589	1.088
7	0.8604	1.351	0.9349	1.144	0.9619	1.081
8	0.8669	1.331	0.9406	1.130	0.9708	1.061

Table 7.2: Minimum values for Z_c, and the corresponding maximum values for ϵ_r, which guarantee the IZP-solution to be realizable.

stellenbosch University http://scholar.sun.ac.za

7.5 Representative numerical results

7.5.1 Small N solutions

Similar to the two-layer trend, it may be seen from Conjecture 3 that the multilayer realizability restriction on ϵ_r is less severe than in the MF-case. With practical low loss foam spacers in mind, IZP solutions are tabulated in Appendix E, for N up to 8 and for various absorption levels.

7.5.2 A twenty-layer IZP-response solution, with $\epsilon_r = 1$.

The $N = 20$, $\epsilon_r = 1$, $\mathcal{R}_{dB} = -20$ dB IZP example clearly illustrates the stability and convergence properties of the IZP-algorithm. In addition, it also unveils an interesting trend in the resistance values. Apart from the much reduced spread (compared to a $N = 20$ MF-solution), it can be seen that the resistances of Table 7.3 increase monotonically to R_{N-1}, with $R_N < R_{N-1}$. This was found whenever too high ripple levels were synthesized, and is a very striking resemblance to the so-called edge-brightening effect in Dolph-Chebyshev linear array pattern synthesis [42].

The corresponding absorption properties is shown in Figure 7.2, and the -20 dB frequency bandwidth was found to be 187.76 %.

R_1	R_6	R_{11}	R_{16}	3.14010	5.15652	10.3179	19.5658
R_2	R_7	R_{12}	R_{17}	3.02978	5.98950	11.7224	22.3751
R_3	R_8	R_{13}	R_{18}	3.29175	6.91294	13.3057	25.7109
R_4	R_9	R_{14}	R_{19}	3.78087	7.93320	15.1055	29.7339
R_5	R_{10}	R_{15}	R_{20}	4.41544	9.06242	17.1709	8.30423

Table 7.3: Normalized resistance values for the $N = 20$, $\epsilon_r = 1$, $\mathcal{R}_{dB} = -20$ dB IZP-response numerical example.

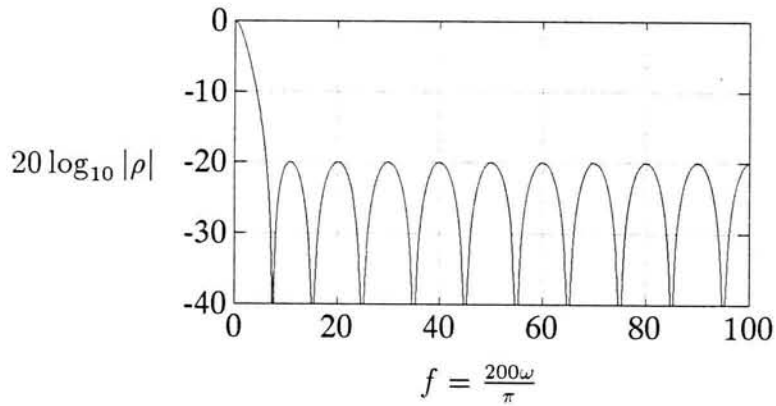

Figure 7.2: Reflection coefficient magnitude versus frequency, for the $N = 20$, $\epsilon_r = 1$, $\mathcal{R}_{dB} = -20$ dB IZP-response numerical example.

stellenbosch University http://scholar.sun.ac.za

7.5.3 High and low maxima intermingled

As an interesting example, a special IZP-response was synthesized with high and low maxima intermingled. Such a response may be obtained by enforcing each maximum in (7.8) to a different level, and the resistance values and absorption properties are tabulated in Table 7.4 and shown in Figure 7.3, respectively.

The reader should note that certain of the combinations of high and low maxima that were investigated, resulted in a final $\mathcal{N}_\rho$ of Class 0, even with $Z_c = 1$. The phenomenon was unexpected, since it was never encountered during the numerous *equiripple* synthesis runs, and it is merely noted here.

R_1	R_6	R_{11}	R_{16}	1.54590	5.39707	9.99184	16.3134
R_2	R_7	R_{12}	R_{17}	2.78692	5.06077	10.7872	33.7878
R_3	R_8	R_{13}	R_{18}	1.89001	5.72967	14.7568	113.862
R_4	R_9	R_{14}	R_{19}	2.23105	7.66598	21.5162	34.7866
R_5	R_{10}	R_{15}	R_{20}	3.95921	9.44380	17.7902	18.3138

Table 7.4: Normalized resistance values for the $N = 20$, IZP-response solution, with $\epsilon_r = 1$, and with high and low maxima intermingled.

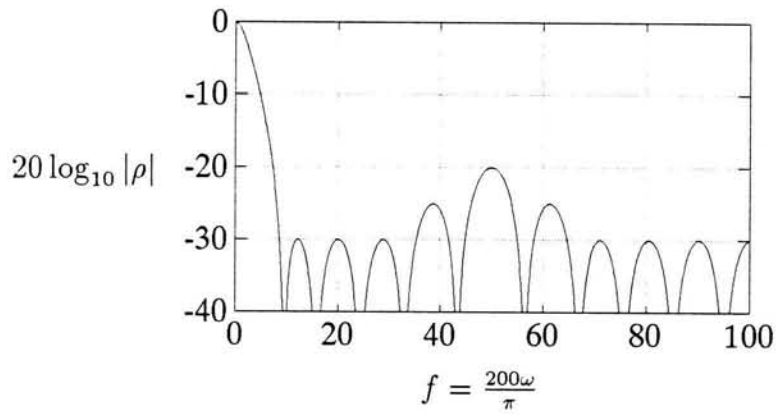

Figure 7.3: Reflection coefficient magnitude versus frequency, for the $N = 20$, IZP-response numerical example, with $\epsilon_r = 1$, and with high and low maxima intermingled.

7.5.4 Application to the Wilkinson power divider problem

In 1960 Wilkinson presented an $N-$output-port hybrid power divider [33]. The structure is probably best known in two output port format, and with two or more output sections to enhance bandwidth. A more recent treatment by Cohn [34] resulted in a design method where the structure is bisected into odd- and even-excitation subcircuits. The even mode problem is simply a multistage impedance transformer, and results in known output section line impedances.

stellenbosch University http://scholar.sun.ac.za

With these impedances known, the odd mode problem reduces to the Jauman topology, and Cohn was able to provide almost optimal two- and three-section design equations, and a general design method for $N > 3$. However, with a slight modification[21] the IZP algorithm is applicable, and results in noticeable bandwidth improvements over Cohn's method.

As a particular example, Cohn's 7 section design will be investigated and improved upon. Normalized characteristic impedances and resistance values from his Table I are repeated[22] in Table 7.5, and the odd-mode reflection properties is shown in Figure 7.4. It is seen that the maximum reflection coefficient ripple is ≈ -23.23 dB, and that not all the reflection zeros are exploited. The IZP-algorithm was invoked, and the improved resistance values and absorption properties are also tabulated and shown, with the bandwidth improvement[23] readily visible in Figure 7.4.

$\Rightarrow i$	1	2	3	4	5	6	7
$Z_{c,i}$	1.7740	1.6597	1.5364	1.4142	1.3017	1.2051	1.1274
R_i^{Cohn}	2.4826	1.2962	2.1758	3.1990	4.4623	6.1615	4.4248
R_i^{IZP}	1.8599	2.5253	3.4225	4.3919	5.5380	7.1026	4.6393

Table 7.5: Normalized resistance and impedance values, for Cohn's 7−section power divider example, and the improved IZP-response solution.

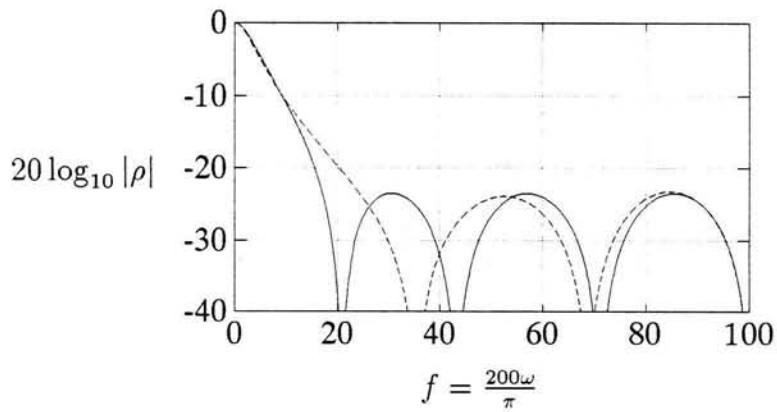

Figure 7.4: Reflection coefficient magnitude versus frequency, for the odd-mode subcircuit of Cohn's 7−section power divider example (dotted), and the improved IZP-response solution (solid).

[21]This dissertation only considers identical spacer impedances. However, the pertinent equations do not change in any fundamental way when the restriction is dropped, although for the sake of conciseness these equations will not be rederived here.

[22]Note that his numbering scheme is from the front towards the PEC, and that the power divider resistance values should first be halved, as part of the bisection approach.

[23]It should be noted that this improvement is in the odd-mode excitation subcircuit only, and that the subsequent improvements in the power-divider output port properties should still be computed.

stellenbosch University http://scholar.sun.ac.za

Chapter 8

MULTILAYERED OPTIMAL (OPT) SOLUTION

8.1 Introduction

Experience gained during the development of the IZP synthesis algorithms indicated that such solutions are very close to local optimality. In particular, numerical minimization packages[1] found small improvements in either the ripple level or the frequency bandwidth (or both). Although these potential improvements are negligible for practical purposes, the phenomenon was quite unexpected, and is important from an academic point of view.

This Chapter introduces an iterative algorithm[2] which will assume a successful multilayered IZP synthesis, and then simultaneously reduce the reflection maxima (over the IZP-solution's bandwidth) as much as possible.

Probably the most interesting property of these optimized responses is the fact that when Chebyshev optimality is applied to the Jauman topology, the reflection coefficient zeros migrate slightly off the $j\Omega$-axis. This phenomenon is not usually encountered in lossless filter synthesis, where Chebyshev optimality usually imply reflection zeros at physical frequencies.

8.2 Iterative synthesis algorithm

The algorithm will operate directly on the conductances, and its objectives will be the simultaneous reduction (and ultimate vanishing) of M errors[3] indicating deviation from equal maxima, and N errors indicative of the deviation from an optimal situation. Together, vanishing of these errors corresponds to a locally optimal equiripple situation, which will be heuristically conjectured to be global. The reader should by now be accustomed to most of the numerical techniques that will be used, and the algorithm will be presented in a concise format.

[1] E.g. a circuit analysis package containing an optimizer.
[2] The algorithm is briefly described in [39].
[3] As in the IZP algorithm, $M = \left[\frac{N}{2}\right]$.

stellenbosch University http://scholar.sun.ac.za

8.2.1 Maxima of interest

The reflection coefficient magnitude behavior (e.g. the maxima positions and general structure of the rippled response) does not change much when an IZP solution is optimized, and the same numbering scheme described in Section 7.2.1 will be employed for the maxima, $m_{1\ldots M}$. Again only the respective values (in dB) are of interest, and not the frequency points where they occur.

To complete the specification, one additional point is of interest, namely the value of $20\log_{10}|\rho|$ at f_c. This value will be denoted by m_{M+1}, with f_c the frequency point which defines the bandwidth of the parent IZP solution. Except for the fact that $|\rho|$ will always be evaluated at f_c, m_{M+1} will be treated in exactly the same way as the other maxima.

8.2.2 Equiripple errors

With the conductances known, the maxima may be computed exactly as in the IZP algorithm (see Section 7.2.3). With these maxima known, the M errors of the first kind are defined as[4]

$$[\mathcal{E}_1,\ldots,\mathcal{E}_M]^T = m_{M+1} - [m_1,\ldots,m_M]^T \ . \tag{8.1}$$

With the optimization starting with an equiripple IZP solution, it follows that these errors will start off being zero. In the first stages of the optimization, however, the maxima will start to differ slightly, finally shrinking back to zero upon convergence.

8.2.3 Optimality errors

Optimality in the present context simply implies that the maxima under investigation must be at a state where they cannot all reduce simultaneously. To formalize this criterion, set up the following matrix equation :

$$\mathbf{Q}\boldsymbol{\lambda} = [A_1\ ,\ A_2\ ,\ \ldots\ ,\ A_{M+1}]^T\ ,\ \text{with} \tag{8.2}$$

$$\mathbf{Q} = [q_{ij}]\ ,\ \text{where}\ q_{ij} = \frac{\partial m_i}{\partial G_j}\ ,\ i = 1\ldots M+1\ ,\ j = 1\ldots N\ , \tag{8.3}$$

with the A_i arbitrary non-zero real numbers with the same sign, and with $\boldsymbol{\lambda} = [\lambda_1\ldots\lambda_N]^T$ to be solved for[5]. Optimality will have been reached when (8.2) has no solution [51], [52], explaining the *no-solution* terminology often associated with this approach.

No solution of (8.2) will have been reached when the $M+1$ rows of $\mathbf{Q}$ exhibit linear dependence, i.e. when $\alpha_{1\ldots M+1}$ (not all zero) exist such that

$$\sum_{i=1}^{M+1} \alpha_i\, q_{ij} = 0\ ,\ \text{for}\ j = 1\ldots N\ , \tag{8.4}$$

[4] See footnote 18, Chapter 7.

[5] The q_{ij} may be approximated by finite differences. In particular, conductance perturbations of $10^{-5}\mho$ were found to be sufficiently small.

stellenbosch University http://scholar.sun.ac.za

and with the signs of all the nonzero α_i the same[6] [53, p. 91].

Since (8.4) will by necessity not be possible during optimization, N optimality errors may now be extracted from it, indicative of the "deviation from linear dependence". Without loss of generality, define $\alpha_{M+1} = -1$, and restate (8.4) as follows :

$$q_{M+1,j} = \sum_{i=1}^{M} \alpha_i \, q_{ij} \ , \text{ for } j = 1 \ldots N \ . \tag{8.5}$$

Notationwise, it will be convenient to segregate $\mathbf{Q}$ into

$$\mathbf{R} = [r_{ij}] \ , \text{ with } r_{ij} = q_{ji} \ , \ i = 1 \ldots N \ , \ j = 1 \ldots M \ , \text{ and}$$

$$\mathbf{t} = [q_{M+1,1} \ , \ q_{M+1,2} \ , \ \cdots \ , \ q_{M+1,N}]^T \ , \tag{8.6}$$

thereby (with $\boldsymbol{\alpha} = [\alpha_1 \ldots \alpha_M]^T$) transforming (8.5) into

$$\mathbf{R}\boldsymbol{\alpha} = \mathbf{t} \ . \tag{8.7}$$

It follows that (8.7) is overdetermined (N equations in M unknowns), and inconsistent in general. One way to find the "best" solution is to solve it in a minimum RMS sense [56, pp. 321 – 322], [53, p. 143],

$$\boldsymbol{\alpha} = (\mathbf{R}^T\mathbf{R})^{-1}\mathbf{R}^T\mathbf{t} \ . \tag{8.8}$$

This solution for $\boldsymbol{\alpha}$ may now be used in (8.7) to obtain N criteria (errors) representing the "deviation from linear dependence" in $\mathbf{Q}$. In particular,

$$[\mathcal{E}_{M+1} \ldots \mathcal{E}_{M+N}]^T = \mathbf{t} - \mathbf{R}\boldsymbol{\alpha} \ . \tag{8.9}$$

8.2.4 Reducing the errors

In order to find the conductances that will yield $\boldsymbol{\mathcal{E}} = 0$, approximate the functional dependence of $\boldsymbol{\mathcal{E}}$ on $\mathbf{G}$ as being linear[7], thereby setting up $M + N$ equations in the N unknown conductance improvements.

Once again this system of equations is overdetermined and inconsistent, and may be solved for in a minimum RMS sense (similar to (8.7) and (8.8)). With the improved conductances, the algorithm may be executed again, and the cycle repeats until the errors are acceptably small, i.e.

$$\max \{|\mathcal{E}_1|, |\mathcal{E}_2|, \ldots, |\mathcal{E}_{M+N}|\} \leq 10^{-6} \ . \tag{8.10}$$

[6]The requirement on the signs of α_i was not mentioned in the initial version of this algorithm, and the need for a clarification was pointed out by Professor I. Navot, during examination. Although this sign requirement will not be enforced, it was satisfied by all the numerous examples worked out. In addition, it is evident in Example 2 of Section 4.3.3, as well as in the worked example of Section 8.3.1.

[7]The partial derivatives should again be approximated by finite differences. Care must be taken with the nested derivatives of (8.3), however. In particular, conductance perturbations of $10^{-4}\mho$ were found to be acceptable.

stellenbosch University http://scholar.sun.ac.za

8.3 Numerical results

8.3.1 Worked example

The OPT-algorithm was applied to the IZP parent solution of Section 7.3, i.e. $N = 3$, $Z_c = 1$, $\mathcal{R}_{dB} = -15$ dB, $f_c = 31.4519$, and $\mathbf{G} = \begin{bmatrix} 0.946448 & 0.494095 & 0.355120 \end{bmatrix}^T$, and intermediate results of the first three iterations in the optimization are shown in Table 8.1. The final solution was $\mathbf{G} = \begin{bmatrix} 1.19577 & 0.490892 & 0.443512 \end{bmatrix}^T$, with a 0.528 dB reduction in the maximum ripple level. The optimized and parent IZP absorption properties are shown in Figure 8.1.

Iteration	Equation	Results
1	(8.1)	$\mathcal{E}_1 = 0$
	(8.3)	$\mathbf{Q} = \begin{bmatrix} -9.7046 & -6.7886 & 15.2929 \\ 1.9935 & -1.8947 & -18.2545 \end{bmatrix}$
	(8.9)	$\mathcal{E}_2 = -5.4158$, $\mathcal{E}_3 = -7.0777$, $\mathcal{E}_4 = -6.5785$
	See Section 8.2.4	$\mathbf{G} = \begin{bmatrix} 1.12254 & 0.508687 & 0.433493 \end{bmatrix}^T$
2	(8.1)	$\mathcal{E}_1 = -0.2985$
	(8.3)	$\mathbf{Q} = \begin{bmatrix} -7.2461 & -6.4480 & 16.8322 \\ 3.5083 & 3.7961 & -10.3095 \end{bmatrix}$
	(8.9)	$\mathcal{E}_2 = -0.7815$, $\mathcal{E}_3 = -0.0212$, $\mathcal{E}_4 = -0.3446$
	See Section 8.2.4	$\mathbf{G} = \begin{bmatrix} 1.19434 & 0.489375 & 0.443681 \end{bmatrix}^T$
3	(8.1)	$\mathcal{E}_1 = -0.0358$
	(8.3)	$\mathbf{Q} = \begin{bmatrix} -6.4652 & -7.2319 & 17.6069 \\ 3.5384 & 3.9051 & -9.7378 \end{bmatrix}$
	(8.9)	$\mathcal{E}_2 = -0.0224$, $\mathcal{E}_3 = -0.0780$, $\mathcal{E}_4 = -0.0403$
	See Section 8.2.4	$\mathbf{G} = \begin{bmatrix} 1.19576 & 0.490890 & 0.443508 \end{bmatrix}^T$

Table 8.1: Intermediate results of the worked example of Section 8.3.1.

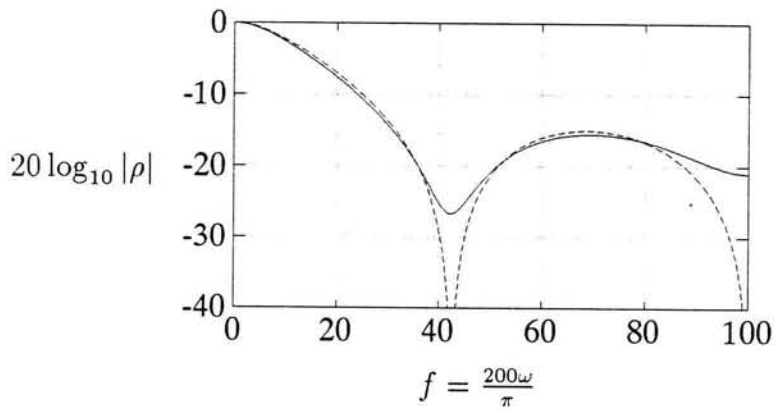

Figure 8.1: Reflection coefficient magnitude versus frequency, for the $N = 3$, $\epsilon_r = 1$, multilayered OPT-response worked example (solid), and the parent IZP solution (dotted).

stellenbosch University http://scholar.sun.ac.za

8.3.2 Representative case

To illustrate the optimal algorithm, the IZP example of Section 7.5.2 was used as parent, and optimization resulted in the normalized resistances of Table 8.2. The corresponding absorption behavior is illustrated in Figure 8.2, and a ripple level reduction of 0.766 dB was achieved over the parent IZP bandwidth of 187.76 %. Tabulated solutions for practical scenarios may be found in Appendix E.

R_1	R_6	R_{11}	R_{16}	0.9059363	4.770628	9.839279	19.27123
R_2	R_7	R_{12}	R_{17}	1.763838	5.619094	11.19513	22.94296
R_3	R_8	R_{13}	R_{18}	2.504997	6.535536	12.73308	29.43759
R_4	R_9	R_{14}	R_{19}	3.229556	7.533020	14.51053	55.29024
R_5	R_{10}	R_{15}	R_{20}	3.978383	8.627533	16.62491	5.249849

Table 8.2: Normalized resistance values for the $N = 20$ OPT-response solution, with $\epsilon_r = 1$.

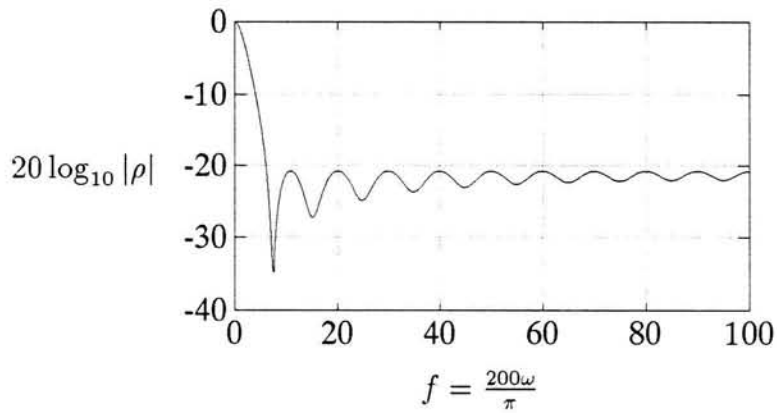

Figure 8.2: Reflection coefficient magnitude versus frequency, for the $N = 20$ ($\epsilon_r = 1$) multilayered OPT-response numerical example.

8.4 Solution Characteristics

- Convergence was found to be stable without exception.
- Although the optimal zero-positions are close to the parent IZP zeros, it was found that they have migrated slightly into the lefth half S-plane.
- The trend in the optimal conductances closely resembles the parent IZP trend, but the conductance values are slightly bigger in general.
- The spacer ϵ_r restriction appears to be slightly less severe than in the IZP case (see Appendix E).
- The behavior of the reflection minima is a subtle reminder of the wealth of undiscovered mathematical intricasies still hidden in this simple topology.

stellenbosch University http://scholar.sun.ac.za

Chapter 9

CONCLUSIONS

9.1 General

This dissertation addressed the design problem associated with electric screen Jauman absorbers. Although the absorber topology is uncomplicated, and example solutions abound in the literature, no rigorous design techniques for multilayered absorbers could be found.

To make available the wealth of existing network analysis and synthesis techniques, the absorber parts and electromagnetic environment were idealized, resulting in a simple equivalent network. Analysis of this structure proved to be almost trivial, and concise equations and algorithms were developed to facilitate this symbolically or numerically. Unfortunately, the formal network synthesis problem proved to be extremely challenging, and remains unsolved. The obstacle was, and remains, the unknown topology-driven realizability constraints[1] on the input port network functions, e.g. the driving-point impedance, and/or reflection coefficient.

Consequently, the research concentrated on tractable and iterative design techniques. The first step was the development of a method to realize reflection zeros at given physical frequencies[2]. This involved solving a set of N highly non-linear equations in the N unknown sheet resistivities, and was achieved with a gradient method algorithm. The algorithm proved to be stable, with excellent convergence properties, and provided a powerful synthesis tool.

Realizing all the reflection zeros at the center frequency will result in a maximally flat absorption behavior, and such solutions have been published for two- and three-layer absorbers. An algorithm was presented which synthesizes such multilayered absorbers for up to at least 20 layers, thereby extending and complementing the available procedures and solutions. It was found that the surface resistivities are spread out over an extreme range, that a severe realizability restriction exists on the spacer ϵ_r, and that these solutions exhibit narrow bandwidths. It is therefore not advisable to implement maximally flat response Jauman absorbers.

[1] This specific problem has been partially addressed by Richards [46].

[2] In fact, this procedure suggested the two zero-placement synthesis algorithms that followed.

stellenbosch University http://scholar.sun.ac.za

Realizing all the reflection zeros at distinct and judiciously chosen frequencies, resulted in rippled absorption behaviors. The number of ripples could be maximized, with the reflection maxima at a chosen level, and it was found that these solutions exhibited wider bandwidths than any comparable examples found in the literature. Numerous practical cases were synthesized, and lookup tables are presented.

An investigation revealed that such rippled responses are very close to being optimal in the Chebyshev sense. Another algorithm was developed, which decreases the reflection maxima as much as possible, without compromising bandwidth. The improvements were found to be extremely small, but to the author's knowledge these solutions solve the optimal Jauman design problem for the first time. In addition, the algorithm is felt to be a novel application of fundamental Chebyshev optimization, and would be applicable to certain general optimization problems with only minor modifications.

Although the synthesis algorithms were designed to operate with low ϵ_r spacers, it was nevertheless surprising to discover that they started to behave erratically with increasing ϵ_r. The phenomenon was investigated, and it is conjectured[3] that these solutions only exist for ϵ_r smaller than an upper bound, which depends on the response characteristics, ripple level and number of layers. These limits are given, and should be adhered to during practical absorber design.

9.2 Unsolved problems

- The synthesis algorithms presented here are not applicable to absorbers with high dielectric constant spacers. However, no reference to such practice could be found[4] in the literature, and this unsolved design problem is relevant only for the sake of academic completeness.

- The seemingly innocuous problem of finding necessary and sufficient conditions for an input impedance to be realizable with the Jauman topology, remains unsolved. Such conditions will be a fundamental and important contribution to network theory.

- Once these evasive realizability conditions are known, the iterative solutions developed in this dissertation should be derived using formal network theoretical techniques[5]. Such an approach might explain many of the intricacies which were noted, and which are not fully understood at the moment, and would be extremely rewarding from an academic viewpoint.

---

[3] Although the non-linear equations are solved in a stable and consistent manner for low ϵ_r, the associated (and inevitable) loss of insight prohibited a more formal investigation.

[4] A heuristic argument might be that the drastic impedance transformation properties of such spacers will cause severe impedance mismatches in the cascaded Jauman topology, thereby causing large reflections, which will be hard to control. This might be the reason why the use of such spacers is avoided in practice.

[5] Specifically, the class of rational reflection coefficient functions associated with the optimal solutions should be investigated.

APPENDICES

stellenbosch University http://scholar.sun.ac.za

Appendix A

Algebraic analysis and synthesis of the Salisbury screen

The theory developed in Chapter 3 readily leads to the following representative equations for the $N = 1$ case :

$$Z_{in}(S) = \frac{SZ_c}{SZ_cG_1 + 1} \ , \ \rho(S) = \frac{SZ_c(1 - G_1) - 1}{SZ_c(1 + G_1) + 1} \ , \text{ and} \tag{A.1}$$

$$|\rho(j\Omega)|^2 = \rho(S)\rho(S)|_{S=j\Omega} = \frac{\Omega^2 Z_c^2(1 - G_1)^2 + 1}{\Omega^2 Z_c^2(1 + G_1)^2 + 1} \ . \tag{A.2}$$

These equations are simple to manipulate[1], and the following design problem[2] will now be solved :

> *With $0 < Z_c \leq 1$, and the maximum acceptable reflection coefficient magnitude $|\rho|_{max} = -\mathcal{R}$, assumed known, what G_1 will maximize the bandwidth (i.e. minimize Ω_c where $|\rho| \leq -\mathcal{R}$ for $\Omega \geq \Omega_c$)?*

With G_1 and Z_c finite and positive, differentiation of (A.2) shows that $|\rho(j\Omega)|^2$ always decreases monotonically from 1 at $\Omega = 0$, to $(1 - G_1)^2/(1 + G_1)^2$ at $\Omega \to \infty$. Enforcing $|\rho(\Omega \to \infty)|^2 \leq \mathcal{R}^2$ results in bounds on G_1, namely $x \leq G_1 \leq \frac{1}{x}$ with $x = (1 + \mathcal{R})/(1 - \mathcal{R})$. Assuming for the moment that this inequality holds, we have from (A.2) that

$$\Omega_c^2 = \frac{1 - \mathcal{R}^2}{Z_c^2\{(1 + G_1)^2\mathcal{R}^2 - (1 - G_1)^2\}} \ , \tag{A.3}$$

with $|\rho| = -\mathcal{R}$ at $\Omega = \Omega_c$. In order to find $\Omega_{c\,(min)}^2$, i.e. maximum bandwidth, differentiate (A.3) and equate to zero. This results in

$$G_{1,optimum} = \frac{1 + \mathcal{R}^2}{1 - \mathcal{R}^2} \ , \tag{A.4}$$

[1]For instance, the maximally flat response, defined as $|\rho|_{\Omega-\infty}^2 = 0$, is obtained when $G_1 = 1$, irrespective of Z_c.

[2]To be compatible with the two-layer development of Chapter 4, $\mathcal{R}$ is defined as $-1 \leq \mathcal{R} \leq 0$.

stellenbosch University http://scholar.sun.ac.za

which always satisfies the inequality $x \leq G_1 \leq \frac{1}{x}$ stated above. To find the frequency bandwidth, use $G_{1,optimum}$ in (A.3), to obtain

$$\mathcal{B} = 200\,\frac{\pi - 2\arctan(\Omega_c)}{\pi}\ \%, \text{ with } \Omega_c = \frac{\mathcal{R}^2 - 1}{2Z_c\mathcal{R}}\ . \tag{A.5}$$

It is interesting to note the following properties exhibited by the optimal bandwidth solution :

- $G_{1,optimum}$ does not depend on Z_c, and is always > 1.
- $\mathcal{B}$ increases[3] with increasing Z_c.
- With $G_{1,optimum}$ it follows that $|\rho(j\Omega \rightarrow \infty)| = |\rho(j\Omega_c)|^2 = \mathcal{R}^2$.

Example: Design a Salisbury screen with optimal bandwidth absorption at the -15 dB level. Use a spacer with $\epsilon_r = 1.1$, i.e. $Z_c = 0.95346$.
$\otimes$ We have $\mathcal{R} = -0.1778$, and from (A.4) the optimal conductance value follows as $G_{1,optimum} = 1.0653$, implying a resistive sheet with surface resistivity of 353.61 Ω/square (see (2.4)). The resulting -15 dB bandwidth is obtained from (A.5) as $\mathcal{B} = 42.89\%$, which improves marginally on the maximally flat ($G_1 = 1$) bandwidth of $\mathcal{B} = 42.25\%$. The absorption behavior is illustrated in Figure A.1.

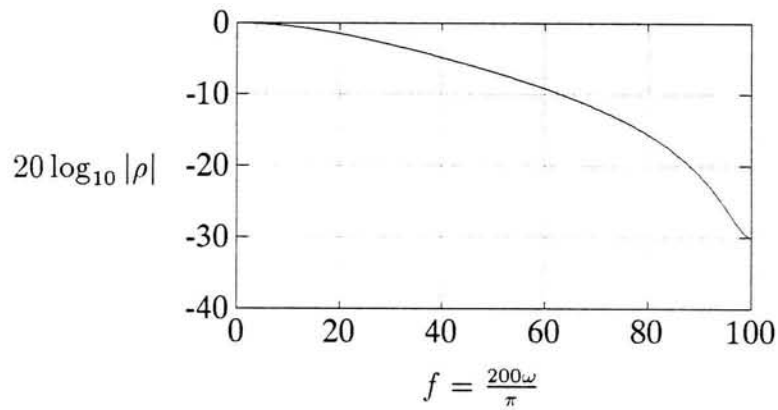

Figure A.1: Reflection coefficient magnitude versus frequency, for a Salisbury screen optimally designed for -15 dB absorption, and with $\epsilon_r = 1.1$.

[3]This is mentioned in the literature on Salisbury screens.

stellenbosch University http://scholar.sun.ac.za

Appendix B

Analysis-related recursive algorithms

B.1 Expressing Z_{in} and ρ in terms of the polynomial set $P_{0\ldots N+1}(S)$

The simple cascaded transmission matrix method of Chapter 3 is sufficient to compute $Z_{in}(S)$ and $\rho(S)$ of multilayered structures. However, with numerical implementation in mind, it will be convenient to express the pertinent properties in terms of a recursive sequence of polynomials[1].

The intermediate matrix $\mathbf{F}_i$, obtained after assembling the first i sections, may be written as[2]

$$\mathbf{F}_i = \begin{bmatrix} A_i & B_i \\ C_i & D_i \end{bmatrix} = \prod_{j=0}^{i-1} \mathbf{T}_{i-j} = \mathbf{T}_i \prod_{j=0}^{i-2} \mathbf{T}_{i-j-1} =$$

$$\mathbf{T}_i \mathbf{F}_{i-1} = \begin{bmatrix} 1 & Z_c S \\ \frac{S}{Z_c} + G_i & Z_c G_i S + 1 \end{bmatrix} \begin{bmatrix} A_{i-1} & B_{i-1} \\ C_{i-1} & D_{i-1} \end{bmatrix} ,$$

$$\text{with } i = 2 \ldots N \text{ , and } \mathbf{F}_1 = \mathbf{T}_1 \text{ .} \tag{B.1}$$

From this it is straightforward to extract the B_i and D_i polynomial buildup in the form of two coupled first order recursion equations :

$$B_i = B_{i-1} + Z_c S D_{i-1} \text{ ,} \tag{B.2}$$

$$D_i = (\frac{S}{Z_c} + G_i) B_{i-1} + (Z_c G_i S + 1) D_{i-1} \text{ ,} \tag{B.3}$$

$$\text{with } i = 2 \ldots N \text{ , } B_1 = Z_c S \text{ , and } D_1 = Z_c G_1 S + 1 \text{ .}$$

[1] Throughout the development N, Z_c and $G_{1\ldots N}$ will be assumed known.

[2] The common radical, $\sqrt{1 - S^2}$, will be assumed absent.

stellenbosch University http://scholar.sun.ac.za

The next step is to decouple these equations, i.e. to obtain independent recursion equations for B_i and D_i. This may be accomplished by substituting $i+1$ for i in (B.2),

$$B_{i+1} = B_i + Z_c S D_i \ , \tag{B.4}$$

substituting D_i from (B.3),

$$B_{i+1} = B_i + (S^2 + G_i Z_c S) B_{i-1} + Z_c S (Z_c G_i S + 1) D_{i-1} \ , \tag{B.5}$$

and finally substituting D_{i-1} from (B.2) to yield the second order recursion equation

$$B_{i+1} = (Z_c G_i S + 2) B_i + (S^2 - 1) B_{i-1} \ ,$$

$$\text{with } i = 1 \ldots N-1 \ , \ B_0 = 0 \ , \text{ and } B_1 = Z_c S \ . \tag{B.6}$$

The same technique may be used to obtain a recursion equation for D_i, with the resulting equation slightly more complicated than (B.6).

However, it will be more convenient to have both B and D expressed in terms of the same recursively derived polynomials. From (B.2), (B.3) and (B.6) it is easy to see[3] that

$$D_i = \frac{1}{Z_c S} \{ (Z_c G_i S + 1) B_i + (S^2 - 1) B_{i-1} \} \ , \ i = 2 \ldots N$$

$$= \frac{1}{Z_c S} \{ B_{i+1} - B_i \} \ , \ i = 1 \ldots N \ . \tag{B.7}$$

The last step is to consolidate (B.6) and (B.7) as follows. For clarity introduce the following notation,

$$P_i = \frac{1}{Z_c S} B_i \ , \tag{B.8}$$

which is valid since we have $B_i(0) = 0$ for all $i = 0 \ldots N+1$. Introduce the physically meaningless quantity $P_0 = 0$ for mathematical completeness, and summarize :

$$P_{i+1} = (Z_c G_i S + 2) P_i + (S^2 - 1) P_{i-1} \ , \text{ with}$$

$$P_0 = 0 \ , \ P_1 = 1 \ , \ i = 1 \ldots N \ . \tag{B.9}$$

It is easily verified that P_i will be a real polynomial in S of degree $i-1$, that it will be a function of $G_1 \ldots G_{i-1}$, and not of G_i, and that the $Z_c G_i$ always appear as paired products[4] in the $P_i(S)$ buildup. This sequence of polynomials, $P_{0 \ldots N+1}(S)$, will form the fundamental building block of most of the analysis and synthesis algorithms to

[3] Note that B_{N+1} is appended for mathematical completeness.

[4] Since no practical realizability restrictions were found when $Z_c = 1$, it might at first look feasible to design such a free space absorber, and to subsequently scale the conductances with $1/Z_c$ for use with the Z_c spacers. This will result in an input impedance which is scaled by Z_c (see (B.10)), which will yield the wanted reflection properties *when embedded in a medium with the same dielectric constant as the spacers.* However, the broadband impedance transformer needed to use the absorber in free space, will in general prohibit such a technique.

stellenbosch University http://scholar.sun.ac.za

be described. In addition, it may be used symbolically for the speedy construction of input port properties for small N structures.

In particular, Z_{in} and ρ, automatically expressed in the standard forms of Section 3.2, are constructed as

$$Z_{in} = \frac{B_N}{D_N} = \frac{Z_c S P_N}{P_{N+1} - P_N} \text{ , and}$$

$$\rho = \frac{B_N - D_N}{B_N + D_N} = \frac{(Z_c S + 1)P_N - P_{N+1}}{(Z_c S - 1)P_N + P_{N+1}} . \tag{B.10}$$

B.2 Recursive algorithm to compute the coefficients of $P_i(S)$

In this section an algorithm will be developed to compute the polynomial coefficients in the following expansion,

$$P_i(S) = \sum_{m=0}^{i-1} p_m^{(i)} S^m \text{ , for } i = 1 \ldots N+1 , \tag{B.11}$$

where the superscript (i) does not denote any mathematical operation, but is simply used as convenient notation.

To be mathematically complete, define

$$p_m^{(i)} \equiv 0 \text{ for } m < 0 \text{ or } m \geq i. \tag{B.12}$$

This automatically includes the first initial condition, $P_0 = 0$. The second condition, $P_1 = 1$, and the recursive equation (B.9) for P_i, may now be implemented with the following algorithm :

- Define the initial state as
$$p_{m=-2\ldots N}^{(i=0\ldots N+1)} = 0 , \tag{B.13}$$
keeping in mind that the ranges of m and i incorporate some implicit bookkeeping.
- Implement $P_1 = 1$ by setting $p_0^{(1)} = 1$.
- Build up the triangular set of coefficients, by computing for each $i = 2 \ldots N+1$,
$$p_m^{(i)} = Z_c G_{i-1} p_{m-1}^{(i-1)} + 2p_m^{(i-1)} + p_{m-2}^{(i-2)} - p_m^{(i-2)} \text{ , } m = 0 \ldots i-1 . \tag{B.14}$$

stellenbosch University http://scholar.sun.ac.za

B.3 Constructing the coefficients of $\mathcal{N}_\rho(S)$

In the conductance reconstruction algorithm of Chapter 5, the coefficients a_i in the expansion[5]

$$\begin{aligned}\mathcal{N}_\rho(S) &= -1 + \sum_{i=1}^{N} a_i S^i \\ &= (Z_c S + 1)P_N - P_{N+1} \ . \end{aligned} \tag{B.15}$$

will be needed. To facilitate this, use (B.11) to obtain[6]

$$a_i = Z_c p_{i-1}^{(N)} + p_i^{(N)} - p_i^{(N+1)} \ , \text{ for } i = 1 \ldots N. \tag{B.16}$$

B.4 Recursive algorithm to compute $\partial a_i / \partial G_j$

In the conductance reconstruction algorithm of Chapter 5, the partial derivatives of a_i with respect to G_j will be needed ($i, j = 1 \ldots N$). These may be computed in a similar way as the a_i themselves, namely with recursive schemes using the intermediate derivatives

$$D_{j,i,m} \stackrel{\text{def}}{=} \frac{\partial p_m^{(i)}}{\partial G_j} \ . \tag{B.17}$$

From (B.14) we have

$$\begin{aligned} D_{j,i,m} = Z_c G_{i-1} D_{j,i-1,m-1} + Z_c p_{m-1}^{(i-1)} \delta(i-j-1) + \\ 2D_{j,i-1,m} + D_{j,i-2,m-2} - D_{j,i-2,m} \ , \end{aligned} \tag{B.18}$$

with $\delta(0) = 1$, $\delta(i \neq 0) = 0$, and with the ranges of j, i, and m carefully selected to accommodate all the initial and edge conditions.

To construct the N triangular sets of D's, perform the following steps :

```
For each j = 1 ... N Do
    Initialize : D_{j,i=0...N+1,m=-1...N} = 0.
    If j = 1, set D_{1,2,1} = Z_c.
    For each i = max (3, j + 1) ... N + 1 Do
        For each m = 1 ... i - 1 Do
            Compute D_{j,i,m} with (B.18).
        Next m.
    Next i.
Next j.
```

Finally, use (B.16) to construct

$$\frac{\partial a_i}{\partial G_j} = Z_c D_{j,N,i-1} + D_{j,N,i} - D_{j,N+1,i} \ , \text{ with } i, j = 1 \ldots N \ . \tag{B.19}$$

---

[5] See (5.2).

[6] Remember from (B.12) that $p_N^{(N)} \equiv 0$.

stellenbosch University http://scholar.sun.ac.za

B.5 Evaluating the ripple behavior of $|\rho|$

At a lobe maximum of $|\rho|$ we have

$$\left.\frac{\partial|\rho|^2}{\partial\Omega}\right|_{f=f_i} = 0 \ .$$

Since $\rho(S)$ is known, the following may be constructed :

$$\rho(S)\rho(-S) = \frac{C(S)}{D(S)} \ ,$$

$$|\rho(j\Omega)|^2 = \rho(S)\rho(-S)|_{S=j\Omega} = \frac{E(\Omega)}{F(\Omega)} \ ,$$

and finally

$$\mathcal{E}(f_i) = \left.\frac{\partial|\rho(j\Omega)|^2}{\partial\Omega}\right|_{\Omega=\tan(\frac{\pi f_i}{200})} = \left.\frac{E(\Omega)\frac{\partial F(\Omega)}{\partial\Omega} - F(\Omega)\frac{\partial E(\Omega)}{\partial\Omega}}{F^2(\Omega)}\right|_{\Omega=\tan(\frac{\pi f_i}{200})} \ . \qquad \text{(B.20)}$$

To find f_i where $\mathcal{E}(f_i) = 0$, assume a linear dependence of $\mathcal{E}$ on f, approximate the derivative numerically with a finite difference, and apply the iterative[7] Newton-Rhapson technique. With the particular f_i known, simply compute

$$m_i = 20\log_{10}|\rho(f = f_i)| \ . \qquad \text{(B.21)}$$

[7]The midpoint of the lobe, i.e. the arithmetic mean of its two boundary zero positions, was found to be a stable starting point in the iteration.

stellenbosch University http://scholar.sun.ac.za

Appendix C

Proof of the maximally flat criterion, $\mathcal{N}_\rho(S) = -1$

Recalling Property 2, the proof starts by renaming $\rho = \frac{A(S)}{B(S)}$, and then constructing

$$|\rho(S = j\Omega)|^2 = \rho(S)\rho(-S)|_{S=j\Omega} =$$

$$\left.\frac{A(S)A(-S)}{B(S)B(-S)}\right|_{S=j\Omega} = \frac{1 + \sum_{i=1}^{N} c_i \Omega^{2i}}{1 + \sum_{i=1}^{N} d_i \Omega^{2i}} \; . \tag{C.1}$$

The next step is to move the maximally flat point to $S = 0$ with the high-to-low pass transformation $S \rightarrow \frac{1}{S}$, to obtain

$$|\rho(j\Omega)|^2 = \frac{\sum_{i=0}^{N-1} c_{(N-i)} \Omega^{2i} + \Omega^{2N}}{\sum_{i=0}^{N-1} d_{(N-i)} \Omega^{2i} + \Omega^{2N}} \; . \tag{C.2}$$

When $S \rightarrow 0$ it follows that $S = j\Omega = j \tan\omega \rightarrow j\omega$ which, with the substitutions $x = \omega^2$ and $g = |\rho|^2$ for clarity, reduce (C.2) to

$$g(x) = \frac{\sum_{i=0}^{N-1} c_{(N-i)} x^i + x^N}{\sum_{i=0}^{N-1} d_{(N-i)} x^i + x^N} \; . \tag{C.3}$$

The maximally flat requirements of (6.1) have now been transformed into

$$g(0) = 0 \; ,$$

$$\left.\frac{\partial^i g(x)}{\partial x^i}\right|_{x=0} = 0 \; , \; i = 1 \ldots N-1 \; . \tag{C.4}$$

It is seen from (C.3) that $g(0) = 0$ immediately enforces $c_N = 0$. Since differentiating (C.3) repetitively in order to enforce all the conditions on the coefficients simultaneously, rapidly becomes unmanageable, proof will continue by induction.

stellenbosch University http://scholar.sun.ac.za

Define

$$f_j(x) = \frac{\sum_{i=j}^{N-1} c_{(N-i)} x^i + x^N}{\sum_{i=0}^{N-1} d_{(N-i)} x^i + x^N} \ , j = 1 \ldots N-1 \ . \tag{C.5}$$

After performing a Taylor expansion on $f_j(x)$ around $x = 0$, it follows that we have, for $j = 1$,

$$f_1(0) = 0 \ , \text{ and } \left.\frac{\partial f_1(x)}{\partial x}\right|_{x=0} = \frac{c_{(N-1)}}{d_N} \ , \tag{C.6}$$

and for $j = 2 \ldots N-1$,

$$f_j(0) = 0 \ , \tag{C.7}$$

$$\left.\frac{\partial^k f_j(x)}{\partial x^k}\right|_{x=0} = 0 \text{ for } k = 1 \ldots j-1 \text{ , and} \tag{C.8}$$

$$\left.\frac{\partial^j f_j(x)}{\partial x^j}\right|_{x=0} = \frac{c_{(N-j)}}{d_N} \ . \tag{C.9}$$

We already have $c_N = 0$, implying $g(x) = f_1(x)$. Turning next to the requirement that

$$\left.\frac{\partial g(x)}{\partial x}\right|_{x=0} = \left.\frac{\partial f_1(x)}{\partial x}\right|_{x=0} = 0 \ , \tag{C.10}$$

we see that it implies $c_{N-1} = 0$, i.e. $g(x) = f_2(x)$. This line of reasoning continues through induction, finally terminating when

$$c_i = 0 \ , i = 1 \ldots N. \tag{C.11}$$

Turning back to (C.1), it follows that $\mathcal{N}_\rho = A(S) = -1$ is equivalent to the MF-criteria defined in (6.1), thereby completing the proof.

stellenbosch University http://scholar.sun.ac.za

Appendix D

Matlab386 routines

D.1 Multilayered synthesis and analysis routines

The iterative synthesis algorithms of Chapters 6, 7 and 8 have been implemented in MATLAB386[1], in the form of function m-files. The filenames and functions are related as follows :

MF.m	:	Maximally flat synthesis,
IZP.m	:	Equiripple synthesis,
OPT.m	:	Optimization of an IZP solution,
VIEW.m	:	Shows the absorption response of a known absorber.

These functions include header sections explaining their usage, which can be accessed with the usual Matlab command, ≫**help** *function name*, and they should accompany this document in electronic format.

D.2 Auxiliary routines

A number of auxiliary support functions are necessary to execute the main routines above, and should be copied into the same (Matlab accessible) directory. These are

a_d_p.m	:	Implementation of Appendices B.2, B.3 and B.4,
ef_coefs.m	:	Implementation of Appendix B.5,
find_bw.m	:	Finds the bandwidth point, f_c,
rho.m	:	Computes $\rho(f)$, given $\mathbf{G}$ and Z_c,
nr_to_g.m	:	Implements the reconstruction algorithm of Chapter 5,
zpit_mxs.m	:	Support function for IZP.m,
zpit_wnr.m	:	Support function for IZP.m,
opt_mxs.m	:	Support function for OPT.m,
opt_noso.m	:	Support function for OPT.m,
opt_shw1.m	:	Support function for OPT.m,
opt_shw2.m	:	Support function for OPT.m.

[1] By MathWorks, Inc.

stellenbosch University http://scholar.sun.ac.za

Appendix E

Tabulated numerical results

Even for moderate N, the Matlab routines of Appendix D may take up to a few minutes to execute. It was therefore decided to run automated versions, and to present the results here in the form of lookup tables. These results represent a comprehensive extension to the rather wide selection of solutions available in the literature, and keeping Conjectures 2 and 3 in mind, were tailored around practical low-loss, low dielectric constant foam spacers.

The maximally flat (MF) and equiripple[1] (IZP) solutions were obtained by executing the appropriate routines from Appendix D, and the reader may verify the results independently. However, the optimal (OPT) solutions were obtained with a slightly modified routine. In particular, the IZP solutions of Tables E.2 to E.4 were used as parent solutions for the OPT routine, resulting (after optimization) in slightly reduced reflection ripple levels over the parent bandwidths. These optimal solutions were then iteratively adjusted[2] and fed back to the modified OPT routine, until the ripple levels returned to those of the parent IZP solutions (in particular, the -20, -30 and -40 dB levels).

It is interesting to note the relaxation in the ϵ_r restriction in the $\mathcal{R} = -30$ dB, $\epsilon_r = 1.2$ case. It is seen that five and six-layered OPT response absorbers are realizable, whereas the corresponding IZP-response absorbers are not. This is a practical illustration of the logical extension of Conjectures 2 and 3, which was mentioned in Chapter 8.

[1] With reflection zeros at physical frequencies.

[2] By increasing the bandwidths in small, judicious increments.

stellenbosch University http://scholar.sun.ac.za

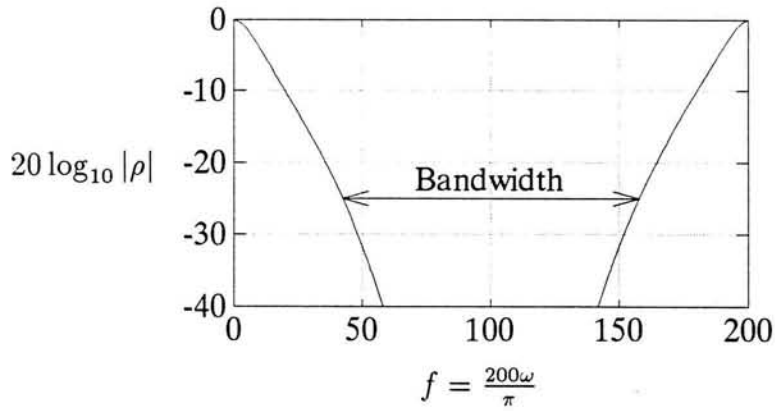

Figure E.1: Generic shape of the tabulated maximally flat solutions of Table E.1.

	$\epsilon_r = 1$	$\epsilon_r = 1.03$	$\epsilon_r = 1.05$	$\epsilon_r = 1.1$	$\epsilon_r = 1.2$
$N = 1$	$R_1 = 1.00000$ $B = 14.28\%$	$R_1 = 1.00000$ $B = 14.07\%$	$R_1 = 1.00000$ $B = 13.94\%$	$R_1 = 1.00000$ $B = 13.62\%$	$R_1 = 1.00000$ $B = 13.05\%$
$N = 2$	$R_1 = 0.707107$ $R_2 = 3.41421$ $B = 50.65\%$	$R_1 = 0.696733$ $R_2 = 3.54152$ $B = 50.26\%$	$R_1 = 0.690066$ $R_2 = 3.63067$ $B = 50.01\%$	$R_1 = 0.674200$ $R_2 = 3.87027$ $B = 49.41\%$	$R_1 = 0.645497$ $R_2 = 4.43649$ $B = 48.30\%$
$N = 3$	$R_1 = 0.608257$ $R_2 = 1.94454$ $R_3 = 9.16207$ $B = 76.22\%$	$R_1 = 0.599334$ $R_2 = 1.91601$ $R_3 = 10.4295$ $B = 75.82\%$	$R_1 = 0.593598$ $R_2 = 1.89768$ $R_3 = 11.4750$ $B = 75.56\%$	$R_1 = 0.579950$ $R_2 = 1.85404$ $R_3 = 15.2290$ $B = 74.93\%$	$R_1 = 0.555260$ $R_2 = 1.77511$ $R_3 = 41.4629$ $B = 73.78\%$
$N = 4$	$R_1 = 0.561038$ $R_2 = 1.49364$ $R_3 = 4.27818$ $R_4 = 22.5545$ $B = 93.54\%$	$R_1 = 0.552807$ $R_2 = 1.47173$ $R_3 = 4.21541$ $R_4 = 33.2137$ $B = 93.16\%$	$R_1 = 0.547517$ $R_2 = 1.45765$ $R_3 = 4.17507$ $R_4 = 48.2231$ $B = 92.92\%$	NO SOLUTION	NO SOLUTION
$N = 5$	$R_1 = 0.535357$ $R_2 = 1.28591$ $R_3 = 2.91767$ $R_4 = 8.79951$ $R_5 = 53.1999$ $B = 105.97\%$	$R_1 = 0.527503$ $R_2 = 1.26705$ $R_3 = 2.87487$ $R_4 = 8.67041$ $R_5 = 238.792$ $B = 105.62\%$	NO SOLUTION	NO SOLUTION	NO SOLUTION
$N = 6$	$R_1 = 0.520602$ $R_2 = 1.17288$ $R_3 = 2.32379$ $R_4 = 5.32786$ $R_5 = 17.6607$ $R_6 = 122.301$ $B = 115.34\%$	NO SOLUTION	NO SOLUTION	NO SOLUTION	NO SOLUTION
$N = 7$	$R_1 = 0.511953$ $R_2 = 1.10625$ $R_3 = 2.00829$ $R_4 = 3.90673$ $R_5 = 9.52448$ $R_6 = 35.1300$ $R_7 = 276.238$ $B = 122.70\%$	NO SOLUTION	NO SOLUTION	NO SOLUTION	NO SOLUTION
$N = 8$	$R_1 = 0.506871$ $R_2 = 1.06546$ $R_3 = 1.82256$ $R_4 = 3.18060$ $R_5 = 6.41672$ $R_6 = 16.9650$ $R_7 = 69.6897$ $R_8 = 615.734$ $B = 128.66\%$	NO SOLUTION	NO SOLUTION	NO SOLUTION	NO SOLUTION

Table E.1: Normalized sheet surface resistivities for maximally flat absorption behaviors. The ϵ_r values are representative of practical low-loss low dielectric constant foams, all computed bandwidths are at the -25 dB level (see Figure E.1), and all resistance values are given to 6 digit accuracy.

stellenbosch University http://scholar.sun.ac.za

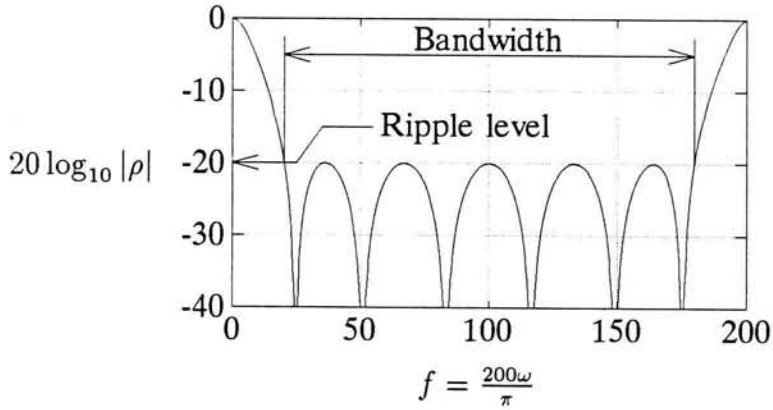

Figure E.2: Generic shape of the tabulated −20 dB IZP solutions of Table E.2. Note that N reflection zeros will reside in the range $0 < f < 200$.

	$\epsilon_r = 1$	$\epsilon_r = 1.03$	$\epsilon_r = 1.05$	$\epsilon_r = 1.1$	$\epsilon_r = 1.2$
$N = 2$	$R_1 = 0.826894$ $R_2 = 2.52955$ $\mathcal{B} = 86.40\%$	$R_1 = 0.812910$ $R_2 = 2.59791$ $\mathcal{B} = 85.88\%$	$R_1 = 0.803952$ $R_2 = 2.64500$ $\mathcal{B} = 85.55\%$	$R_1 = 0.782734$ $R_2 = 2.76845$ $\mathcal{B} = 84.74\%$	$R_1 = 0.744697$ $R_2 = 3.04334$ $\mathcal{B} = 83.23\%$
$N = 3$	$R_1 = 0.838716$ $R_2 = 1.94817$ $R_3 = 3.84076$ $\mathcal{B} = 120.69\%$	$R_1 = 0.823232$ $R_2 = 1.91887$ $R_3 = 4.03772$ $\mathcal{B} = 120.28\%$	$R_1 = 0.813333$ $R_2 = 1.90005$ $R_3 = 4.17892$ $\mathcal{B} = 120.01\%$	$R_1 = 0.789942$ $R_2 = 1.85534$ $R_3 = 4.57236$ $\mathcal{B} = 119.36\%$	$R_1 = 0.748214$ $R_2 = 1.77467$ $R_3 = 5.59167$ $\mathcal{B} = 118.14\%$
$N = 4$	$R_1 = 0.896298$ $R_2 = 1.75683$ $R_3 = 3.28899$ $R_4 = 4.79759$ $\mathcal{B} = 139.71\%$	$R_1 = 0.878576$ $R_2 = 1.72844$ $R_3 = 3.24334$ $R_4 = 5.13014$ $\mathcal{B} = 139.38\%$	$R_1 = 0.867263$ $R_2 = 1.71023$ $R_3 = 3.21399$ $R_4 = 5.37564$ $\mathcal{B} = 139.17\%$	$R_1 = 0.840582$ $R_2 = 1.66706$ $R_3 = 3.14417$ $R_4 = 6.09308$ $\mathcal{B} = 138.66\%$	$R_1 = 0.793171$ $R_2 = 1.58945$ $R_3 = 3.01781$ $R_4 = 8.21620$ $\mathcal{B} = 137.70\%$
$N = 5$	$R_1 = 0.975877$ $R_2 = 1.70002$ $R_3 = 2.86558$ $R_4 = 4.74914$ $R_5 = 5.49659$ $\mathcal{B} = 151.49\%$	$R_1 = 0.955448$ $R_2 = 1.67112$ $R_3 = 2.82228$ $R_4 = 4.68707$ $R_5 = 5.95104$ $\mathcal{B} = 151.23\%$	$R_1 = 0.942420$ $R_2 = 1.65262$ $R_3 = 2.79449$ $R_4 = 4.64716$ $R_5 = 6.29390$ $\mathcal{B} = 151.06\%$	$R_1 = 0.911745$ $R_2 = 1.60881$ $R_3 = 2.72846$ $R_4 = 4.55211$ $R_5 = 7.33340$ $\mathcal{B} = 150.64\%$	$R_1 = 0.857404$ $R_2 = 1.53030$ $R_3 = 2.60941$ $R_4 = 4.37986$ $R_5 = 10.7805$ $\mathcal{B} = 149.86\%$
$N = 6$	$R_1 = 1.07070$ $R_2 = 1.69661$ $R_3 = 2.68251$ $R_4 = 4.09579$ $R_5 = 6.28190$ $R_6 = 6.02222$ $\mathcal{B} = 159.46\%$	$R_1 = 1.04720$ $R_2 = 1.66647$ $R_3 = 2.63988$ $R_4 = 4.03689$ $R_5 = 6.20351$ $R_6 = 6.58139$ $\mathcal{B} = 159.23\%$	$R_1 = 1.03222$ $R_2 = 1.64719$ $R_3 = 2.61255$ $R_4 = 3.99906$ $R_5 = 6.15309$ $R_6 = 7.01024$ $\mathcal{B} = 159.09\%$	$R_1 = 0.997001$ $R_2 = 1.60160$ $R_3 = 2.54771$ $R_4 = 3.90910$ $R_5 = 6.03294$ $R_6 = 8.34865$ $\mathcal{B} = 158.74\%$	$R_1 = 0.934754$ $R_2 = 1.52016$ $R_3 = 2.43108$ $R_4 = 3.74662$ $R_5 = 5.81502$ $R_6 = 13.2433$ $\mathcal{B} = 158.09\%$
$N = 7$	$R_1 = 1.17776$ $R_2 = 1.72238$ $R_3 = 2.59707$ $R_4 = 3.77571$ $R_5 = 5.41532$ $R_6 = 7.86210$ $R_7 = 6.42951$ $\mathcal{B} = 165.19\%$	$R_1 = 1.15088$ $R_2 = 1.69048$ $R_3 = 2.55420$ $R_4 = 3.71836$ $R_5 = 5.34048$ $R_6 = 7.76747$ $R_7 = 7.07770$ $\mathcal{B} = 164.99\%$	$R_1 = 1.13376$ $R_2 = 1.67009$ $R_3 = 2.52673$ $R_4 = 3.68156$ $R_5 = 5.29239$ $R_6 = 7.70659$ $R_7 = 7.58123$ $\mathcal{B} = 164.87\%$	$R_1 = 1.09355$ $R_2 = 1.62195$ $R_3 = 2.46164$ $R_4 = 3.59416$ $R_5 = 5.17798$ $R_6 = 7.56150$ $R_7 = 9.18968$ $\mathcal{B} = 164.57\%$	$R_1 = 1.02259$ $R_2 = 1.53619$ $R_3 = 2.34484$ $R_4 = 3.43664$ $R_5 = 4.97106$ $R_6 = 7.29817$ $R_7 = 15.5939$ $\mathcal{B} = 164.01\%$
$N = 8$	$R_1 = 1.29513$ $R_2 = 1.76763$ $R_3 = 2.56200$ $R_4 = 3.59991$ $R_5 = 4.95560$ $R_6 = 6.80274$ $R_7 = 9.47503$ $R_8 = 6.75346$ $\mathcal{B} = 169.50\%$	$R_1 = 1.26464$ $R_2 = 1.73356$ $R_3 = 2.51829$ $R_4 = 3.54310$ $R_5 = 4.88296$ $R_6 = 6.71179$ $R_7 = 9.36425$ $R_8 = 7.47744$ $\mathcal{B} = 169.33\%$	$R_1 = 1.24523$ $R_2 = 1.71182$ $R_3 = 2.49030$ $R_4 = 3.50666$ $R_5 = 4.83633$ $R_6 = 6.65333$ $R_7 = 9.29296$ $R_8 = 8.04566$ $\mathcal{B} = 169.22\%$	$R_1 = 1.19966$ $R_2 = 1.66053$ $R_3 = 2.42405$ $R_4 = 3.42022$ $R_5 = 4.72550$ $R_6 = 6.51419$ $R_7 = 9.12304$ $R_8 = 9.89563$ $\mathcal{B} = 168.96\%$	$R_1 = 1.11935$ $R_2 = 1.56938$ $R_3 = 2.30543$ $R_4 = 3.26473$ $R_5 = 4.52549$ $R_6 = 6.26233$ $R_7 = 8.81453$ $R_8 = 17.8319$ $\mathcal{B} = 168.47\%$

Table E.2: Normalized sheet surface resistivities for −20 dB IZP absorption behaviors. The ϵ_r values are representative of practical low-loss low dielectric constant foams, all computed bandwidths are at the −20 dB level (see Figure E.2), and all resistance values are given to 6 digit accuracy.

stellenbosch University http://scholar.sun.ac.za

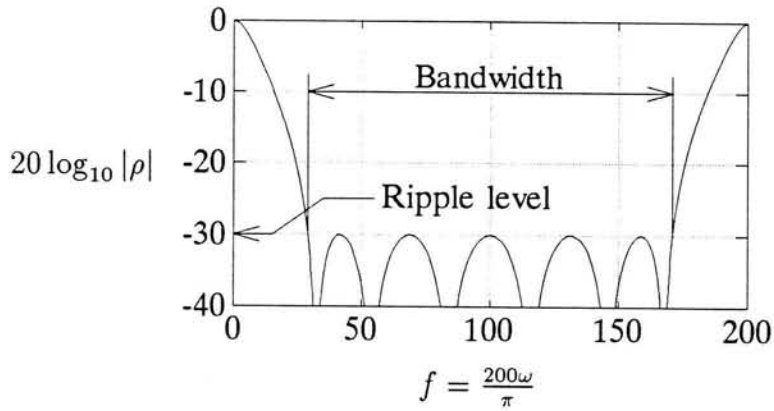

Figure E.3: Generic shape of the tabulated −30 dB IZP solutions of Table E.3. Note that N reflection zeros will reside in the range $0 < f < 200$.

	$\epsilon_r = 1$	$\epsilon_r = 1.03$	$\epsilon_r = 1.05$	$\epsilon_r = 1.1$	$\epsilon_r = 1.2$
$N = 2$	$R_1 = 0.740516$ $R_2 = 3.07887$ $\mathcal{B} = 51.97\%$	$R_1 = 0.729158$ $R_2 = 3.18190$ $\mathcal{B} = 51.61\%$	$R_1 = 0.721866$ $R_2 = 3.25361$ $\mathcal{B} = 51.38\%$	$R_1 = 0.704540$ $R_2 = 3.44451$ $\mathcal{B} = 50.83\%$	$R_1 = 0.673283$ $R_2 = 3.88545$ $\mathcal{B} = 49.80\%$
$N = 3$	$R_1 = 0.688225$ $R_2 = 1.93226$ $R_3 = 5.86018$ $\mathcal{B} = 89.90\%$	$R_1 = 0.677196$ $R_2 = 1.90395$ $R_3 = 6.34415$ $\mathcal{B} = 89.53\%$	$R_1 = 0.670121$ $R_2 = 1.88576$ $R_3 = 6.70913$ $\mathcal{B} = 89.29\%$	$R_1 = 0.653329$ $R_2 = 1.84247$ $R_3 = 7.81492$ $\mathcal{B} = 88.72\%$	$R_1 = 0.623110$ $R_2 = 1.76417$ $R_3 = 11.4737$ $\mathcal{B} = 87.65\%$
$N = 4$	$R_1 = 0.682415$ $R_2 = 1.63239$ $R_3 = 3.55269$ $R_4 = 8.60235$ $\mathcal{B} = 114.50\%$	$R_1 = 0.671092$ $R_2 = 1.60749$ $R_3 = 3.50403$ $R_4 = 9.76662$ $\mathcal{B} = 114.19\%$	$R_1 = 0.663835$ $R_2 = 1.59150$ $R_3 = 3.47272$ $R_4 = 10.7225$ $\mathcal{B} = 113.98\%$	$R_1 = 0.646628$ $R_2 = 1.55347$ $R_3 = 3.39813$ $R_4 = 14.1224$ $\mathcal{B} = 113.48\%$	$R_1 = 0.615719$ $R_2 = 1.48482$ $R_3 = 3.26283$ $R_4 = 36.5390$ $\mathcal{B} = 112.55\%$
$N = 5$	$R_1 = 0.693078$ $R_2 = 1.51331$ $R_3 = 2.84978$ $R_4 = 5.49086$ $R_5 = 11.0045$ $\mathcal{B} = 130.68\%$	$R_1 = 0.681220$ $R_2 = 1.48970$ $R_3 = 2.80821$ $R_4 = 5.42045$ $R_5 = 13.0463$ $\mathcal{B} = 130.41\%$	$R_1 = 0.673623$ $R_2 = 1.47454$ $R_3 = 2.78150$ $R_4 = 5.37512$ $R_5 = 14.8628$ $\mathcal{B} = 130.24\%$	$R_1 = 0.655629$ $R_2 = 1.43853$ $R_3 = 2.71792$ $R_4 = 5.26701$ $R_5 = 22.6034$ $\mathcal{B} = 129.81\%$	NO SOLUTION
$N = 6$	$R_1 = 0.712041$ $R_2 = 1.45639$ $R_3 = 2.54526$ $R_4 = 4.30062$ $R_5 = 7.65510$ $R_6 = 13.0320$ $\mathcal{B} = 141.88\%$	$R_1 = 0.699498$ $R_2 = 1.43331$ $R_3 = 2.50695$ $R_4 = 4.24062$ $R_5 = 7.56247$ $R_6 = 16.0453$ $\mathcal{B} = 141.65\%$	$R_1 = 0.691468$ $R_2 = 1.41850$ $R_3 = 2.48234$ $R_4 = 4.20203$ $R_5 = 7.50280$ $R_6 = 18.9282$ $\mathcal{B} = 141.51\%$	$R_1 = 0.672463$ $R_2 = 1.38333$ $R_3 = 2.42382$ $R_4 = 4.11014$ $R_5 = 7.36040$ $R_6 = 33.9158$ $\mathcal{B} = 141.15\%$	NO SOLUTION
$N = 7$	$R_1 = 0.736379$ $R_2 = 1.42751$ $R_3 = 2.38354$ $R_4 = 3.75470$ $R_5 = 5.94749$ $R_6 = 9.98126$ $R_7 = 14.7312$ $\mathcal{B} = 150.03\%$	$R_1 = 0.723037$ $R_2 = 1.40460$ $R_3 = 2.34698$ $R_4 = 3.70007$ $R_5 = 5.86789$ $R_6 = 9.86633$ $R_7 = 18.7403$ $\mathcal{B} = 149.84\%$	$R_1 = 0.714502$ $R_2 = 1.38990$ $R_3 = 2.32350$ $R_4 = 3.66495$ $R_5 = 5.81667$ $R_6 = 9.79226$ $R_7 = 22.8333$ $\mathcal{B} = 149.71\%$	$R_1 = 0.694316$ $R_2 = 1.35500$ $R_3 = 2.26769$ $R_4 = 3.58140$ $R_5 = 5.69462$ $R_6 = 9.61540$ $R_7 = 49.3349$ $\mathcal{B} = 149.39\%$	NO SOLUTION
$N = 8$	$R_1 = 0.764827$ $R_2 = 1.41376$ $R_3 = 2.28753$ $R_4 = 3.45199$ $R_5 = 5.12368$ $R_6 = 7.75772$ $R_7 = 12.4258$ $R_8 = 16.1611$ $\mathcal{B} = 156.20\%$	$R_1 = 0.750589$ $R_2 = 1.39080$ $R_3 = 2.25198$ $R_4 = 3.40050$ $R_5 = 5.05148$ $R_6 = 7.65774$ $R_7 = 12.2887$ $R_8 = 21.1493$ $\mathcal{B} = 156.03\%$	$R_1 = 0.741486$ $R_2 = 1.37607$ $R_3 = 2.22915$ $R_4 = 3.36742$ $R_5 = 5.00505$ $R_6 = 7.59338$ $R_7 = 12.2002$ $R_8 = 26.5460$ $\mathcal{B} = 155.92\%$	$R_1 = 0.719973$ $R_2 = 1.34111$ $R_3 = 2.17490$ $R_4 = 3.28873$ $R_5 = 4.89451$ $R_6 = 7.43994$ $R_7 = 11.9890$ $R_8 = 71.2811$ $\mathcal{B} = 155.64\%$	NO SOLUTION

Table E.3: Normalized sheet surface resistivities for −30 dB IZP absorption behaviors. The ϵ_r values are representative of practical low-loss low dielectric constant foams, all computed bandwidths are at the −30 dB level (see Figure E.3), and all resistance values are given to 6 digit accuracy.

stellenbosch University http://scholar.sun.ac.za

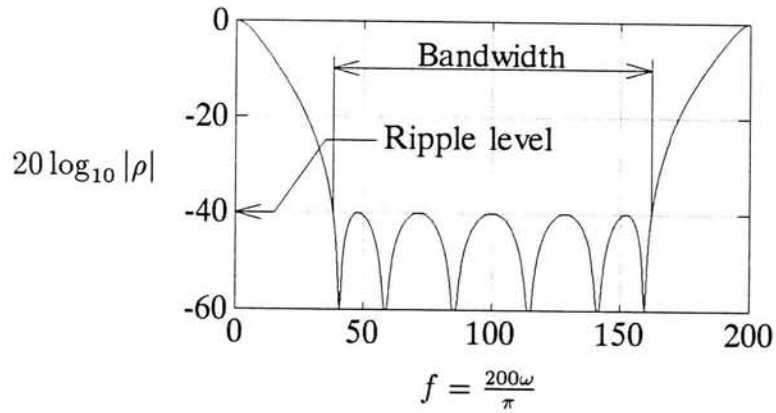

Figure E.4: Generic shape of the tabulated −40 dB IZP solutions of Table E.4. Note that N reflection zeros will reside in the range $0 < f < 200$.

	$\epsilon_r = 1$	$\epsilon_r = 1.03$	$\epsilon_r = 1.05$	$\epsilon_r = 1.1$	$\epsilon_r = 1.2$
$N = 2$	$R_1 = 0.717280$ $R_2 = 3.30118$ $\mathcal{B} = 29.93\%$	$R_1 = 0.706609$ $R_2 = 3.42003$ $\mathcal{B} = 29.72\%$	$R_1 = 0.699753$ $R_2 = 3.50310$ $\mathcal{B} = 29.58\%$	$R_1 = 0.683445$ $R_2 = 3.72561$ $\mathcal{B} = 29.24\%$	$R_1 = 0.653970$ $R_2 = 4.24739$ $\mathcal{B} = 28.63\%$
$N = 3$	$R_1 = 0.641022$ $R_2 = 1.93723$ $R_3 = 7.36039$ $\mathcal{B} = 64.27\%$	$R_1 = 0.631270$ $R_2 = 1.90887$ $R_3 = 8.14888$ $\mathcal{B} = 63.98\%$	$R_1 = 0.625007$ $R_2 = 1.89064$ $R_3 = 8.76749$ $\mathcal{B} = 63.79\%$	$R_1 = 0.610119$ $R_2 = 1.84726$ $R_3 = 10.7801$ $\mathcal{B} = 63.34\%$	$R_1 = 0.583241$ $R_2 = 1.76878$ $R_3 = 19.3901$ $\mathcal{B} = 62.51\%$
$N = 4$	$R_1 = 0.615632$ $R_2 = 1.57492$ $R_3 = 3.80185$ $R_4 = 12.6322$ $\mathcal{B} = 91.00\%$	$R_1 = 0.606097$ $R_2 = 1.55126$ $R_3 = 3.74881$ $R_4 = 15.3508$ $\mathcal{B} = 90.72\%$	$R_1 = 0.599976$ $R_2 = 1.53606$ $R_3 = 3.71469$ $R_4 = 17.8863$ $\mathcal{B} = 90.53\%$	$R_1 = 0.585433$ $R_2 = 1.49992$ $R_3 = 3.63342$ $R_4 = 30.1223$ $\mathcal{B} = 90.09\%$	NO SOLUTION
$N = 5$	$R_1 = 0.607756$ $R_2 = 1.42798$ $R_3 = 2.87193$ $R_4 = 6.28655$ $R_5 = 18.3051$ $\mathcal{B} = 110.19\%$	$R_1 = 0.598204$ $R_2 = 1.40620$ $R_3 = 2.83005$ $R_4 = 6.20398$ $R_5 = 24.8433$ $\mathcal{B} = 109.94\%$	$R_1 = 0.592074$ $R_2 = 1.39222$ $R_3 = 2.80313$ $R_4 = 6.15082$ $R_5 = 32.4858$ $\mathcal{B} = 109.77\%$	$R_1 = 0.577514$ $R_2 = 1.35897$ $R_3 = 2.73907$ $R_4 = 6.02406$ $R_5 = 133.457$ $\mathcal{B} = 109.37\%$	NO SOLUTION
$N = 6$	$R_1 = 0.607554$ $R_2 = 1.35451$ $R_3 = 2.48483$ $R_4 = 4.54029$ $R_5 = 9.30127$ $R_6 = 23.8450$ $\mathcal{B} = 124.11\%$	$R_1 = 0.597877$ $R_2 = 1.33366$ $R_3 = 2.44774$ $R_4 = 4.47652$ $R_5 = 9.18624$ $R_6 = 36.5137$ $\mathcal{B} = 123.88\%$	$R_1 = 0.591668$ $R_2 = 1.32027$ $R_3 = 2.42390$ $R_4 = 4.43550$ $R_5 = 9.11214$ $R_6 = 56.1690$ $\mathcal{B} = 123.73\%$	NO SOLUTION	NO SOLUTION
$N = 7$	$R_1 = 0.611444$ $R_2 = 1.31308$ $R_3 = 2.28316$ $R_4 = 3.79698$ $R_5 = 6.56209$ $R_6 = 12.7485$ $R_7 = 29.0019$ $\mathcal{B} = 134.48\%$	$R_1 = 0.601577$ $R_2 = 1.29274$ $R_3 = 2.24861$ $R_4 = 3.74177$ $R_5 = 6.47347$ $R_6 = 12.5994$ $R_7 = 50.4168$ $\mathcal{B} = 134.28\%$	$R_1 = 0.595248$ $R_2 = 1.27968$ $R_3 = 2.22642$ $R_4 = 3.70629$ $R_5 = 6.41644$ $R_6 = 12.5033$ $R_7 = 98.1511$ $\mathcal{B} = 134.15\%$	NO SOLUTION	NO SOLUTION
$N = 8$	$R_1 = 0.617884$ $R_2 = 1.28803$ $R_3 = 2.16345$ $R_4 = 3.40222$ $R_5 = 5.36271$ $R_6 = 8.90869$ $R_7 = 16.5435$ $R_8 = 33.6927$ $\mathcal{B} = 142.45\%$	$R_1 = 0.607783$ $R_2 = 1.26798$ $R_3 = 2.13043$ $R_4 = 3.35177$ $R_5 = 5.28693$ $R_6 = 8.79291$ $R_7 = 16.3594$ $R_8 = 66.7722$ $\mathcal{B} = 142.27\%$	$R_1 = 0.601306$ $R_2 = 1.25510$ $R_3 = 2.10923$ $R_4 = 3.31934$ $R_5 = 5.23820$ $R_6 = 8.71838$ $R_7 = 16.2408$ $R_8 = 188.966$ $\mathcal{B} = 142.15\%$	NO SOLUTION	NO SOLUTION

Table E.4: Normalized sheet surface resistivities for −40 dB IZP absorption behaviors. The ϵ_r values are representative of practical low-loss low dielectric constant foams, all computed bandwidths are at the −40 dB level (see Figure E.4), and all resistance values are given to 6 digit accuracy.

stellenbosch University http://scholar.sun.ac.za

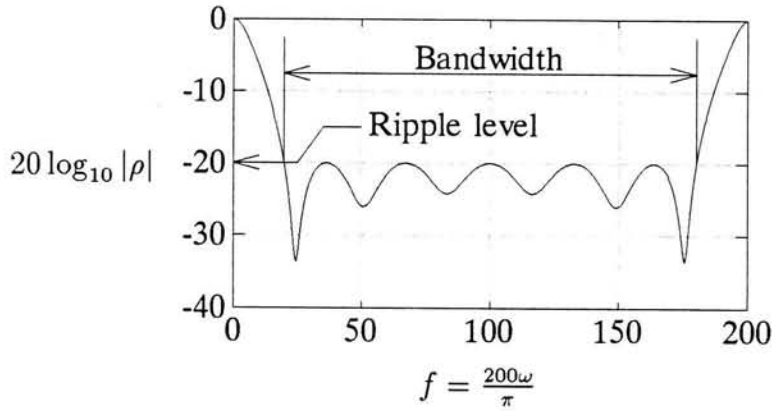

Figure E.5: Generic shape of the tabulated -20 dB OPT solutions of Table E.5. Note that N reflection minima will reside in the range $0 < f < 200$.

	$\epsilon_r = 1$	$\epsilon_r = 1.03$	$\epsilon_r = 1.05$	$\epsilon_r = 1.1$	$\epsilon_r = 1.2$
$N = 2$	$R_1 = 0.790001$ $R_2 = 2.31363$ $\mathcal{B} = 87.18\%$	$R_1 = 0.777107$ $R_2 = 2.37078$ $\mathcal{B} = 86.65\%$	$R_1 = 0.768841$ $R_2 = 2.40999$ $\mathcal{B} = 86.31\%$	$R_1 = 0.749242$ $R_2 = 2.51221$ $\mathcal{B} = 85.48\%$	$R_1 = 0.714034$ $R_2 = 2.73687$ $\mathcal{B} = 83.95\%$
$N = 3$	$R_1 = 0.760552$ $R_2 = 1.90474$ $R_3 = 3.23075$ $\mathcal{B} = 121.77\%$	$R_1 = 0.747693$ $R_2 = 1.87516$ $R_3 = 3.36944$ $\mathcal{B} = 121.35\%$	$R_1 = 0.739451$ $R_2 = 1.85620$ $R_3 = 3.46750$ $\mathcal{B} = 121.07\%$	$R_1 = 0.719913$ $R_2 = 1.81124$ $R_3 = 3.73492$ $\mathcal{B} = 120.41\%$	$R_1 = 0.684833$ $R_2 = 1.73043$ $R_3 = 4.39037$ $\mathcal{B} = 119.17\%$
$N = 4$	$R_1 = 0.767007$ $R_2 = 1.68882$ $R_3 = 3.23865$ $R_4 = 3.77565$ $\mathcal{B} = 140.83\%$	$R_1 = 0.753815$ $R_2 = 1.66163$ $R_3 = 3.18990$ $R_4 = 3.97977$ $\mathcal{B} = 140.50\%$	$R_1 = 0.745360$ $R_2 = 1.64420$ $R_3 = 3.15866$ $R_4 = 4.12675$ $\mathcal{B} = 140.28\%$	$R_1 = 0.725313$ $R_2 = 1.60287$ $R_3 = 3.08463$ $R_4 = 4.53916$ $\mathcal{B} = 139.76\%$	$R_1 = 0.689315$ $R_2 = 1.52859$ $R_3 = 2.95174$ $R_4 = 5.62773$ $\mathcal{B} = 138.78\%$
$N = 5$	$R_1 = 0.781686$ $R_2 = 1.61910$ $R_3 = 2.75740$ $R_4 = 4.75326$ $R_5 = 4.10571$ $\mathcal{B} = 152.57\%$	$R_1 = 0.768171$ $R_2 = 1.59221$ $R_3 = 2.71489$ $R_4 = 4.68207$ $R_5 = 4.35601$ $\mathcal{B} = 152.30\%$	$R_1 = 0.759506$ $R_2 = 1.57499$ $R_3 = 2.68763$ $R_4 = 4.63650$ $R_5 = 4.53826$ $\mathcal{B} = 152.12\%$	$R_1 = 0.738956$ $R_2 = 1.53415$ $R_3 = 2.62296$ $R_4 = 4.52863$ $R_5 = 5.05893$ $\mathcal{B} = 151.70\%$	$R_1 = 0.702031$ $R_2 = 1.46085$ $R_3 = 2.50665$ $R_4 = 4.33541$ $R_5 = 6.50276$ $\mathcal{B} = 150.90\%$
$N = 6$	$R_1 = 0.797876$ $R_2 = 1.59606$ $R_3 = 2.57263$ $R_4 = 3.94280$ $R_5 = 6.44053$ $R_6 = 4.31436$ $\mathcal{B} = 160.46\%$	$R_1 = 0.784103$ $R_2 = 1.56898$ $R_3 = 2.53161$ $R_4 = 3.88375$ $R_5 = 6.34292$ $R_6 = 4.59655$ $\mathcal{B} = 160.24\%$	$R_1 = 0.775270$ $R_2 = 1.55164$ $R_3 = 2.50532$ $R_4 = 3.84589$ $R_5 = 6.28051$ $R_6 = 4.80351$ $\mathcal{B} = 160.09\%$	$R_1 = 0.754312$ $R_2 = 1.51053$ $R_3 = 2.44296$ $R_4 = 3.75606$ $R_5 = 6.13296$ $R_6 = 5.40178$ $\mathcal{B} = 159.73\%$	$R_1 = 0.716622$ $R_2 = 1.43678$ $R_3 = 2.33090$ $R_4 = 3.59450$ $R_5 = 5.86937$ $R_6 = 7.11706$ $\mathcal{B} = 159.07\%$
$N = 7$	$R_1 = 0.813430$ $R_2 = 1.59356$ $R_3 = 2.48273$ $R_4 = 3.62175$ $R_5 = 5.22681$ $R_6 = 8.30589$ $R_7 = 4.45160$ $\mathcal{B} = 166.12\%$	$R_1 = 0.799464$ $R_2 = 1.56612$ $R_3 = 2.44214$ $R_4 = 3.56575$ $R_5 = 5.14991$ $R_6 = 8.17724$ $R_7 = 4.75604$ $\mathcal{B} = 165.92\%$	$R_1 = 0.790505$ $R_2 = 1.54854$ $R_3 = 2.41612$ $R_4 = 3.52984$ $R_5 = 5.10062$ $R_6 = 8.09506$ $R_7 = 4.98039$ $\mathcal{B} = 165.80\%$	$R_1 = 0.769238$ $R_2 = 1.50689$ $R_3 = 2.35445$ $R_4 = 3.44465$ $R_5 = 4.98371$ $R_6 = 7.90105$ $R_7 = 5.63413$ $\mathcal{B} = 165.49\%$	$R_1 = 0.730960$ $R_2 = 1.43218$ $R_3 = 2.24371$ $R_4 = 3.29145$ $R_5 = 4.77353$ $R_6 = 7.55539$ $R_7 = 7.55226$ $\mathcal{B} = 164.92\%$
$N = 8$	$R_1 = 0.827640$ $R_2 = 1.60137$ $R_3 = 2.43715$ $R_4 = 3.44990$ $R_5 = 4.75290$ $R_6 = 6.59900$ $R_7 = 10.3609$ $R_8 = 4.54487$ $\mathcal{B} = 170.36\%$	$R_1 = 0.813537$ $R_2 = 1.57351$ $R_3 = 2.39653$ $R_4 = 3.39514$ $R_5 = 4.68106$ $R_6 = 6.50282$ $R_7 = 10.1959$ $R_8 = 4.86507$ $\mathcal{B} = 170.19\%$	$R_1 = 0.804486$ $R_2 = 1.55566$ $R_3 = 2.37050$ $R_4 = 3.36003$ $R_5 = 4.63499$ $R_6 = 6.44119$ $R_7 = 10.0906$ $R_8 = 5.10184$ $\mathcal{B} = 170.08\%$	$R_1 = 0.782994$ $R_2 = 1.51338$ $R_3 = 2.30882$ $R_4 = 3.27678$ $R_5 = 4.52569$ $R_6 = 6.29508$ $R_7 = 9.84235$ $R_8 = 5.79556$ $\mathcal{B} = 169.81\%$	$R_1 = 0.744281$ $R_2 = 1.43752$ $R_3 = 2.19812$ $R_4 = 3.12715$ $R_5 = 4.32909$ $R_6 = 6.03264$ $R_7 = 9.40127$ $R_8 = 7.86466$ $\mathcal{B} = 169.31\%$

Table E.5: Normalized sheet surface resistivities for -20 dB OPT absorption behaviors. The ϵ_r values are representative of practical low-loss low dielectric constant foams, all computed bandwidths are at the -20 dB level (see Figure E.5), and all resistance values are given to 6 digit accuracy.

stellenbosch University http://scholar.sun.ac.za

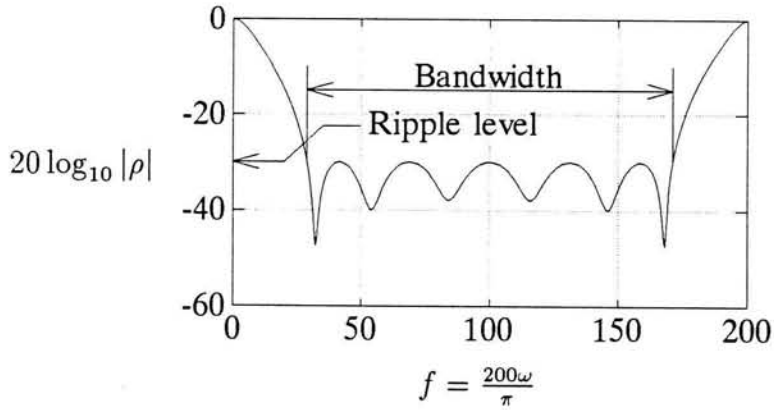

Figure E.6: Generic shape of the tabulated −30 dB OPT solutions of Table E.6. Note that N reflection minima will reside in the range $0 < f < 200$.

	$\epsilon_r = 1$	$\epsilon_r = 1.03$	$\epsilon_r = 1.05$	$\epsilon_r = 1.1$	$\epsilon_r = 1.2$
$N = 2$	$R_1 = 0.731516$ $R_2 = 2.99586$ $\mathcal{B} = 52.11\%$	$R_1 = 0.720422$ $R_2 = 3.09333$ $\mathcal{B} = 51.75\%$	$R_1 = 0.713297$ $R_2 = 3.16107$ $\mathcal{B} = 51.52\%$	$R_1 = 0.696361$ $R_2 = 3.34098$ $\mathcal{B} = 50.96\%$	$R_1 = 0.665788$ $R_2 = 3.75425$ $\mathcal{B} = 49.93\%$
$N = 3$	$R_1 = 0.670939$ $R_2 = 1.88297$ $R_3 = 5.44051$ $\mathcal{B} = 90.25\%$	$R_1 = 0.660419$ $R_2 = 1.85566$ $R_3 = 5.85472$ $\mathcal{B} = 89.88\%$	$R_1 = 0.653666$ $R_2 = 1.83810$ $R_3 = 6.16382$ $\mathcal{B} = 89.64\%$	$R_1 = 0.637629$ $R_2 = 1.79632$ $R_3 = 7.08367$ $\mathcal{B} = 89.06\%$	$R_1 = 0.608725$ $R_2 = 1.72073$ $R_3 = 9.95920$ $\mathcal{B} = 87.98\%$
$N = 4$	$R_1 = 0.656444$ $R_2 = 1.58614$ $R_3 = 3.40904$ $R_4 = 7.62912$ $\mathcal{B} = 114.96\%$	$R_1 = 0.645914$ $R_2 = 1.56220$ $R_3 = 3.36267$ $R_4 = 8.53028$ $\mathcal{B} = 114.64\%$	$R_1 = 0.639157$ $R_2 = 1.54682$ $R_3 = 3.33284$ $R_4 = 9.24999$ $\mathcal{B} = 114.43\%$	$R_1 = 0.623119$ $R_2 = 1.51026$ $R_3 = 3.26179$ $R_4 = 11.6722$ $\mathcal{B} = 113.93\%$	$R_1 = 0.594243$ $R_2 = 1.44422$ $R_3 = 3.13295$ $R_4 = 23.6587$ $\mathcal{B} = 112.99\%$
$N = 5$	$R_1 = 0.656689$ $R_2 = 1.46876$ $R_3 = 2.73978$ $R_4 = 5.20869$ $R_5 = 9.37907$ $\mathcal{B} = 131.18\%$	$R_1 = 0.645977$ $R_2 = 1.44609$ $R_3 = 2.70021$ $R_4 = 5.14184$ $R_5 = 10.8225$ $\mathcal{B} = 130.90\%$	$R_1 = 0.639107$ $R_2 = 1.43154$ $R_3 = 2.67478$ $R_4 = 5.09882$ $R_5 = 12.0433$ $\mathcal{B} = 130.73\%$	$R_1 = 0.622803$ $R_2 = 1.39695$ $R_3 = 2.61425$ $R_4 = 4.99627$ $R_5 = 16.6677$ $\mathcal{B} = 130.30\%$	$R_1 = 0.593469$ $R_2 = 1.33453$ $R_3 = 2.50472$ $R_4 = 4.81010$ $R_5 = 64.8250$ $\mathcal{B} = 129.50\%$
$N = 6$	$R_1 = 0.663013$ $R_2 = 1.41200$ $R_3 = 2.45276$ $R_4 = 4.09566$ $R_5 = 7.20866$ $R_6 = 10.7338$ $\mathcal{B} = 142.39\%$	$R_1 = 0.652057$ $R_2 = 1.38988$ $R_3 = 2.41619$ $R_4 = 4.03898$ $R_5 = 7.12026$ $R_6 = 12.6992$ $\mathcal{B} = 142.15\%$	$R_1 = 0.645032$ $R_2 = 1.37569$ $R_3 = 2.39270$ $R_4 = 4.00253$ $R_5 = 7.06337$ $R_6 = 14.4407$ $\mathcal{B} = 142.00\%$	$R_1 = 0.628363$ $R_2 = 1.34196$ $R_3 = 2.33682$ $R_4 = 3.91572$ $R_5 = 6.92773$ $R_6 = 21.7903$ $\mathcal{B} = 141.64\%$	$R_1 = 0.598389$ $R_2 = 1.28115$ $R_3 = 2.23584$ $R_4 = 3.75842$ $R_5 = 6.68136$ $R_6 = 1413.97$ $\mathcal{B} = 140.95\%$
$N = 7$	$R_1 = 0.672239$ $R_2 = 1.38222$ $R_3 = 2.30041$ $R_4 = 3.59275$ $R_5 = 5.61879$ $R_6 = 9.36566$ $R_7 = 11.7796$ $\mathcal{B} = 150.53\%$	$R_1 = 0.661018$ $R_2 = 1.36032$ $R_3 = 2.26545$ $R_4 = 3.54091$ $R_5 = 5.54397$ $R_6 = 9.25458$ $R_7 = 14.2135$ $\mathcal{B} = 150.33\%$	$R_1 = 0.653822$ $R_2 = 1.34626$ $R_3 = 2.24299$ $R_4 = 3.50758$ $R_5 = 5.49584$ $R_6 = 9.18310$ $R_7 = 16.4525$ $\mathcal{B} = 150.19\%$	$R_1 = 0.636754$ $R_2 = 1.31288$ $R_3 = 2.18961$ $R_4 = 3.42828$ $R_5 = 5.38116$ $R_6 = 9.01268$ $R_7 = 26.8581$ $\mathcal{B} = 149.88\%$	NO SOLUTION
$N = 8$	$R_1 = 0.682913$ $R_2 = 1.36666$ $R_3 = 2.20975$ $R_4 = 3.31400$ $R_5 = 4.87086$ $R_6 = 7.28066$ $R_7 = 11.6561$ $R_8 = 12.5922$ $\mathcal{B} = 156.68\%$	$R_1 = 0.671424$ $R_2 = 1.34479$ $R_3 = 2.17571$ $R_4 = 3.26496$ $R_5 = 4.80268$ $R_6 = 7.18694$ $R_7 = 11.5209$ $R_8 = 15.4323$ $\mathcal{B} = 156.51\%$	$R_1 = 0.664058$ $R_2 = 1.33075$ $R_3 = 2.15386$ $R_4 = 3.23345$ $R_5 = 4.75884$ $R_6 = 7.12663$ $R_7 = 11.4340$ $R_8 = 18.1248$ $\mathcal{B} = 156.39\%$	$R_1 = 0.646585$ $R_2 = 1.29744$ $R_3 = 2.10192$ $R_4 = 3.15850$ $R_5 = 4.65447$ $R_6 = 6.98290$ $R_7 = 11.2268$ $R_8 = 31.7466$ $\mathcal{B} = 156.11\%$	NO SOLUTION

Table E.6: Normalized sheet surface resistivities for −30 dB OPT absorption behaviors. The ϵ_r values are representative of practical low-loss low dielectric constant foams, all computed bandwidths are at the −30 dB level (see Figure E.6), and all resistance values are given to 6 digit accuracy.

stellenbosch University http://scholar.sun.ac.za

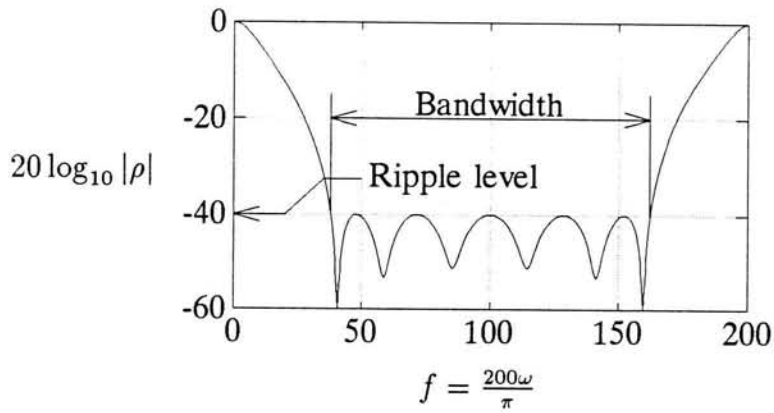

Figure E.7: Generic shape of the tabulated −40 dB OPT solutions of Table E.7. Note that N reflection minima will reside in the range $0 < f < 200$.

	$\epsilon_r = 1$	$\epsilon_r = 1.03$	$\epsilon_r = 1.05$	$\epsilon_r = 1.1$	$\epsilon_r = 1.2$
$N = 2$	$R_1 = 0.714644$ $R_2 = 3.27270$ $\mathcal{B} = 29.96\%$	$R_1 = 0.704049$ $R_2 = 3.38947$ $\mathcal{B} = 29.74\%$	$R_1 = 0.697242$ $R_2 = 3.47104$ $\mathcal{B} = 29.60\%$	$R_1 = 0.681048$ $R_2 = 3.68936$ $\mathcal{B} = 29.27\%$	$R_1 = 0.651771$ $R_2 = 4.20032$ $\mathcal{B} = 28.65\%$
$N = 3$	$R_1 = 0.635433$ $R_2 = 1.90932$ $R_3 = 7.12073$ $\mathcal{B} = 64.38\%$	$R_1 = 0.625832$ $R_2 = 1.88160$ $R_3 = 7.85541$ $\mathcal{B} = 64.09\%$	$R_1 = 0.619666$ $R_2 = 1.86378$ $R_3 = 8.42814$ $\mathcal{B} = 63.91\%$	$R_1 = 0.605004$ $R_2 = 1.82137$ $R_3 = 10.2696$ $\mathcal{B} = 63.45\%$	$R_1 = 0.578523$ $R_2 = 1.74461$ $R_3 = 17.7871$ $\mathcal{B} = 62.61\%$
$N = 4$	$R_1 = 0.607539$ $R_2 = 1.54794$ $R_3 = 3.69298$ $R_4 = 11.8594$ $\mathcal{B} = 91.19\%$	$R_1 = 0.598224$ $R_2 = 1.52487$ $R_3 = 3.64208$ $R_4 = 14.2215$ $\mathcal{B} = 90.91\%$	$R_1 = 0.592242$ $R_2 = 1.51006$ $R_3 = 3.60933$ $R_4 = 16.3688$ $\mathcal{B} = 90.72\%$	$R_1 = 0.578024$ $R_2 = 1.47481$ $R_3 = 3.53130$ $R_4 = 26.0380$ $\mathcal{B} = 90.27\%$	NO SOLUTION
$N = 5$	$R_1 = 0.597199$ $R_2 = 1.40207$ $R_3 = 2.79442$ $R_4 = 6.02243$ $R_5 = 16.7045$ $\mathcal{B} = 110.43\%$	$R_1 = 0.587941$ $R_2 = 1.38086$ $R_3 = 2.75408$ $R_4 = 5.94443$ $R_5 = 21.9785$ $\mathcal{B} = 110.17\%$	$R_1 = 0.581997$ $R_2 = 1.36723$ $R_3 = 2.72814$ $R_4 = 5.89421$ $R_5 = 27.7489$ $\mathcal{B} = 110.00\%$	$R_1 = 0.567873$ $R_2 = 1.33483$ $R_3 = 2.66640$ $R_4 = 5.77444$ $R_5 = 78.3222$ $\mathcal{B} = 109.60\%$	NO SOLUTION
$N = 6$	$R_1 = 0.594226$ $R_2 = 1.32903$ $R_3 = 2.42140$ $R_4 = 4.37429$ $R_5 = 8.80180$ $R_6 = 21.2058$ $\mathcal{B} = 124.36\%$	$R_1 = 0.584928$ $R_2 = 1.30873$ $R_3 = 2.38557$ $R_4 = 4.31353$ $R_5 = 8.69450$ $R_6 = 30.6603$ $\mathcal{B} = 124.13\%$	$R_1 = 0.578960$ $R_2 = 1.29570$ $R_3 = 2.36254$ $R_4 = 4.27444$ $R_5 = 8.62537$ $R_6 = 43.4068$ $\mathcal{B} = 123.98\%$	NO SOLUTION	NO SOLUTION
$N = 7$	$R_1 = 0.594990$ $R_2 = 1.28768$ $R_3 = 2.22736$ $R_4 = 3.67279$ $R_5 = 6.26485$ $R_6 = 11.9413$ $R_7 = 25.2117$ $\mathcal{B} = 134.74\%$	$R_1 = 0.585604$ $R_2 = 1.26790$ $R_3 = 2.19393$ $R_4 = 3.61991$ $R_5 = 6.18126$ $R_6 = 11.8035$ $R_7 = 39.9615$ $\mathcal{B} = 134.54\%$	$R_1 = 0.579580$ $R_2 = 1.25519$ $R_3 = 2.17246$ $R_4 = 3.58591$ $R_5 = 6.12746$ $R_6 = 11.7147$ $R_7 = 65.0126$ $\mathcal{B} = 134.41\%$	NO SOLUTION	NO SOLUTION
$N = 8$	$R_1 = 0.597845$ $R_2 = 1.26238$ $R_3 = 2.11210$ $R_4 = 3.29967$ $R_5 = 5.15042$ $R_6 = 8.43466$ $R_7 = 15.3653$ $R_8 = 28.6957$ $\mathcal{B} = 142.71\%$	$R_1 = 0.588342$ $R_2 = 1.24289$ $R_3 = 2.08013$ $R_4 = 3.25117$ $R_5 = 5.07838$ $R_6 = 8.32640$ $R_7 = 15.1962$ $R_8 = 49.6333$ $\mathcal{B} = 142.53\%$	$R_1 = 0.582244$ $R_2 = 1.23038$ $R_3 = 2.05959$ $R_4 = 3.21999$ $R_5 = 5.03205$ $R_6 = 8.25671$ $R_7 = 15.0872$ $R_8 = 95.5521$ $\mathcal{B} = 142.41\%$	NO SOLUTION	NO SOLUTION

Table E.7: Normalized sheet surface resistivities for −40 dB OPT absorption behaviors. The ϵ_r values are representative of practical low-loss low dielectric constant foams, all computed bandwidths are at the −40 dB level (see Figure E.7), and all resistance values are given to 6 digit accuracy.

stellenbosch University http://scholar.sun.ac.za

Bibliography

[1] W.H. Emerson, "Electromagnetic wave absorbers and anechoic chambers through the years," *IEEE Trans. Antennas Propagat.*, vol. 21, no. 4, pp. 484 – 490, Jul. 1973.

[2] H.A. Schade, "Schornsteinfeger," U.S. Tech. Mission to Europe, Tech. Rep. 90 – 45 AD–47746, May 1945.

[3] G.G. MacFarlane, "Radar camouflage, research and development by the Germans," T. 1905, M/99, TRE, Jul. 23, 1945.

[4] O. Halpern and M.J. Johnson, Jr., "Radar, summary report of HARP project," OSRD Div. 14, vol. 1, pt. π, chs. 9 – 12.

[5] W.W. Salisbury, "Absorbent body for electromagnetic waves," US Patent 2 599 944, filed May 11, 1943, granted Jun. 10, 1952.

[6] B. Sweetman, "Lifting the curtain," *International Defense Review*, vol. 2, pp. 159 – 162, 1992.

[7] P. Bedard, "Stealth cars," *Car and Driver*, vol. 26, no. 6, pp. 140 *et seq*, Dec. 1980.

[8] L.K. Neher, "Non-reflecting background for testing microwave equipment," U.S Patent 2 656 535, filed Aug. 6, 1945, granted Oct. 20, 1953.

[9] R.L. Fante and M.T. McCormack, "Reduction of reflections using Salisbury screens," *1988 IEEE AP-S/URSI Int. Symp.*, Syracuse, NY., Symp. Digest, p. 63.

[10] R.L. Fante and M.T. McCormack, "Reflection properties of the Salisbury screen," *IEEE Trans. Antennas Propagat.*, vol. 36, no. 10, pp. 1443 – 1454, Oct. 1988.

[11] H. Dominik and E. Eckert, "Hochfrequenz-absorbierende materialien," *Electromagnetische Vertraglichkeit*, ntz. Bd. 41, Heft 5, pp. 280 – 283, 1988.

[12] K. Naishadham and P.K. Kadaba, "Measurement of the microwave conductivity of a polymeric material with potential applications in absorbers and shielding," *IEEE Trans. Microwave Theory Tech.*, vol. 39, no. 7, pp. 1158 – 1164, Jul. 1991.

stellenbosch University http://scholar.sun.ac.za

[13] H. Jasik, ed., *Antenna Engineering Handbook.* New York: McGraw-Hill, 1961.

[14] Salisbury Screen, Type SS (Tuned), Product note from Advanced Absorbers, 170 West Road, Portsmouth, NH 03801.

[15] E.F. Knott, J.F. Schaeffer and M.T. Tuly, *Radar Cross Section, Its Prediction, Measurement and Reduction.* Norwood: Artech House, 1985.

[16] M.I. Skolnik, editor, *Radar Handbook.* New York: McGraw-Hill, 2nd ed., 1990.

[17] G.T. Ruck, D.E. Barrick, W.D. Stuart and C.K. Krichbaum, *Radar Cross Section Handbook.* New York: Plenum Press, 1970, vol. 2.

[18] H. Severin, "Nonreflecting absorbers for microwave radiation," *IRE Trans. Antennas Propagat.*, vol. 4, pp. 385 – 392, Jul. 1956.

[19] R. Becker, "The reflection of electromagnetic waves at a medium consisting of layers," Rep. Institut für Theoretische Physik der Universität, Göttingen, Germany, 1943, not published.

[20] R.E. Collin, *Foundations for Microwave Engineering.* New York: McGraw-Hill, 1966.

[21] C.G. Montgomery, R.H. Dicke, and E.M. Purcell, *Principles of Microwave Circuits.* M.I.T. Rad. Lab. Ser., vol. 8, New York: McGraw-Hill, 1948.

[22] J.R. Nortier, C.A. Van der Neut and D.E. Baker, "Tables for the design of Jaumann microwave absorber," *Microwave Journal*, pp. 219 – 222, Sep. 1987.

[23] F. Gross and J.R. Nortier, Letters to the Editor, *Microwave Journal*, pp. 206 – 207, Jan. 1988.

[24] T.M. Connolly and E.J. Luoma, "Microwave absorbers," U.S. Patent 4 038 660, Jul. 26, 1977.

[25] E.F. Knott and K.B. Langseth, "Performance degradation of Jaumann absorbers due to curvature," *IEEE Trans. Antennas Propagat.*, vol. 28, no. 1, pp. 137 – 139, Jan. 1980.

[26] R.D. Graglia and P.L.E. Uslenghi, "Anisotropic layered absorbers on cylindrical structures," *Electromagnetics*, vol. 7, no. 2, 1987.

[27] L.J. du Toit and J.H. Cloete, "A design process for Jaumann absorbers," *1989 IEEE AP-S/URSI Int. Symp.*, San Jose, CA., Symp. Digest, pp. 1558 – 1561.

[28] E. Marouby, J.P. Gouy and J.R. Levrel, "Optimization of radar absorbing material with the CAD software Touchstone," *1992 IEEE AP-S/URSI Int. Symp.*, Chicago, IL., Symp. Digest, pp. 280 – 283.

stellenbosch University http://scholar.sun.ac.za

[29] D.L. Jaggard, N. Engheta and J.C. Liu, "*Chiroshield*† : The chiral Salisbury shield," *1990 IEEE AP-S/URSI Int. Symp.*, Dallas, TX., Symp. Digest, p. 137.

[30] F.B. Gross and E.J. Kuster, "An optimized polarization sensitive Salisbury screen," *IEEE Trans. Antennas Propagat.*, vol. 35, no. 12, pp. 1492 – 1495, Dec. 1987.

[31] R.M. Walser, "A study of thin-film magnetodielectrics," *Doctoral Dissertation*, The University of Michigan, Ann Arbor, 1967.

[32] R.S. Zich, editor, "Frequency selective surfaces," Special Issue, *Electromagnetics*, vol. 5, no. 4, 1985.

[33] E.J. Wilkinson, "An N-way hybrid power divider," *IRE Trans. Microwave Theory Tech.*, vol. 8, pp. 116 – 118, Jan 1960.

[34] S.B. Cohn, "A class of broadband three-port TEM-mode hybrids," *IEEE Trans. Microwave Theory Tech.*, vol. 16, no. 2, pp. 110 – 116, Feb. 1968.

[35] L.J. du Toit and J.H. Cloete, "Plane wave specular reflection from an infinite planar conductor coated with lossy layers," *1988 SAIEE Joint AP-S/MTT Symp.*, Pretoria, South Africa, Symp. Digest, pp. 24.1 – 24.12.

[36] _____, "Specular reflection of plane waves by a planar conductor coated with lossy layers," *Trans. SAIEE*, pp. 9 – 13, Mar. 1991.

[37] O. Brune, "Synthesis of a finite two-terminal network whose driving-point impedance is a prescribed function of frequency," J. Math. Phys., vol. 10, no. 3, pp. 191 – 236, 1931.

[38] L.J. du Toit and J.H. Cloete, "Advances in the design of Jaumann absorbers," *1990 IEEE AP-S/URSI Int. Symp.*, Dallas, TX., Symp. Digest, pp. 1212–1215.

[39] _____, "Optimal equiripple solution to the Jauman absorber problem," *1992 IEEE AP-S/URSI Int. Symp.*, Chicago, IL., Symp. Digest, pp. 703 – 706.

[40] R.S. Elliott and G.J. Stern, "A new technique for shaped beam synthesis of equispaced arrays," *IEEE Trans. Antennas Propagat.*, vol. 32, no. 10, pp. 1129–1133, Oct. 1984.

[41] H.J. Orchard, R.S. Elliott and G.J. Stern, "Optimizing the synthesis of shaped beam antenna patterns," *Proc. IEEE*, vol. 132, no. 1, pp. 63 – 68, Feb. 1985.

[42] C.L. Dolph, "A current distribution for broadside arrays which optimizes the relationship between beam width and side-lobe level," *Proc. IRE*, pp. 335–348, Jun. 1946.

[43] T.B.A. Senior, "Backscattering from resistive strips," *IEEE Trans. Antennas Propagat.*, vol. 27, no. 6, pp. 808 – 813, Nov. 1979.

stellenbosch University http://scholar.sun.ac.za

[44] S. Ramo, J.R. Whinnery and T. van Duzer, *Fields and Waves in Communication Electronics.* New York: John Wiley & Sons, 1965.

[45] J.A. Stratton, *Electromagnetic Theory.* New York: McGraw-Hill, 1941.

[46] P.I. Richards, "Resistor-transmission-line circuits," *Proc. IRE*, vol. 36, pp. 217–220, Feb. 1948.

[47] G.C. Temes and J.W. LaPatra, *Circuit Synthesis and Design.* Tokyo: McGraw-Hill, 1977.

[48] I. Navot, private communication.

[49] I. Navot, "Analysis of the Jauman absorber equivalent network," private communication, Nov. 1989.

[50] A.C. Bartlett, *The Theory of Artificial Lines and Filters.* Chapman & Hall, 1930.

[51] P.R. Clement, "The Chebyshev approximation method," *Quarterly App. Math.*, vol. 11, no. 2, pp. 167 – 183, Jul. 1953.

[52] I. Navot, "Some comments on Chebyshev approximation," notes from a lecture given at the Department of Electrical and Electronic Engineering, University of Stellenbosch, Stellenbosch, South Africa, Aug. 18, 1989.

[53] B. Noble, *Applied Linear Algebra.* Prentice Hall, 1969.

[54] G. Dahlquist, A. Björk and N. Anderson, *Numerical Methods.* Englewood Cliffs: Prentice Hall, 1974.

[55] I. Navot, private communication, Jan. 8, 1990.

[56] K.C. Gupta, R. Garg and R. Chadha, *Computer-Aided Design of Microwave Circuits.* Massachusetts: Artech House, 1981.